Processing of Trace Metals in Atmospheric Particulate Matter

by

Aurelie Rose Marcotte

A Dissertation Presented in Partial Fulfillment
of the Requirements for the Degree
Doctor of Philosophy

Approved April 2015 by the
Graduate Supervisory Committee:

Pierre Herckes (Co-Chair)
Ariel Anbar (Co-Chair)
Matthew Fraser
Mark Hayes

ARIZONA STATE UNIVERSITY

May 2015

ABSTRACT

Particulate trace metals can enter the atmosphere as mineral dust, sea spray, anthropogenic emissions, biomass burning, etc. Once in the atmosphere they can undergo a variety of transformations including aqueous phase (cloud) processing, photochemical reactions, interact with gases, and ultimately deposit. Metals in aerosols are of particular interest because of their natural and anthropogenic sources as well as their effects on local (human health) and global (climate change) scales. This work investigates the metal component of atmospheric particles and how it changes during physical and chemical processes at local, regional and global scales, through laboratory and field studies. In the first part of this work, the impact of local dust storms (haboobs) on ambient metal concentrations and speciation is investigated in Tempe, AZ. It was found that metal concentrations substantially increase (> 10 times) during these events before returning to pre-storm levels. In a second part of this work, the impact of fog processing on metal concentrations, solubility and speciation is examined through field observations in California's Central Valley. The observations show that fog processing has a profound effect on local metal concentrations but the trends are not consistent between sites or even between events, indicating complex processes that need further investigation. For example, fogs have an effect on scavenging and solubility of iron in Davis, while in Fresno soluble iron content is indicative of the source of the aerosol. The last part of the thesis investigates the role of particle size on the solubilization of iron from mineral dust aerosols during global atmospheric transport through laboratory experiments. The experiments showed that mineralogy and pH have the greatest effect on iron solubility in

atmospheric aerosols in general while particle size and photochemistry impact mainly the solubility of iron oxides.

DEDICATION

"Tell me and I forget, teach me and I may remember, involve me and I learn."

–Benjamin Franklin

To all of my mentors; past, present, and future. Thank you for believing in my abilities and helping me become better scientist and mentor to the next generation of scientists.

"The delicate balance of mentoring someone is not creating them in your own image, but giving them the opportunity to create themselves."

–Steven Spielberg

To my greatest mentors of all; my parents. Thank you for the encouragement to discover myself; without your love and support none of this would have been possible.

ACKNOWLEDGMENTS

I would first like to acknowledge my advisors Pierre Herckes and Ariel Anbar, whose guidance over the past 5 years has made me a better scientist and prepared for what lies ahead. I would also like to acknowledge my supervisory committee members, Matthew Fraser and Mark Hayes as well as Everett Shock, Hiliary Hartnett and Paul Westerhoff for all of their advice and assistance with my dissertation projects.

I would like to acknowledge my collaborators Brian Majestic, Benton Cartledge, Chris Mead, Marin Robinson, and Jeff Collett. I would also like to acknowledge all of the help I have received from Gwyn Gordon, Steve Romaniello, Panjai Prapaipong, Sisouk Phrasavath, Andrea Clements and Dan Meritz.

I would like to acknowledge all of my current and past labmates in the Herckes Group at ASU: Nabin Upadhyay, Jim Hutchings, Youliang Wang, Jershon Eagar, Jinwei Zhang, Sarah Frey, Denise Napolitano, Christy Rose, Taka Nosaka, Alyssa Sherry, Kevin Shaffer, Kirt Reed, Amanda Moore, Joana Sipe, and Blanca Rodriguez. Thank you to all of the Arizona State University Department of Chemistry and Biochemistry staff for their hard work. I would also like to acknowledge my funding sources including the National Science Foundation (AGS-0964810 and AGS-0847710), CAP-LTER 2014 Graduate Grant and Environment Canada.

Finally, I would like to acknowledge all the help and support from my friends at ASU. I would especially like to acknowledge Iolanda Klein, who has been a great friend throughout my graduate school career, and Dayn Sommer, who was an amazing support system throughout this dissertation process.

TABLE OF CONTENTS

Page

LIST OF TABLES ix

LIST OF FIGURES x

CHAPTER

1 INTRODUCTION AND BACKGROUND 1

Properties of Atmospheric Aerosols 1

Sources of Atmospheric Aerosols 4

Transportation of Atmospheric Aerosols 8

Fate and Implications of Atmospheric Aerosols 10

Aerosol and Fog Sampling 13

Rationale and Objectives 15

2 CHARACTERIZATION OF HABOOB PARTICULATE MATTER IN TEMPE, AZ 19

Introduction 19

Materials and Methods 23

Sample Collection 23

Trace Metal Analysis 23

Enrichment Factors 24

Principal Components Analysis 24

Results and Discussion 25

Particulate Matter Concentrations 25

Elemental Concentrations 27

CHAPTER Page

Enrichment Factors 29

Temporal Duration and Effect of Haboobs 35

Conclusions 40

3 FOG PROCESSING OF TRACE METALS IN CALIFORNIA'S CENTRAL VALLEY 41

Introduction 41

Materials and Methods 43

Sample Collection 44

Trace Metal Analysis 44

Scavenging Efficiency 45

Results and Discussion 46

Metal Concentrations in Fog and Cloud Water Samples 46

Metal Processing by Fog Events 49

Observed Trace Metals Scavenging Efficiencies for Davis and Fresno Fog Events 54

Conclusions 57

4 PROCESSING OF ATMOPSHERIC AEROSOLS IN RURAL AND URBAN ENVIRONMENTS: SOLUBLE IRON CONTENT 59

Introduction 59

Materials and Methods 61

Sample Collecton 61

Sample Extraction 62

CHAPTER Page

Soluble Iron Analysis 63

Results and Discussion 64

Conclusions 71

5 EFFECT OF PARTICLE SIZE ON IRON SOLUBULITY IN ATMOPSHERIC AEROSOLS 72

Introduction 72

Materials and Methods 76

Reagents 76

Sample Preparation 77

Scanning Electron Microscopy (SEM) 77

Surface Area Measurements 78

Inductively Coupled Plasma Mass Spectrometry (ICP-MS) Analysis 78

UV-Vis Spectroscopy Analysis 78

Photochemical Experiments 79

Results and Discussion 80

Confirmation of Particle Size Distribution by SEM and BET 80

Iron Dissolution of Minerals 83

Iron Speciation of Minerals in Simulated Cloud Water 88

Impact of Photochemistry on Iron Solubility in Minerals 89

Variable and Unexpected Results for Goethite 93

Conclusions 94

CHAPTER Page

6 SUMMARY 95

REFERENCES..... 99

APPENDIX

A SAMPLE INFORMATION FOR FOG WATER AND AEROSOL SAMPLES COLLECTED IN FRESNO AND DAVIS, CALIFORNIA..... 113

LIST OF TABLES

Table Page

2.1 Average PM_{10} and $PM_{2.5}$ Concentrations (μg m^{-3}) in Tempe, AZ 25

2.2 Elemental Concentrations (ng m^{-3}) in $PM_{2.5}$ Samples Collected in 2013.....27

2.3 Elemental Concentrations (ng m^{-3}) in $PM_{2.5}$ Samples Collected in 2014.....28

3.1 Selected Metal Concentrations (μg L^{-1}) in Fog and Cloud Studies around the World, Past and Present 47

4.1 Percent of Total Soluble Fe that is Fe(II) in $PM_{2.5}$ Samples 70

5.1 Composition of Extraction Solutions in Solubility Experiments.....76

5.2 Surface Area Measurements of Kaolinite and Magnetite made by the BET Method.....83

LIST OF FIGURES

Figure Page

1.1 Schematic of Different Particle Size Modes and how Particles come to be in that Size Category 2

1.2 A Schematic Representation of the Influence of Particles and Gases on Cloud/Fog Drop Composition. Reactions Between Several of the Dissolved Species Shown Here can Also be Important. 3

1.3 An Image Taken by the Moderate Resolution Imaging Spectroradiometer (MODIS) on NASA's Terra Satellite on June 10, 2010 6

1.4 Radiative Forcing by Emissions, Their Uncertainties, and Our Level of Confidence/Understanding. The Lower Plot Shows the Total Anthropogenic Radiative Forcing (RF) in 2011 Relative to 1750 13

1.5 Diagrams of a CASCC (A), RAC (B), and a CSU 5-Stage (C) 15

2.1 Average Enrichment Factors of $PM_{2.5}$ Samples Collected During Non-Haboob and Haboob Periods in 2013. Elements Represented in A have Enrichment Factors Less than 5, While Elements Represented in B have enrichment factors greater than 5. Enrichment Factors of Elements of Interest are Normalized to Al (i.e. Al=1) 30

2.2 Average enrichment factors of $PM_{2.5}$ Samples Collected During Non-Haboob and Haboob Periods in 2014. Elements Represented in A have Enrichment Factors Less than 5, While Elements Represented in B have Enrichment Factors Greater than 5. Enrichment Factors of Elements of Interest are Normalized to Al (i.e. Al=1). 31

Figure Page

2.3 Principal Components 1 (Mineral Dust) vs 2 (Anthropogenic) from Principal Component Analysis (PCA) of $PM_{2.5}$ Samples Collected during Summer 2013 at ASU-Tempe Campus. 32

2.4 Principal Components 1 (Mineral Dust) vs 2 (Anthropogenic) from Principal Component Analysis (PCA) of $PM_{2.5}$ Samples Collected during Summer 2014 at ASU-Tempe Campus 33

2.5 Particulate Matter (PM) Concentrations of Al (Blue; A) in µg m^{-3} and Cd (Red; B) in ng m^{-3} in Aerosol Samples Collected During the Summer of 2013 at ASU Tempe Campus. Arrows Represent Periods During which Haboobs Occurred. $PM_{2.5}$ (gray) Concentrations are Plotted on the Primary y-axis (µg m^{-3})..... 35

2.6 Al (Blue; A) and Cd (Red, B) Concentrations in $PM_{2.5}$ Samples Collected during 2014 at the ASU Tempe Campus in µg and ng m^{-3}, Respectively 37

2.7 Enrichment factors (EF) of Mg (purple; A) and Cu and Sb (orange and teal; B) in $PM_{2.5}$ Samples Collected during the Summer of 2013 at ASU Tempe Campus. Arrows Represent Periods during which Haboobs Occurred. $PM_{2.5}$ Concentrations (grey) is Plotted on the Secondary y-axis 39

Figure Page

3.1 Box and Whisker Plots for Major (A) and Minor (B) Element Concentrations in Fog and Cloud Water Collected in Whistler, BC (Blue), Fresno, CA (Green) and Davis, CA (Purple). The Black Line Represents the Median, Whiskers Represent Range, the Top and Bottom of the Boxes Indicate the 75th and 25th Percentile, Respectively, Circles Represent Outliers and Asterisks Represent Extreme Outliners 46

3.2 $PM_{2.5}$ Concentrations of Al and Fe (**A**) and Sb, Pb, and Cd (**B**) (ng m^{-3}) from Fresno, CA. Grey Bars Represent Periods of Fog 50

3.3 $PM_{2.5}$ Concentrations of Al and Fe (A) and Sb, Pb, and Cd (B) (ng m^{-3}) from Davis, CA. Grey Bars Represent Periods of Fog. 51

3.4 Calculated Scavenging Efficiencies in Fresno (A) and Davis (B), CA. Circles Represent Medians and Lines Represent Maximum and Minimum Values 55

4.1 Percent Soluble Iron in $PM_{2.5}$ Samples Collected from Various Sites. Bars Represent Averages and Black Line Represents Maximum and Minimum Values. Grey Represents Urban Areas, Blue Represents Ocean Regions, Green Represents Agricultural Areas, and Brown Represents Areas with Mineral Dust Aerosol Sources. All Samples were Analyzed Similarly to make a More Accurate Comparison..... 64

Figure Page

4.2 Soluble Iron Content in $PM_{2.5}$ Samples Collected in Fresno, CA during the Winter of 2010. Grey Bars Represent Periods of Fog. (Data from Upadhyay et al., 2011) 66

4.3 Soluble Iron Content in $PM_{2.5}$ and $PM_{>2.5}$ Samples Collected in Davis, CA during the Winter of 2011. Grey Bars Represent Periods of Fog 67

4.4 Soluble Iron Content in $PM_{2.5}$ and $PM_{>2.5}$ Samples Collected in Bakersfield, CA during the Winter of 2013. The Grey Bar Represents a Period of Haze (RH > 90%) 68

4.5 Soluble Iron Content in $PM_{2.5}$ Samples Collected in Tempe, AZ during the Summer 2013 Monsoon Season. Blue Bars Represent Periods of Rain. Green Arrows Represent Haboob Events 69

5.1 Distribution of HNLC Regions in the Oceans 73

5.2 Schematic Diagram of Atmospheric Processing and Transport of Mineral Dust Aerosols to the Open Ocean 75

5.3 Schematic Diagram of Photochemical Experimental Set Up 80

5.4 Scanning Electron Microscopy (SEM) Images for Illite (A) and Magnetite (B). The SEM Images are Shown at the Same Magnification, 6500x, with a Scale of 2μm. 82

Figure Page

5.5 Total Soluble Iron Content (as a Percentage) of the Extracted Mineral Samples into Simulated Cloudwater and a Marine Aerosol Solution at the Various Size Fractions. The Graphs on the Left Show the Two Clay Minerals, while the Graphs on the Right Show the Three Iron (Oxyhydr)oxide Minerals, which are Substantially Less Soluble. Error Bars are Representative of the Standard Deviation of Three Replicate Experiments. 86

5.6 Percent Soluble Iron Normalized to Surface Area (SA) for Hematite (Blue) and Magnetite (Purple). Error Bars Represent 3 Replicate Experiments.....88

5.7 Soluble Iron Fraction (as a Percentage) and Speciation of the Size Fractionated Minerals. The Graphs on the Left Show the Two Clay Minerals, while the Graphs on the Right Show the Three Iron (Oxyhydr)oxide Minerals, which are Substantially Less Soluble. Fe(II) (Shaded) is Stacked on Top of Fe(III) (Solid) and Total Soluble Iron is shown as the Height of the Column. Error Bars are Representative of the Standard Deviation of Three Replicate Experiments..... 89

Figure Page

5.8 The Fraction of Soluble Iron (as a Percentage) of the Iron (Oxyhydr)oxide Minerals Studied as a Function of the Time (in Minutes) of the Photochemical Reaction in the Marine Aerosol Solution (pH 1-2). Circles are Representative of Relative Particle Size with Non-Irradiated Samples in Black and Irradiated Samples in Yellow... 91

5.9 The Fraction of Soluble Iron (as a Percentage) of the Clay Minerals Studied as a Function of the Time (in Minutes) of the Photochemical Reaction in the Marine Aerosol Solution (pH 1-2). Circles are Representative of Relative Particle Size with Non-Irradiated Samples in Black and Irradiated Samples in Yellow 92

CHAPTER 1

INTRODUCTION AND BACKGROUND

Properties of atmospheric aerosols

Aerosols are generally defined in the atmospheric community as suspended matter as a liquid or solid dispersed in a gas. Aerosols can be characterized by their physical, chemical and optical properties which can include size, shape, composition, etc. Aerosols are found throughout the atmosphere from ground level, through the troposphere, up in the stratosphere, and beyond. In this work, aerosol will refer to a solid particle in the troposphere.

The sizes of aerosol particles generally range from a few nanometers (nm) to tens of microns (μm) in diameter. Particles are split by their size into two categories: particles greater than 2.5μm, or "coarse" mode, and particles less than 2.5μm, or "fine" mode. This is an important distinction in atmospheric chemistry as these types of particles have different sources, atmospheric residence times, composition, optical properties, and health effects.

Figure 1.1 shows different particles modes characterized according to their size. The fine mode described above is split into two sub-modes: the nuclei and accumulation modes. The nuclei mode consists of particles from approximately 0.005 to 0.1μm in diameter and although generally have highest particle numbers, they account only for a small fraction of atmospheric particle mass because of their small size. These particles are generated through the nucleation, condensation and coagulation of gaseous vapors and can coagulate to form particles that fall into the accumulation mode. Accumulation mode particles fall in the range of 0.1 to 2.5μm in diameter and can act as cloud

condensation nuclei (CCN), which allow them to be rained or washed out in some cases; however, most particle removal mechanisms are not successful in this mode (hence "accumulation" term). Coarse mode particles, diameters greater than 2.5µm, make up most of the mass of aerosol particles because of their large size. These particles are created though natural and man-made, mechanical processes and have the shortest residence times in the atmosphere because their settling velocities are higher.

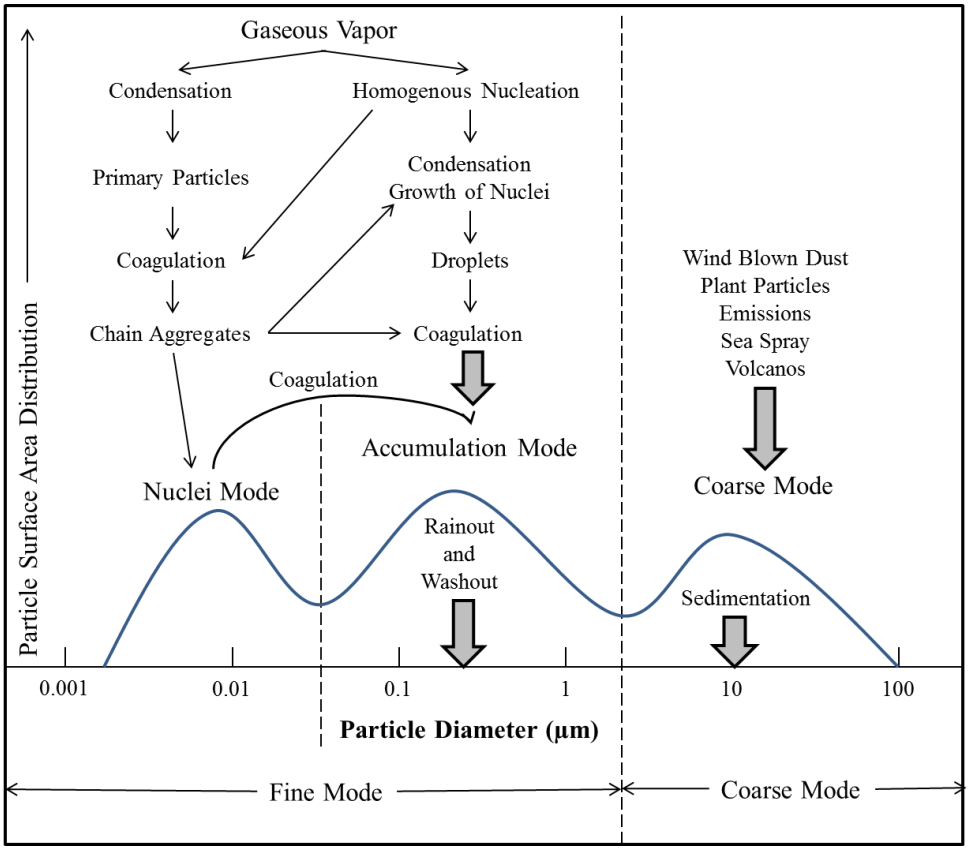


Figure 1.1. Schematic of different particle size modes and how particles come to be in that size category (adapted from Whitby and Cantrell, 1976).

The composition of tropospheric aerosols typically originates from their sources, but transformations during atmospheric transport also affect their chemical properties. Common components of tropospheric aerosols include nitrate, sulfate, ammonium, chloride, sodium, carbonaceous material (elemental and organic carbon), trace metals,

and water (Seinfeld and Pandis, 2006). Aerosols can undergo gas and aqueous phase processing during transport, which can result in chemical transformation of the particle. Figure 1.2 shows potential components in the aqueous layer around a cloud condensation particle, which forms in high humidity conditions (particle deliquescence depends on chemical composition of the particle). These components can come from dissolution of the particle (condensation nucleus) that the droplet forms on, partitioning of gas phase species into the aqueous phase, or from scavenging of other particles by collision. Gas phase reactions with particles under lower humidity conditions are also possible, altering the chemistry of the aerosol (Kong et al., 2014). This work will focus on trace metals in atmospheric aerosols.

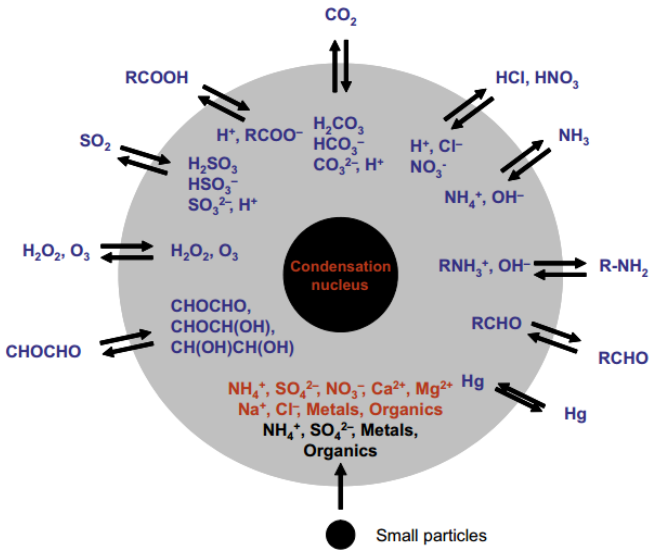


Figure 1.2. A schematic representation of the influence of particles and gases on cloud/fog drop composition. Reactions between several of the dissolved species shown here can also be important. (From Herckes and Collett, Encyclopedia of Atmospheric Sciences, 2015).

The optical properties of aerosols also have an impact on a global and local scale. Globally, aerosol particles can absorb or scatter light, affecting the radiative budget of the

Earth. On a local scale, small aerosol particles can scatter or absorb light as well, which is the main cause of visibility impairment. The optical properties of the aerosol particles are dependent on aerosol optical thickness (aerosol numbers), phase function (angular dependence of light scattering) and single scattering albedo (ratio of scattering to absorption + scattering), which make up the radiative transport function, as well as the particle size, shape, and characterization (physical and chemical properties) (Dubovik et al., 2001).

Sources of atmospheric aerosols

Aerosols can enter the atmosphere in a variety of ways. Natural sources include mineral dust and sea spray aerosols, anthropogenic sources include combustion aerosols, such as vehicle and industrial emissions, and some processes are both natural and anthropogenic such as biomass burning aerosols and secondary organic aerosol formation. The chemical composition of particles originating from each source is complex with organic and inorganic components. In this work, the inorganic components will be examined and are thus described hereafter.

Mineral dust aerosols are classified as ejected minerals into the atmosphere through wind-blown suspension of soil material. Location strongly influences what type of mineralogy is ejected. Mineral dust aerosols are generally on the larger end of the aerosol size range, "coarse" mode particles, with a median size of 1-10μm (Reid et al., 2003), but particles from tens of nanometers to hundreds of micrometers have been measured. Mineral dust particles in the accumulation mode (0.005-0.1μm) seem to have the greatest effect on atmospheric reactivity as they have the greatest surface area (Usher et al., 2003). Mineral dust aerosol morphology is largely dependent on the type of

mineral, which can affect its reactivity in the atmosphere. One of the largest sources of mineral dust aerosols are from Saharan dust storms, ejecting material high in the troposphere, which subsequently gets transported over the Atlantic Ocean (Figure 1.3). Australia, Asia and southern Africa are other locations which have large mineral dust emission events such as these. On a global scale, these events are exceptionally important for the transport of nutrients such as soluble Fe, P, Al, Mn and Si to the open ocean (Baker et al., 2006). Global mineral dust emissions are in the range of 1,000 – 3,000 Tg yr^{-1} (Bauer et al., 2004; Cakmur et al., 2006). On a regional scale, dust storms in Saudi Arabia, inland Australia, and the southwestern United States transport mineral dust aerosols tens to hundreds of miles away from their source. These dust storms have an effect on visibility on short time scales, but the influx of non-native material may have a significant influence on agriculture in the long term (influx of nutrients). Mineral dust aerosols are almost always found in atmospheric aerosol samples as one of the most prominent components. Major elements (> 1 wt%) in mineral dust samples are the typical components of the upper continental crust including Al, Ca, Fe, K, Mg, Na and Si (Rudnick and Gao, 2005).

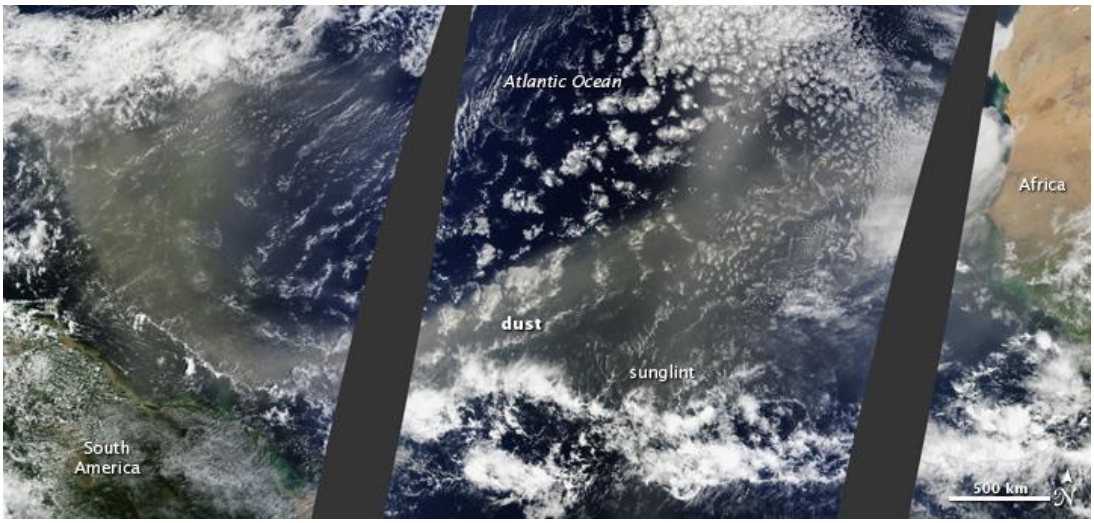


Figure 1.3 An image taken by the Moderate Resolution Imaging Spectroradiometer (MODIS) on NASA's Terra satellite on June 10, 2010 (NASA image courtesy Jeff Schmaltz, MODIS Rapid Response Team at NASA GSFC).

Marine aerosols, or sea-spray aerosols, can be injected from strong winds across the ocean surface, breaking waves, or popping bubbles. Sea-spray aerosols have global emission ranges of 2,000 - 10,000 Tg yr^{-1} (Gantt and Meskhidze, 2013). Although this is a large global mass contribution, particle number counts are low, around 300 - 600cm^{-3} (O'Dowd et al., 1997). Secondary organic aerosols can also form from volatile compounds, dimethyl sulfide for example, over high biologically producing marine environments (Charlson et al., 1987). Since there is mechanical and chemical generation of particles, the size range of marine aerosol particles spans over 5 orders of magnitude. Secondary organic aerosols formed from marine by-products are generally in the nucleation and accumulation mode (sub-micron range and as small as a few nanometers in size) while bubble bursting on the surface can generate particles 1 - 2μm in diameter, but even more in the sub-micron range (Woolfe et al., 1987). Strong winds across the surface of the ocean cause an emission of a wide range of particles as well; although low concentrations are found in the larger size fractions. O'Dowd et al. (1997) shows a size

distribution of sea-spray aerosols from 0.05 - 150μm at wind speeds up for 17 m s^{-1}, as sea-salt number and mass concentrations are highly dependent on wind speed.

Inorganic composition of marine aerosols varies with size region due to inputs of anthropogenic and mineral dust aerosols. In pristine marine environments, Na^{+}, Cl^{-}, Ca^{2+}, Mg^{2+}, and K^{+} are found in high concentrations in coarse mode (> 2.5μm) particles. Inorganic ions, such as NO_3^{-}, SO_4^{2-}, and NH_4^{+}, are also found in high concentrations but in fine mode (sub-micron) particles (Harrison and Pio, 1983). Other trace metals found in marine aerosols include Sr and Fe.

Biomass burning aerosols result from the burning of biological material, which usually happens in large quantities on regional scales, especially in the tropics, as well as on temporal scales. Biomass burning happens all over the world in locations such as South America, Canada, southern Africa, the southeastern United States, and southern Europe. Biomass burning aerosols emission ranges are approximately 60 - 150 Tg yr^{-1} (Kiehl and Rodhe, 1995) and have a median diameter in the sub-micron range. Major components of plants are cellulose and hemicelluloses and lignin, but also proteins, amino acids, volatile compounds, minerals, and water. Because of the major starting material composition, typical emissions from biomass burning include CO_2, H_2O, NO, N_2O, N_2, and SO_2, but also a multitude of other intermediate compounds that can be released (CO, CH_4, H_2, C_2H_4, C_2H_2, PAHs, and soot particles) (Andreae and Merlet, 2001). Major trace elements detected in biomass burning aerosols from the African savanna included P, Cl, S, K, Cu, and Zn. In addition, Al and Fe have been found in high concentrations close to the source (prescribed savanna fires in Lamto, Ivory Coast) as a result of soil remobilization during burning (Gaudiechet et al., 1995).

Major sources of combustion aerosols to the atmosphere are anthropogenic processes, which include industrial, vehicular, smelting, etc. emissions. Aerosols from these combustion sources can be from direct emissions (primary aerosols) or can form from gases through atmospheric processes (secondary organic aerosols). Primary aerosol emissions, such as fly ash and tire wear particles, are generated through human activities. These sources contribute a considerable amount of brown and black carbon, which absorb in the IR, contribute to global warming, and have been found to increase the rate of melting in the Arctic ice sheets (Dumont et al., 2014). These anthropogenic emissions can be enriched in trace crustal elements such as Pb, Cd, and Cu.

In addition to the production of primary particles, human activities produce gases that can undergo gas to particle conversion; called secondary organic aerosols (see Figure 1.1 for particle growth). Most of these combustion particles are less than 0.1μm in diameter and are in high concentration close to their source, but decreases significantly as they travel away from the source (nuclei and accumulation mode particles). Although secondary organic aerosols are a significant fraction of atmospheric aerosols, they were not examined in this work.

Transportation of atmospheric aerosols

Aerosol transport is largely dependent on particle size and meteorological conditions. Large particles are heavier and therefore have higher settling velocities than smaller particles (Hinds, 2012). Large particles (> 30 μm) do not travel far and have more of an effect on a local than global scale. Small particles, however, have the ability to travel further distances because of their long residence times and have greater global impacts. Because residence times of particles are minutes to months (based on size),

meteorology becomes the determinant in atmospheric aerosol transportation. Intra-hemispherically, the transport of particles from east to west happens more rapidly (weeks), since longitudinal wind speeds are on the order of 10 m s^{-1}, than north to south (months), which have meridional wind speeds on the order of 1 m s^{-1}. Inter-hemispheric transport occurs much more slowly (> 1 year) as there is a lack of thermal mixing equatorially (Jacob, 1999). Transport of aerosols vertically, between different layers of the atmosphere, is also very difficult. Since it takes years for aerosol particles to cross from the troposphere to the stratosphere, volcanic eruptions are the only major source of aerosols from the troposphere to the stratosphere.

During atmospheric transport there are a variety of different processes an aerosol particle can undergo that fall generally into two categories: aqueous and heterogeneous processes. Both of these processes can alter the chemical speciation of the aerosol particle changing their reactivity in the environment.

Aerosol particles might act as cloud condensation nuclei and hence be transformed into atmospheric droplets (Andreae and Rosenfeld, 2008). Particles may also be scavenged by collisional processes into droplets. In the droplets, the particles might undergo aqueous phase processing, during which dissolution and subsequent chemical reactions can occur altering the original composition of the particle. Aqueous phase atmospheric processing is especially important when it comes to aerosol solubility (Spokes et al., 1994; Desboeufs et al., 2001). Approximately 10-15% of droplets precipitate while the rest will undergo a cyclic process by which water condenses on the particle (CCN) and then evaporates approximately 5-10 times before it's removed from

the atmosphere (Seinfeld and Pandis, 2006). The average lifetime of a CCN is approximately one week.

During transport, particles can also undergo photochemical surface reactions or photochemical reactions in the aqueous phase (cf above). Photochemical (oxidation) reactions in the troposphere are of significant importance because they cause aerosol aging and the formation of secondary organic aerosols (SOA) (Alfarra et al., 2006). SOA formation has also been shown to be catalyzed by iron (II), which can be present in a particle from the photochemical reduction of iron (III) to iron (II). That photochemical reduction pathway also affects the dissolution properties of an aerosol as iron (II) has been shown to be more soluble than iron (III) (investigated in Chapter 5).

Interactions with SO_x and NO_x gases are also an important part of aerosol chemistry. Gases can cause reactions to occur directly on the surface of particles or can partition into the aqueous phases through Henry's Law. Anthropogenic SO_2 emissions can partition into the liquid phase or be converted from gas to liquid by nucleation and form sulfuric acid (Finlayson-Pitts and Pitts Jr, 2000; Seinfeld and Pandis, 2006) which can lead to particle acidification affecting aqueous phase and gas-particle reactions.

Fate and implications of atmospheric aerosols

After aerosols are emitted and transported it is important to consider their fate and implications. Generally, aerosols can undergo dry, wet or occult deposition. Dry deposition generally happens with larger particles when they fall out as part of gravitational settling. Wet deposition happens when aerosols are rained out either because they were incorporated in liquid droplets as cloud condensation nuclei or they are picked up on the way down. Occult deposition occurs when droplets, which contain particles

(CCN), hit a surface (i.e. fog hitting a building). Where aerosols are deposited can have an effect on human health, biologic systems and our climate.

Aerosol particles can be split into two size categories for their health effects: particles greater than or equal to 2.5μm ($PM_{>2.5}$ or coarse mode) or particles less than 2.5μm ($PM_{2.5}$ or fine mode). $PM_{2.5}$ is regarded as particles that can get into our lungs and cause health effects including respiratory, circulatory, and even possible neurological issues (Schwartz et al., 2002; Lim et al., 2012; Smith et al., 2014). $PM_{>2.5}$ has a large enough mass that it cannot navigate the L-shaped curve of the human esophagus and instead impacts on the walls of our throat and go into the stomach where they are digested (Heyder et al., 1986; Carvalho et al., 2011). $PM_{2.5}$ is lighter and can navigate the sharp curve carried by the airstream. Once in the lungs particles deposit onto the alveoli or walls of the lungs causing inflammation largely due to the formation of reactive oxygen species (ROS) (Gurgueira et al., 2002; Tao et al., 2003). It has been suggested that nanoparticulate material can cross through the blood barrier (Nemmar et al., 2002) and travel to other parts of the body.

Aerosols deposit onto land and sea affecting terrestrial and aquatic ecosystems. Aerosols, especially ones which have been solubilized during transport, can provide a broad range of nutrients (e.g. nitrate and phosphate) to environmental communities. In areas of the ocean where nitrate and phosphate concentrations are high but chlorophyll is low (HNLC regions), iron was found to be a limiting nutrient (Martin, 1990). The main source of iron to the open ocean is from aerosol particles, predominately mineral dust, but also anthropogenic and biomass burning particles.

In terms of climate impacts, aerosols can cause warming or cooling by direct and indirect effects. Aerosol direct effects refer to direct interaction of radiation with the particles. For instance, sulfate aerosols reflect light back to space having a cooling effect on our climate while black carbon absorbs IR radiation having a warming effect on our climate. Aerosol indirect effects refer to a secondary process or effect caused by aerosols. An example of an aerosol indirect effect would be iron-bearing mineral dust deposition into the ocean to seed phytoplankton growth. If more soluble iron is deposited to the ocean then phytoplankton blooms would increase which would subsequently increase the amount of CO_2 uptaken by the ocean which has a cooling effect on our climate. Aerosol direct and indirect effects on climate have some of the largest uncertainty in the global radiative forcing budget (IPCC; Figure 1.4). These large uncertainties make it essential for more research to be done to fully understand these effects and improve climate models.

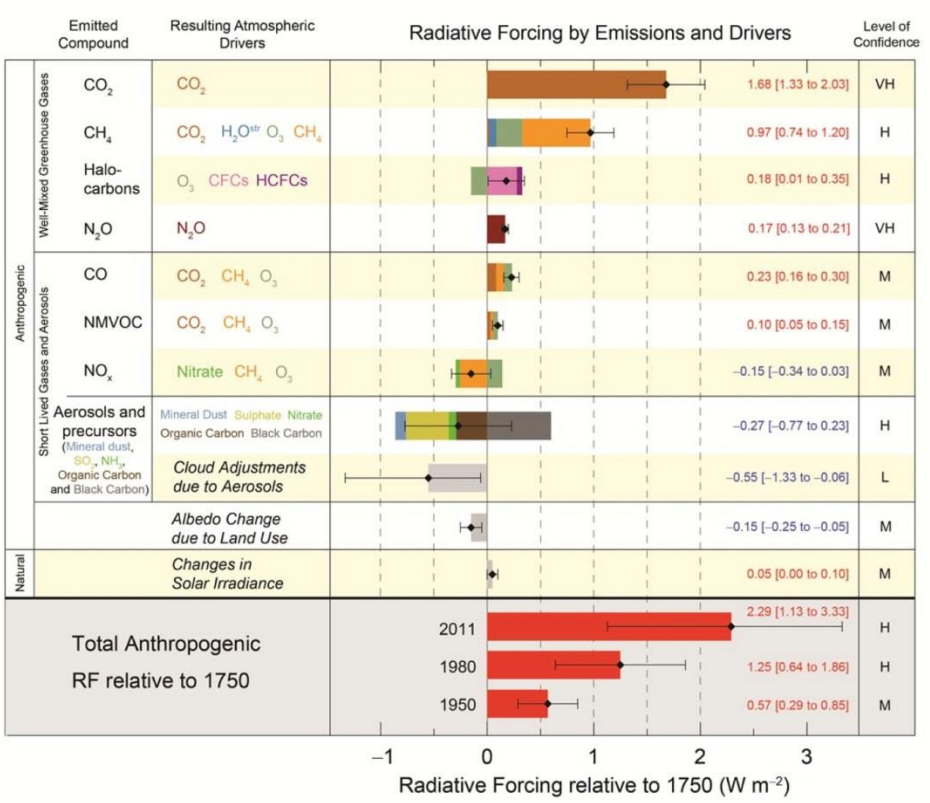


Figure 1.4. Radiative forcing by emissions, their uncertainties, and our level of confidence/understanding. The lower plot shows the total anthropogenic radiative forcing (RF) in 2011 relative to 1750 (from the IPCC 4th Assessment Report (AR4) of Climate Change 2007).

Aerosol and fog sampling

Aerosol sampling can be done in a variety of fashions and is based on the interest of the researcher. Aerosols can be measured remotely based on their optical properties or *in situ* either immediately in the field or collected and brought back to a lab for analysis. In this work, we are most concerned with particle composition, although mass and size distributions of atmospheric particles are also important. Particle composition can be measured by a variety of techniques. Aerosol samples that are collected in the field and brought back to the lab are usually collected on filters or substrates using a pump, but collection of aerosols by dry deposition can also be performed. Filter and substrate samples can be collected as total suspended particles (TSP) or as size segregated particles

using a multi-stage impact sampler or a cyclone (Liu et al., 1976). Aerosol mass spectrometers (AMS) can measure particle composition real time and particle into liquid samplers (PILS) have good time resolution but only measure ions or total organic carbon.

In this work, we focus on offline aerosol sampling methods as samples were collected in the field and brought back to the lab for analysis. A Tisch high volume aerosol sampler (flow rate = 1.13 m^3 min^{-1}) equipped with a $PM_{2.5}$ impactor stage to collect samples split into two size fractions, $PM_{>2.5}$ and $PM_{2.5}$, was used to collect aerosols on acid cleaned cellulose filters for metals analysis by digestion and inductively coupled plasma mass spectrometry (ICP-MS). Chapter 5 focuses on iron solubility in simulated mineral dust aerosol samples. In this case, individual mineral phases were ground, resuspended, and size fractionated using a PM_{10} cyclone followed by a personal cascade impactor sampler (PCIS), which separated particles into five different size fractions. Particle sizes were confirmed by scanning electron microscopy and surface area was measured by Brunauer–Emmett–Teller (BET) theory using nitrogen (N_2) adsorption.

This work also examines how trace metals in aerosols are processed by fog; therefore, in some cases, fog samples were collected simultaneously with aerosol samples. In this work, fog sampling was done using a plastic CalTech Active Strand Cloudwater Collector (CASCC). In a CASCC, droplets are collected via impaction on Teflon strands, which subsequently drop into a plastic bottle, as the air is "sucked" through the collector by a fan (Daube et al., 1987; Monger et al., 1989; Demoz et al., 1996; Figure 1.5A). Another fog collection technique is the Rotating Arm Collector, which is based on the principal of inertial impaction. The sampler is placed facing the wind and the rod at the end of the sampling unit rotates allowing the samples to impact

and flow to the end of the rod into a plastic bottle where it is collected (Jacob et al., 1984; Collett et al., 1990; Krämer and Schültz, 1994; Figure 1.5B). Fog/cloud water can also be collected based on droplet size. The Colorado State University 5-stage cloud water collector (CSU 5-stage; Figure 1.5C) uses cascade inertial impaction to separate droplets in five sizes. As an air mass flows through the sampler, larger droplets that have greater inertia will impact in the earlier stages while the smaller droplets continue and impact at a later stage as the velocity of the air stream increases (Moore et al., 2002).

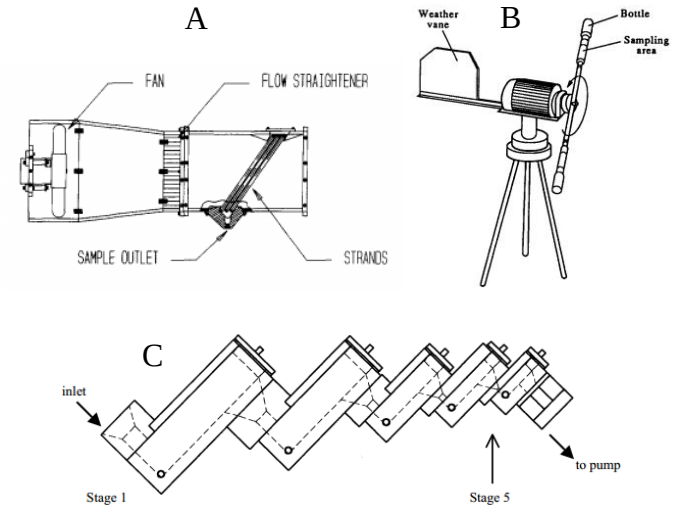


Figure 1.5. Diagrams of a CASCC (A), RAC (B), and a CSU 5-Stage (C).

Rationale and objectives

This work focuses on the inorganic composition of atmospheric particles and the processing of aerosols through field studies and laboratory experiments from local to global scale. This dissertation is structured to start with local aerosol composition moving to larger impacts as the dissertation proceeds. The first research chapter focuses on limited aerosol processing for a local phenomenon. Next, the processing of aerosols by fog at a regional scale is examined. Then, differences between rural and urban environments on aerosol processing with a focus on iron are discussed. Finally,

laboratory experiments simulating multiple atmospheric processes are presented with respect to iron. Iron was chosen as a specific element of interest because it is naturally abundant, but also has anthropogenic sources. It has been shown to solubilize in the atmosphere providing interesting chemical reactions to study and is considered a limiting nutrient in parts of the ocean. This work contributes significantly to *in situ* aerosol and fog measurements as well as global atmospheric processing of iron which has been shown to indirectly effect climate.

Characterization of haboob particulate matter in Tempe, AZ

During this summer months in Arizona temperature and humidity profiles increase significantly as the monsoon season rolls through. In the Phoenix area, monsoons are not the only massive weather event to happen. As cells move and converge to the south large downdrafts on arid land causes the resuspension of dust which move with the storm system, called haboobs. These dust events bring large influxes of dust in short periods of time affecting not only visibility and air conditions, but also can affect ecology. During the summers of 2013 and 2014, aerosol samples were collected in Tempe, AZ with the goal of characterizing and determining the duration of effect a haboob has. It was hypothesized that dust storms fundamentally alter atmospheric compositions, specifically with regards to trace metals, on short time scales.

Fog processing of trace metals in aerosols in California's Central Valley

Fog processing of atmospheric aerosols is important when considering the solubility and deposition of trace metals in the atmosphere. These liquid droplets that form around the aerosols provide an aqueous medium for reactions to occur, but they also allow scavenging of aerosol particles. In this work, aerosol and fog water samples were

collected from two locations in the Central Valley, CA, which has some of the worst air quality in the U.S. Cloud water was also collected in Whistler, BC, a pristine environment, for a comparison. Samples were collected before, during, and after fog events to determine the effect of fog processing on trace metals in atmospheric aerosols. It was hypothesized that regional fog events substantially alter atmospheric trace metal concentrations in an urban environment.

Processing of atmospheric aerosols in rural and urban environments: soluble iron content

The type of particles that are emitted in rural and urban environments is substantially different. In order to further examine fog, cloud, and humidity processing of aerosols, one element, iron, was chosen to be studied. Iron solubility and speciation can be used as a tracer of fog, cloud, and humidity processing as well as an indicator of difference sources and processing by anthropogenic gases. The liquid water of clouds provides an aqueous medium for solubilization to occur and dissolved anthropogenic gases can decrease the pH of a cloud droplet which increases iron solubility. In this work, the soluble iron content of aerosol samples collected in a variety of locations was determined. It was hypothesized that samples with higher soluble iron content have undergone a greater degree of atmospheric processing.

Effect of particle size on iron solubility in atmospheric aerosols

Iron and its solubility are important on a global scale. In certain parts of the worlds' oceans there are enough nutrients, such as nitrates and phosphates, for phytoplankton to bloom, but do not. HNLC ocean regions are limited by iron, and more specifically, soluble iron. One of the main sources of iron to the open ocean is mineral

dust aerosols. Studies have found that the solubility of these mineral dust aerosols is low; therefore, it is important to understand what happens during atmospheric transport that may contribute to its solubilization. In this work, the role of particle size of mineral dust aerosols on iron solubility during atmospheric transport was examined. Clay and iron oxide minerals are commonly found in Saharan dust, which has a large input of dust into the open ocean, so they were chosen to be studied. The role of processing by clouds and marine aerosols was examined as well as the role of photochemistry. It was hypothesized that as particle size decreases, iron solubility will increase and iron speciation will change with the addition of photochemical reactions.

CHAPTER 2

CHARACTERIZATION OF HABOOB PARTICULATE MATTER IN TEMPE, AZ

Introduction

Haboobs, a special class of dust storms, can occur in many different regions (Sudan, Australia, Texas, etc.) and are particularly interesting because they occur suddenly and resuspend large quantities of dust. A haboob formation occurs when fast moving downdrafts from dissipating thunderstorms hit the ground and, in arid regions (e.g. Arizona), cause the resuspension of dust. In Arizona, these thunderstorms usually develop along the mountain range on the Cochise and Pima county border as well as southeast of Tucson around noon, and then travel slowly northwest towards Phoenix.

Although haboobs in Arizona are less frequent than in Sudan (approximately 2-3 haboobs per year as compared to 24 at Khartoum, Sudan), they can be just as dramatic. These turbulent air masses travel at approximately 30 mph, can be up to 60 miles wide and are an average of 4,000 – 8,000 feet in height. Dust storms can last from minutes to hours and have the potential to alter the aerosol content greatly on short time scales. Haboobs in Phoenix usually last around 30 minutes and causes an intense drop in temperature, pressure, with an increase in wind speed and relative humidity (Idso et al., 1972).

Although haboobs occur all over the world and can affect a large amount of people, especially in the southwestern United States, their chemical composition is not well studied. Several studies have examined the formation and structure of haboobs as well as changes in humidity, temperature, and air pressure that can happen during a haboob event (Lawson, 1971; Idso et al., 1972; Chen and Fryrear, 2002; Miller et al.,

2008). Particulate matter flux, concentration, and size distributions of haboobs have also been studied (Gillies et al., 1996; Chen and Fryrear, 2002), but much less is known about the composition of haboobs. Raman et al. (2014) published a study examining a 2011 haboob in Phoenix using satellite, radar, and ground based measurements. In this work, Raman and coworkers state that haboob occurrences in Arizona have been more extreme (PM_{10} > 48.5 μg m^{-3}) since 2007 and there has been an increasing trend of daily PM_{10} concentration during the summer months from 2001-2011 (according to IMPROVE network data). Of the very few studies examining composition, one study in Tempe, AZ collected dust that deposited on a roof as a proxy for haboob aerosol particles and used XRF to determine the mineral composition of the haboob (Pewe, 1981). The results indicated that 58-61% of haboob dust is SiO_2, 11-15% is Al_2O_3, 4-5% is Fe_2O_3, and 1-4% is $CaCO_3$. Studies have not actively collected *in situ* haboob dust storm samples or characterized the trace metals in haboobs. It is important to use active collection (actively drawing air through a filter) to collect aerosol haboob samples because not all particles settle at the same rate, and therefore only a fraction of what is present in the atmosphere will be collected using passive approaches such as dust on a roof (Pewe, 1981). Another disadvantage to passive sampling is low collection mass. Active samplers allow for shorter collection times with enough mass collected for a variety of analyses.

There are several studies that have studied the composition of Arizona soils and particulate matter (PM). Upadhyay et al. (2011) collected $PM_{2.5}$ samples during the winter in Phoenix and Tempe and found the average PM concentration to be 13.0 and 8.8μg m^{-3}, respectively (24-hr interval). $PM_{2.5}$ samples from these sites comprised of mainly (55 ± 9%) elemental carbon (EC), organic carbon (OC), and soil elements,

specifically Al, Fe, K, and Ca. From the 18 trace metals analyzed Al, Fe, K, Ca, and Mn contributed 99% to the trace metal PM composition (~16% of the total PM composition). South of Phoenix, where haboobs generally originate, in Pinal County, Upadhyay et al. (2015; in press) collected soil samples and resuspended them to simulate aerosols in the region. Resuspended native soil samples showed elevated concentrations of As and Sb, while soils adjacent to roads showed elevated concentrations of Cu, Sb, and Zn. High concentrations of organic carbon (OC) and PO_4^{3-} were found in samples collected from cattle feedlots in the area as well. These aerosol components have the ability to become entrained during haboob events. Using this information we could infer the influx of various metals during a haboob event, but *in situ* sampling is still be the most accurate way to determine the chemical composition.

Studying haboobs in the Phoenix area is important because these intense dust storms have the potential to affect the health of over 3 million people. In Arizona, it has been suggested that haboobs may bring in a large influx of the fungus, *Coccidioidomycosis*, which causes Valley Fever and affects 15-30% of the population (CDC reports). In this study, Valley Fever was not examined, but while a large fraction of the PM in a dust storm is greater than 2.5μm (mineral dust contribution), fine PM (< 2.5μm) can also be resuspended. Particulate matter that is 2.5μm or less can be harmful to human health because particles are small enough to be inhaled and retained in our lungs (Schwartz et al., 2002). Since these dust storms move through an urban area, it is possible that anthropogenic PM, which tends to be fine, can be resuspended during these dust storms. Metals and their speciation are especially important to consider in this fine fraction because of the formation of reactive oxygen species in the lungs which causes

inflammation and other health effects (Chapman et al., 1997; Prahalad et al., 1999; Karlsoon et al., 2005).

Haboobs can bring a large influx of non-native dust into an area, which may be the case in Phoenix. This has the possibility to impact soil composition, possibly influencing agriculture as soil nutrients could be imported by the storms. After haboob events there is one common and easily visual indication of a large influx of nutrients; algal blooms in pools. Although there have been no studies published on this, residents of the greater Phoenix area are very familiar with this phenomenon.

In this work, particulate matter (PM) samples were collected before, during and after haboob events on the Arizona State University Tempe Campus to determine the impact of haboobs on aerosol composition in the greater Phoenix area. Fine PM was a specific focus of this work because of their ability to stay resuspended for longer periods of time and their potential health effects. It was hypothesized that as a haboob passes through Phoenix, there will be a large influx of mineral dust, but also smaller, more processed, anthropogenic PM will be resuspended. In addition to a substantial change in aerosol composition during haboob events, it was hypothesized that the perturbation would last for several hours after the haboob has passed, especially for fine PM. PM samples were collected during the summers of 2013 and 2014 were analyzed for a variety of organic (alkanes, PAHs, etc.) and inorganic compounds. This work will focus on the trace metal composition of the aerosol samples.

Materials and Methods

Sample collection

The sampling site was located on the roof of the Life Sciences A-wing building (~50 feet high) on the Arizona State University Tempe Campus. Tempe is part of the greater Phoenix area of Arizona, which during the summer monsoon season experiences large dust storms, or haboobs, originating from the south. Sampling was conducted between July 2, 2013 and September 5, 2013 and between June 30, 2014 and September 8, 2014.

Haboob particulate matter was collected using Tisch High Volume Samplers (Tisch Environmental, Village of Cleves, OH; 1.13 m^3 min^{-1}). Samples were collected on cellulose filters (Whatman 41; GE Heathcare Life Sciences) and split into $PM_{2.5}$ and $PM_{>2.5}$ using $PM_{2.5}$ impactor plates (Tisch Environmental Inc., TE 231). Field blanks were taken before and after the sampling period. Ambient samples (before haboob) were collected at 24-hr intervals. During a haboob event, samples were collected for at least an hour to ensure enough particle (mass) loading for analysis. After a haboob event, samples were collected for at least 2 hour intervals to ensure enough particle (mass) loading for analysis; however, after haboob samples were variable in length overall. After PM collection, samples were stored in a freezer until analysis.

Trace metal analysis

Trace metal samples on cellulose filters were digested using a microwave assisted acid digestion (adapted from Upadhyay et al., 2009); in brief, a 5 x 5 cm section of filter was cut up and placed in a digestion vessel to which concentrated nitric (OmniTrace, EMD, Darmstadt, Germany, 70%) and hydrofluoric acid (EMD; 48%) was added and

digested (Mars 5 Microwave Digestion System, CEM Corporation, Matthews, NC). After digestion, samples were dried down then brought up in 2% nitric acid (OmniTrace, EMD) for analysis by a quadrupole inductively coupled plasma mass spectrometer (X-Series 2 ICP-MS; Thermo Electron). Samples were analyzed for 41 elements total. Reagent blanks, filter blanks, and standard reference materials (SRM2709 and SRM1649a) were treated in the same manner as samples.

Enrichment factors

Enrichment factors are used to examine the composition of a sample as compared to its natural abundance in the upper continental crust (Han et al., 2006; Majestic et al., 2009; Upadhyay et al., 2011) using the equation:

$$EF(X) = (X_{sample} / Al_{sample}) / (X_{crust} / Al_{crust}) \quad (1)$$

Where X is the metal of interest and "crust" is the concentration of the element in the upper continental crust (Rudnick and Gao, 2005). Al is used as the reference metal since it's naturally abundant and its concentration is relatively constant in the upper continental crust.

Principal component analysis

Principal component analysis (PCA) is a useful statistical tool to group samples by commonalities, which can then be used to help determine sources based on elements (Hopke et al., 1991; Upadhyay et al., 2011; Gonzalez-Maddux et al., 2014). In this statistical analysis, a large data set is reduced to principal components (PCs) and based on the correlation coefficient in that PC for an element, sources can be determined. The statistical packet used in this work was IBM SPSS (Version 22) to perform a varimax rotated PCA.

Results and Discussion

Particulate matter concentrations

During the 2013 and 2014 sampling periods, 51 and 70 $PM_{2.5}$ samples were collected, respectively. During the collection periods there were 7 and 3 haboob events in 2013 and 2014, respectively. Haboob samples were classified by their distinct frontal wall of dust. This is different from other dust storms, which are just blowing dust events with no characteristic "dust wall", as well as days with high PM, where wind is not typically a factor. High PM is described as days that exceed the national standards: 150 $\mu g\ m^{-3}$ and 12 $\mu g\ m^{-3}$ for PM_{10} and $PM_{2.5}$, respectively (24-hour average standard, EPA, 2012).

Table 2.1. Average PM_{10} and $PM_{2.5}$ concentrations ($\mu g\ m^{-3}$) in Tempe, AZ.

Average ($\mu g\ m^{-3}$)	**2013 (7/2 - 9/6)**	**2014 (6/30 - 9/9)**
Annual PM_{10}[1]	108	110
Annual $PM_{2.5}$[1]	12.1	12.6
Sampling Period PM_{10}[*]	26.7	34.4
Sampling Period $PM_{2.5}$[*]	7.2	6.3
Haboob PM_{10}[**]	246	842
Haboob $PM_{2.5}$[**]	17.7	48.5

[1]From EPA Air Quality Index Daily Values Report. All other data from Arizona Department of Environmental Quality.
[*]Excludes haboob events.
[**]Time period is not 24-hr standard. Average concentrations over 3-hr.

Table 2.1 shows the average concentrations of PM_{10} and $PM_{2.5}$ annually, during the sampling periods, and during collected haboob events in Tempe, AZ. On average, Tempe was below the national standards in 2013 and 2014 for PM_{10}, but slightly above the $PM_{2.5}$ standard. Additionally, Tempe had a record 133 days in exceedance of the national standards, 131 of which were determined to be "exceptional events" by the EPA

(Lee, 2014; The Arizona Republic). During the sampling periods, PM concentrations were relatively low, which is common for Phoenix as the wintertime typically has high PM due to inversion events. In 2013, the average concentrations of PM_{10} and $PM_{2.5}$ over a 3-hr period during haboob events were 246µg m^{-3} and 17.7µg m^{-3}, respectively; however, during a particularly large dust storm on August 20th, 2013, concentrations reached 1033µg m^{-3} and 85.9µg m^{-3} for PM_{10} and $PM_{2.5}$ over 1-hr, respectively. In 2014, there were fewer haboob events, but they were more intense as the average PM_{10} and $PM_{2.5}$ concentrations over a 3-hr period during haboob events were 842µg m^{-3} and 48.5µg m^{-3}, respectively. During two haboob events in 2014, July 25th and September 6th, PM_{10} concentrations over 1-hr reached 1500µg m^{-3}, and on September 6th $PM_{2.5}$ concentrations over 1-hr reached 109µg m^{-3}. When comparing ambient PM concentrations to elevated PM concentrations during a haboob in 2013, on average, PM_{10} and $PM_{2.5}$ increase by 232µg m^{-3} and 12µg m^{-3} over a 1-hr period, respectively. In 2014, the increase was more significant with PM_{10} and $PM_{2.5}$ increasing by an average of 979µg m^{-3} and 49µg m^{-3} over a 1-hr period, respectively. Raman et al. (2014) found that during a haboob on July 5th, 2011, concentrations of PM_{10} and $PM_{2.5}$ peaked at 1974 µg m^{-3} and 907 µg m^{-3}, respectively, which is much higher than the events shown here. The haboob described in the paper was a particularly large dust event and lasted slightly longer than most events.

Elemental concentrations

Table 2.2. Elemental concentrations (ng m^{-3}) in $PM_{2.5}$ samples collected in 2013.

	Tempe, AZ			Non-Haboob			Haboob		
Element	**Median**	**Min.**	**Max.**	**Median**	**Min.**	**Max.**	**Median**	**Min.**	**Max.**
Al	1596	319	21763	1424	319	3898	13178	5618	21763
As	0.543	0.124	3.41	0.501	0.124	1.00	2.61	1.33	3.41
Ba	24.0	6.08	198	21.7	6.08	56.1	109	51.5	198
Ca	1059	277	10514	994	277	2714	6845	3344	10514
Cd	0.072	0.003	0.397	0.066	0.003	0.194	0.191	0.105	0.397
Ce	2.09	0.45	26.1	1.88	0.45	4.61	15.2	6.74	26.1
Co	0.444	0.088	4.77	0.413	0.088	0.862	3.27	1.34	4.77
Cs	0.194	0.040	3.48	0.186	0.040	0.566	1.92	0.807	3.48
Cu	64.4	20.6	303	57.9	20.6	273	108	75.7	303
Dy	0.12	0.025	1.67	0.110	0.025	0.290	0.993	0.433	1.67
Er	0.071	0.015	0.972	0.065	0.015	0.171	0.584	0.252	0.972
Eu	0.040	0.008	0.479	0.037	0.008	0.091	0.290	0.131	0.479
Fe	968	190	10561	915	190	2108	7684	3191	10561
Ga	0.486	0.096	6.63	0.445	0.096	1.16	3.98	1.69	6.63
Gd	0.156	0.033	2.11	0.142	0.033	0.373	1.25	0.563	2.11
Hf	0.085	0.023	1.05	0.076	0.023	0.173	0.523	0.235	1.05
Ho	0.024	0.005	0.335	0.022	0.005	0.058	0.200	0.086	0.335
K	580	127	7448	542	127	1950	4682	1843	7448
La	1.04	0.222	13.0	0.939	0.222	2.34	7.84	3.52	13.0
Mg	448	121	5139	401	121	1084	3010	1486	5139
Mn	22.9	4.2	265	19.9	4.2	48.7	162	68.7	265
Mo	0.326	0	1.73	0.312	0	1.52	0.807	0	1.73
Na	551	128	3245	504	128	1305	1811	1013	3245
Nb	0.533	0.127	7.25	0.468	0.127	1.24	3.83	1.79	7.25
Nd	0.883	0.182	11.3	0.780	0.182	2.02	6.74	3.07	11.3
P	44	<DL	429	40.3	<DL	107	259	93.5	429
Pb	2.91	0.457	18.2	2.58	0.457	4.70	12.4	5.11	18.2
Pr	0.247	0.049	3.10	0.21	0.049	0.542	1.81	0.83	3.10
Rb	2.46	0.484	36.6	2.23	0.484	6.01	21.6	8.61	36.6
Sb	0.897	0.407	2.61	0.804	0.407	2.61	1.89	0.904	2.10
Se	0.853	0.194	5.85	0.801	0.194	3.64	4.27	1.81	5.85
Sm	0.171	0.034	2.22	0.149	0.034	0.394	1.34	0.600	2.22
Sn	0.651	0.228	2.49	0.619	0.228	1.58	1.75	0.813	2.49
Sr	9.20	2.76	86.2	8.66	2.76	23.5	51.3	26.4	86.2
Th	0.279	0.057	4.21	0.250	0.057	0.719	2.24	1.03	4.21
Ti	108	22.2	1347	98.4	22.2	233	712	330	1347
U	0.067	0.017	0.791	0.059	0.017	0.158	0.478	0.217	0.791
V	2.54	0.505	22.9	2.42	0.505	6.91	14.1	6.31	22.9
W	1.22	0.133	6.40	1.18	0.133	6.40	1.27	0.726	3.79
Zn	16.7	3.36	81.2	15.1	3.36	38.3	53.7	31.6	81.2
Zr	3.20	0.949	36.4	3.05	0.949	6.10	18.6	8.42	36.4

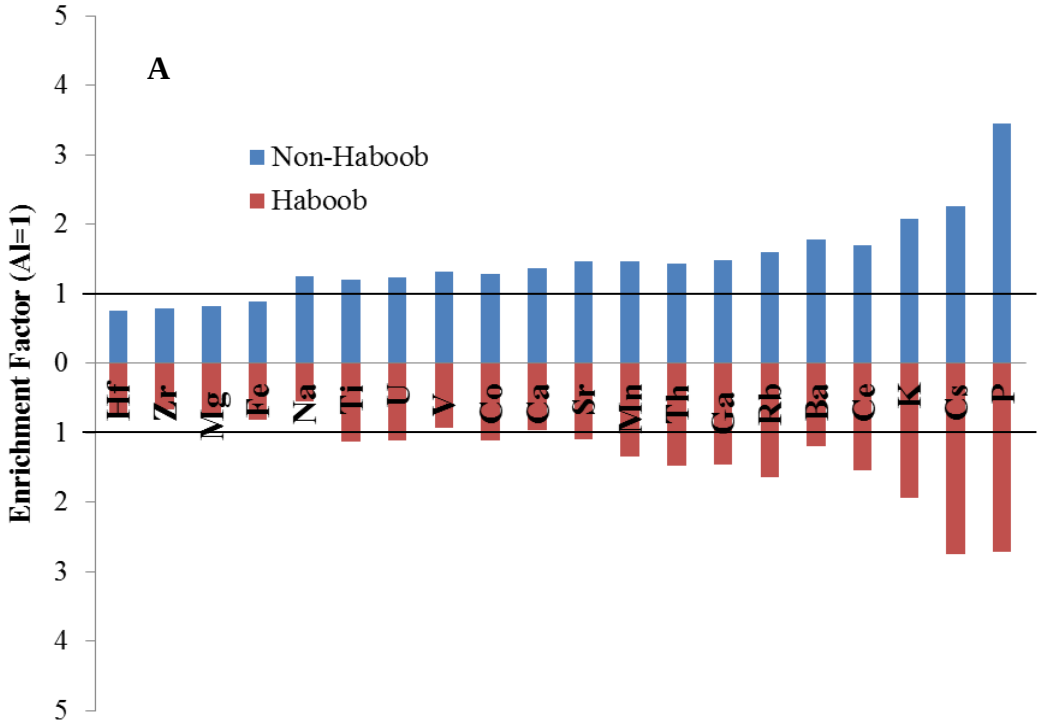
Table 2.3. Elemental concentrations (ng m^{-3}) in $PM_{2.5}$ samples collected in 2014.

	Tempe, AZ			Non-Haboob			Haboob		
Element	**Median**	**Min.**	**Max.**	**Median**	**Min.**	**Max.**	**Median**	**Min.**	**Max.**
Al	1269	55.0	123237	1249	55.0	7983	4012	2329	123237
As	0.35	0.007	9.53	0.35	0.007	2.21	1.23	0.30	9.53
Ba	15.8	2.95	926	15.7	2.95	71.0	60.0	21.5	926
Ca	1150	168	75323	1068	168	5648	4202	1514	75323
Cd	0.06	0.014	1.56	0.06	0.014	0.50	0.21	0.05	1.56
Ce	1.64	0.33	142	1.58	0.33	10.30	5.39	2.71	142
Co	0.32	0.04	24.1	0.32	0.04	1.63	1.20	0.50	24.1
Cs	0.16	0.03	17.5	0.15	0.03	1.30	0.52	0.32	17.5
Cu	105	39.1	438	104	39.1	313	417	116	438
Dy	0.099	0.017	9.63	0.097	0.017	0.66	0.33	0.18	9.63
Er	0.056	0.010	5.48	0.055	0.010	0.38	0.19	0.10	5.48
Eu	0.031	0.006	2.68	0.030	0.006	0.19	0.10	0.05	2.68
Fe	963	145	78337	944	145	5483	3606	1573	78337
Gd	0.20	0.04	19.0	0.20	0.04	1.34	0.68	0.34	19.0
Hf	0.06	0.01	5.85	0.06	0.01	0.33	0.27	0.11	5.85
Ho	0.02	0.00	1.93	0.02	0.00	0.13	0.07	0.04	1.93
K	521	100	44751	516	100	3389	1795	891	44751
La	0.82	0.15	69.6	0.78	0.15	5.04	2.61	1.37	69.6
Mg	397	67	30697	388	67	2301	1438	592	30697
Mn	19.7	2.58	1576	19.5	2.58	95.9	68.3	31.4	1576
Mo	0.37	0.07	6.25	0.37	0.07	1.35	1.38	0.32	6.25
Na	676	112	20154	668	112	1405	3368	603	20154
Nb	0.42	0.07	39.3	0.42	0.074	2.73	1.36	0.75	39.3
Nd	0.70	0.13	64.1	0.67	0.132	4.55	2.25	1.18	64.1
P	23	0.15	1651	22.4	0.15	119	91.1	29.7	1651
Pb	2.02	0.61	69.2	1.95	0.61	7.81	6.00	2.39	69.2
Rb	1.88	0.30	175	1.85	0.30	13.3	5.94	3.44	175
Se	0.37	0.15	5.61	0.37	0.15	1.47	1.41	0.41	5.61
Sm	0.14	0.03	13.0	0.14	0.03	0.91	0.44	0.24	13.0
Sr	7.08	1.18	620	6.96	1.18	37.6	25.6	10.2	620
Th	0.23	0.04	23.2	0.23	0.04	1.55	0.73	0.43	23.2
Ti	71.8	14.4	8732	69.3	14.4	485	241	134	8732
U	0.05	0.009	4.31	0.05	0.009	0.27	0.18	0.09	4.31
V	2.39	0.55	155	2.24	0.552	12.5	10.9	3.19	155
W	1.69	0.11	57.0	1.66	0.108	11.1	5.49	1.13	57.0
Zn	16.9	2.43	440	16.9	2.43	42.5	52.0	15.8	440
Zr	2.78	0.54	223	2.71	0.54	13.2	11.8	4.50	223

Tables 2.2 and 2.3 show the elemental concentrations in $PM_{2.5}$ samples collected in 2013 and 2014 in Tempe, AZ. Tables are split by average, maximum, and minimum

values for Tempe, AZ during the sampling period as well as non-haboob versus haboob samples. All elemental concentrations increased during haboob events, which is consistent with a short sampling period of extreme PM concentrations. When compared to $PM_{2.5}$ collected in Phoenix during the winter (Upadhyay et al., 2011), elements associated with natural sources (i.e. mineral dust) such as Al, Ca, Fe, Mg, etc. are higher in concentration. Elements associated with anthropogenic sources (As, Pb, Sb, etc.), however, were similar in concentration or lower in Tempe, AZ summer samples.

Enrichment factors



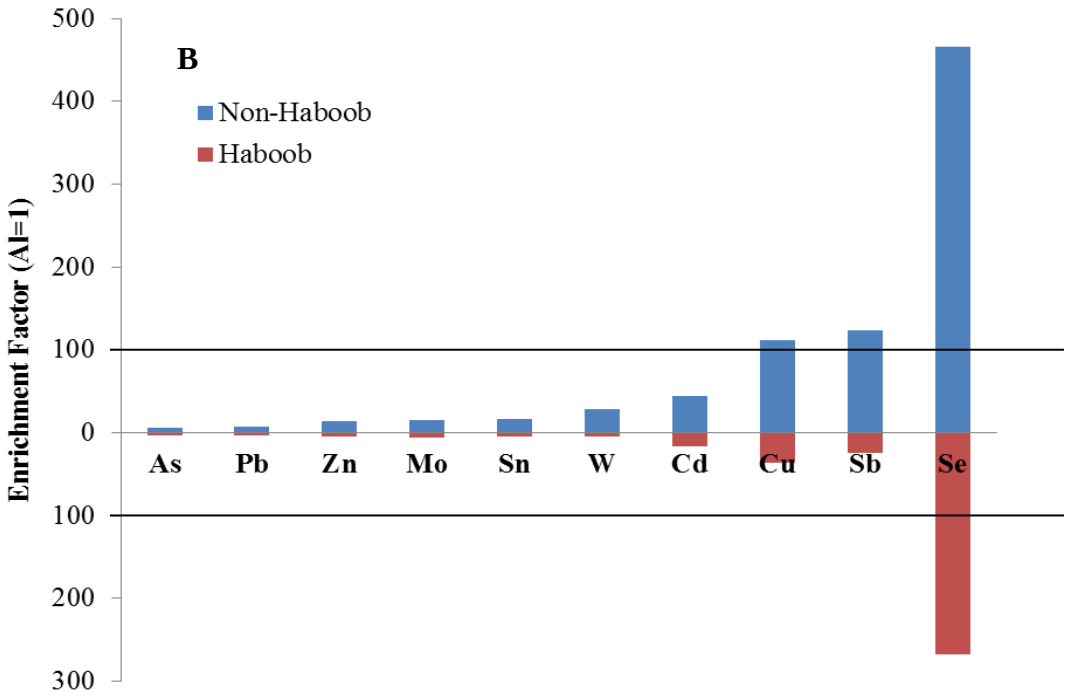
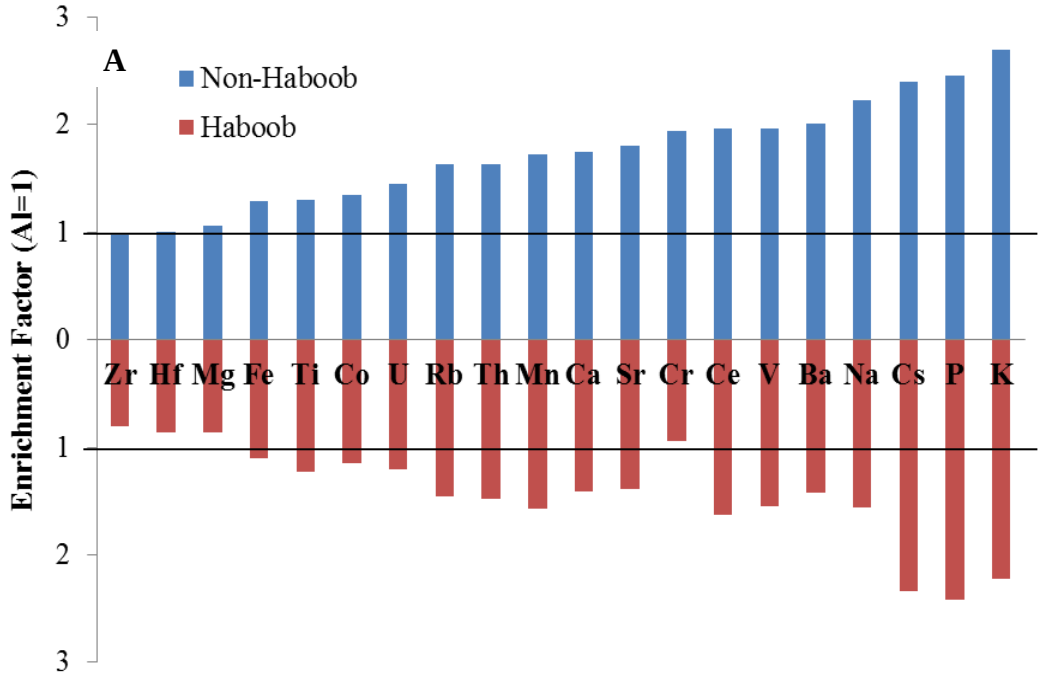


Figure 2.1. Average enrichment factors of $PM_{2.5}$ samples collected during non-haboob and haboob periods in 2013. Elements represented in A have enrichment factors less than 5 (black lines represent 1:1 X:Al, where X is element of interest), while elements represented in B have enrichment factors greater than 5 (black lines represent 100:1 X:Al). Enrichment factors of elements of interest are normalized to Al (i.e. Al=1).



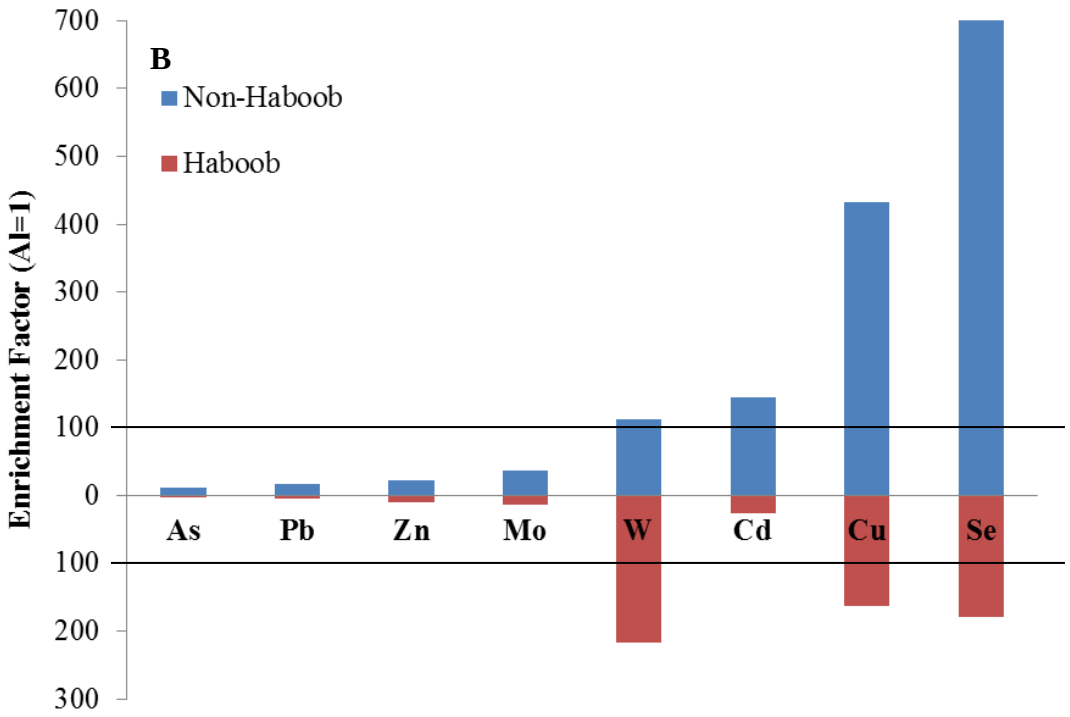


Figure 2.2. Average enrichment factors of $PM_{2.5}$ samples collected during non-haboob and haboob periods in 2014. Elements represented in A have enrichment factors less than 5 (black lines represent 1:1 X:Al, where X is element of interest), while elements represented in B have enrichment factors greater than 5 (black lines represent 100:1 X:Al). Enrichment factors of elements of interest are normalized to Al (i.e. Al=1).

The enrichment of elements compared to Al, a major trace metal in the upper continental crust, was determined for $PM_{2.5}$ samples collected in Tempe, AZ. Ten elements were found to be enriched (EF > 5) in $PM_{2.5}$ samples: As, Pb, Zn, Mo, Sn, W, Cd, Cu, Sb, and Se. Figure 2.1 shows these ten enriched elements and their enrichment in ambient and haboob samples in 2013. Figure 2.2 shows eight of these enriched elementas and their enrichment in ambient and haboob samples: As, Pb, Zn, Mo, W, Cd, Cu, and Se. Sb and Sn are missing from this list as they were not analyzed in the 2014 samples. The differences in enrichment factors of haboob versus non-haboob samples will be discussed later.

$PM_{2.5}$ samples collected in South Phoenix showed similar elements to be enriched as this study including As, Ba, Cr, Cu, K, Ni, Pb, Sb, Se, Sr, and Zn (Upadhyay et al., 2011). Differences in enrichment factors is likely due to differences in sampling season as south Phoenix samples were collected in the wintertime while these samples were collected in the summer. Source samples were collected in Pinal County, which is also the origin of haboob dust storms, and resuspended to simulate $PM_{2.5}$ and PM_{10} from these sources as part of another study by Upadhyay et al. (2015). Source samples were enriched in elements such as As, Ca, Cu, Ni, P, Pb, Sb and Zn, which is in good agreement with our findings. Upadhyay and coworkers noted that all the samples including the natural and agricultural samples were enriched in As and Sb, which they suggest is a local pollutant source and is from long range transport.

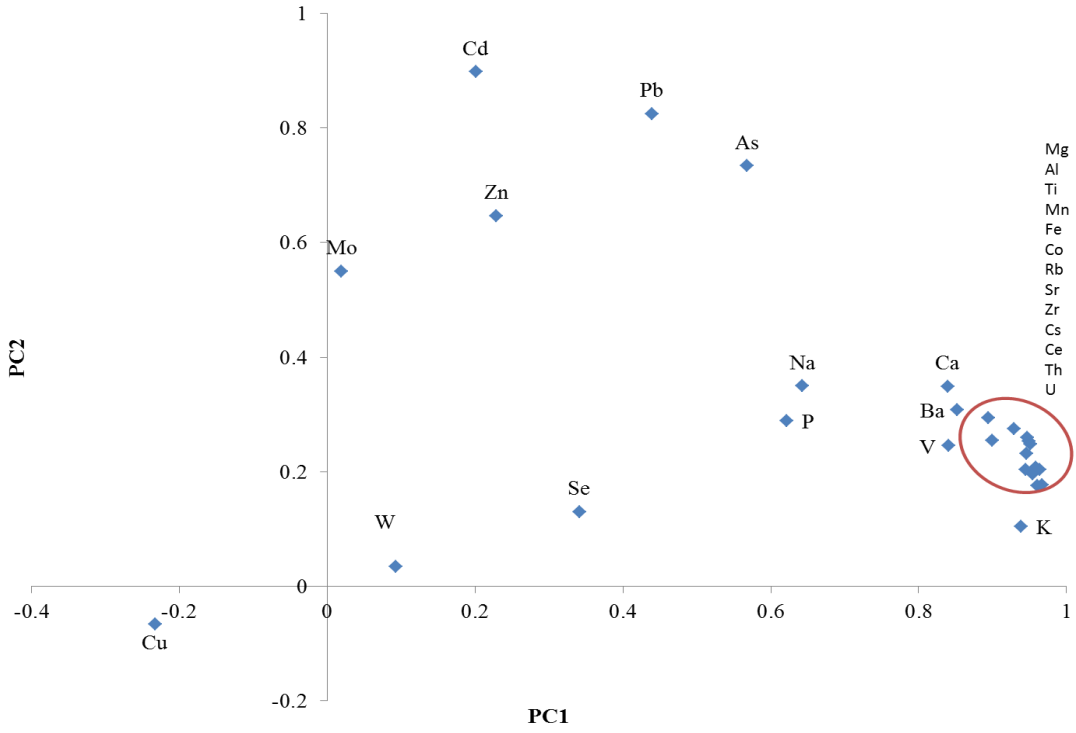


Figure 2.3. Principal components 1 (mineral dust) vs 2 (anthropogenic) from principal component analysis (PCA) of $PM_{2.5}$ samples collected during summer 2013 at ASU-Tempe Campus.

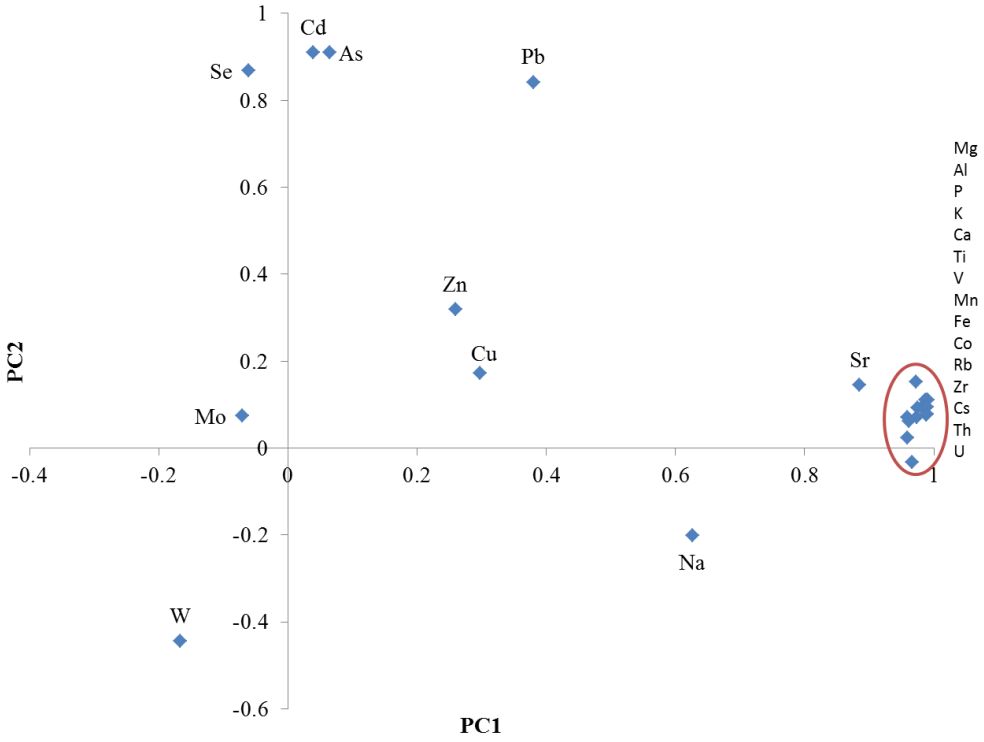


Figure 2.4. Principal components 1 (mineral dust) vs 2 (anthropogenic) from principal component analysis (PCA) of $PM_{2.5}$ samples collected during summer 2014 at ASU-Tempe Campus.

$PM_{2.5}$ samples from 2013 were analyzed (26 elements) by PCA (Figure 2.3). The first principal component (PC1) accounted for 60% of the total variance and was determined to be soil derived as it had strong influences from elements such as Al, Mg, Ca, Ti, etc. A high mineral dust contribution is consistent with low enrichment factors of these elements and with other studies who have examined soil compositions in the desert Southwest (Majestic et al., 2009; Upadhyay et al., 2011; Gonzalez-Maddux et al., 2014). The second (PC2), third (PC3), and fourth (PC4) principal components accounted for 15%, 7%, and 6% of the total variance. These components are likely derived from industrial sources such as coal combustion (Cu; Xu et al., 2004), vehicle emissions (Cd,

Mo, Cu, Pb, Zn; Solomon and Hopke, 2008), and possibly non-ferrous smelting processes (Cu, As, Pb; Ramadan et al., 2000).

$PM_{2.5}$ samples collected in 2014 were analyzed (26 elements) by PCA. 65% of the variance was accounted for by the first principal component (PC1), which was attributed to natural sources (i.e. mineral dust), similar to the samples from 2013. The second (PC2) and third (PC3) principal components accounted for 14% and 9% of the variance, respectively. Similar to samples collected in 2013, PC2 and PC3 were attributed to anthropogenic sources.

Upadhyay et al. (2011) performed PCA analysis on $PM_{2.5}$ samples collected in South Phoenix during the wintertime. In their study, PC1, which accounted for 55% of the variance, was dominated by combustion sources, while PC2, which accounted for 25% of the variance, was dominated by soil sources. During the wintertime in Phoenix, there is a large inversion layer that forms, which traps all the emissions in the area; air quality is Phoenix in the wintertime is particularly poor. Since the samples in this work were collected during the summer, PC1, which accounted for 60% and 65% of the total variance in 2013 and 2014, respectively, was attributed to soil sources due to the summer monsoon season.

Temporal duration and effect of haboobs

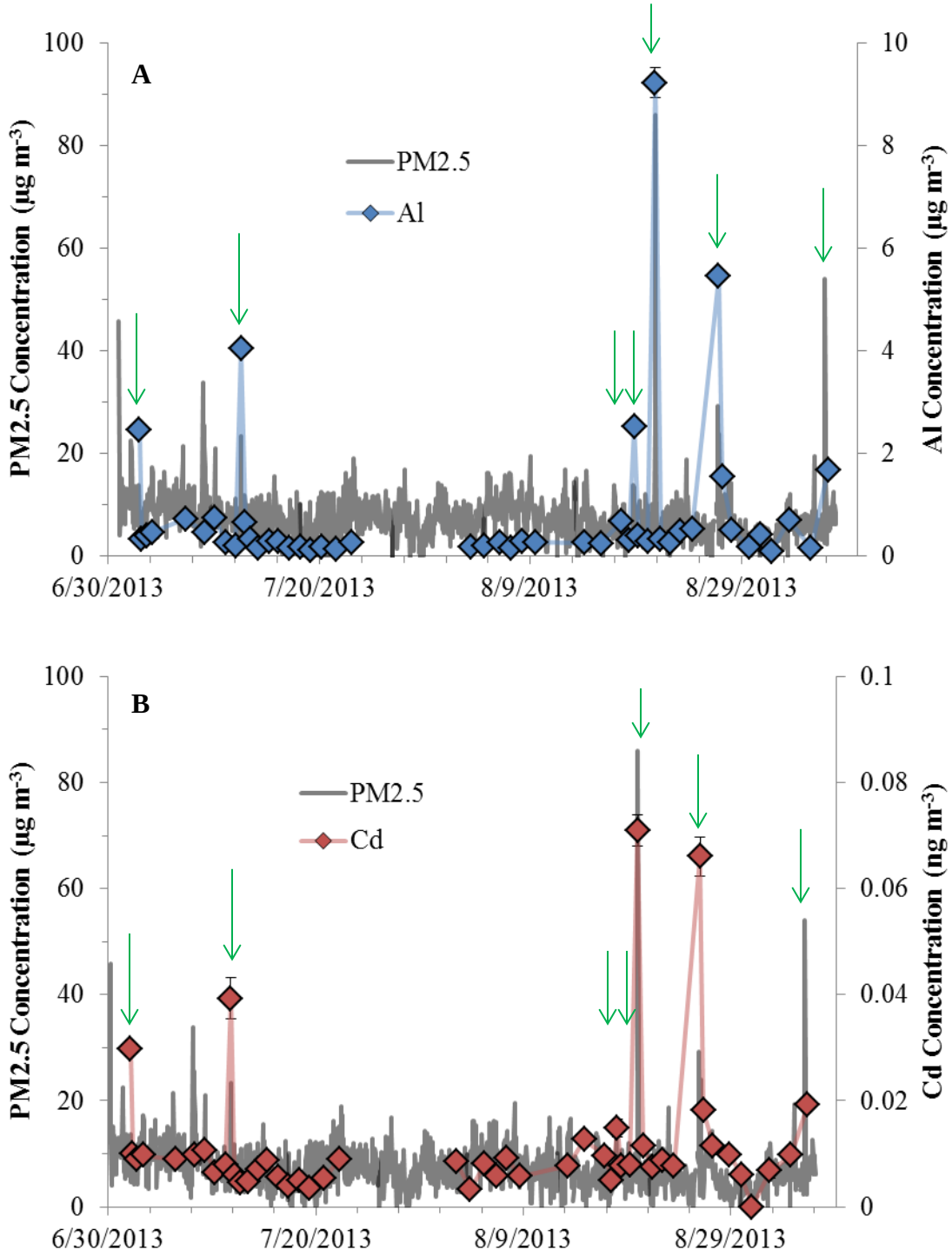
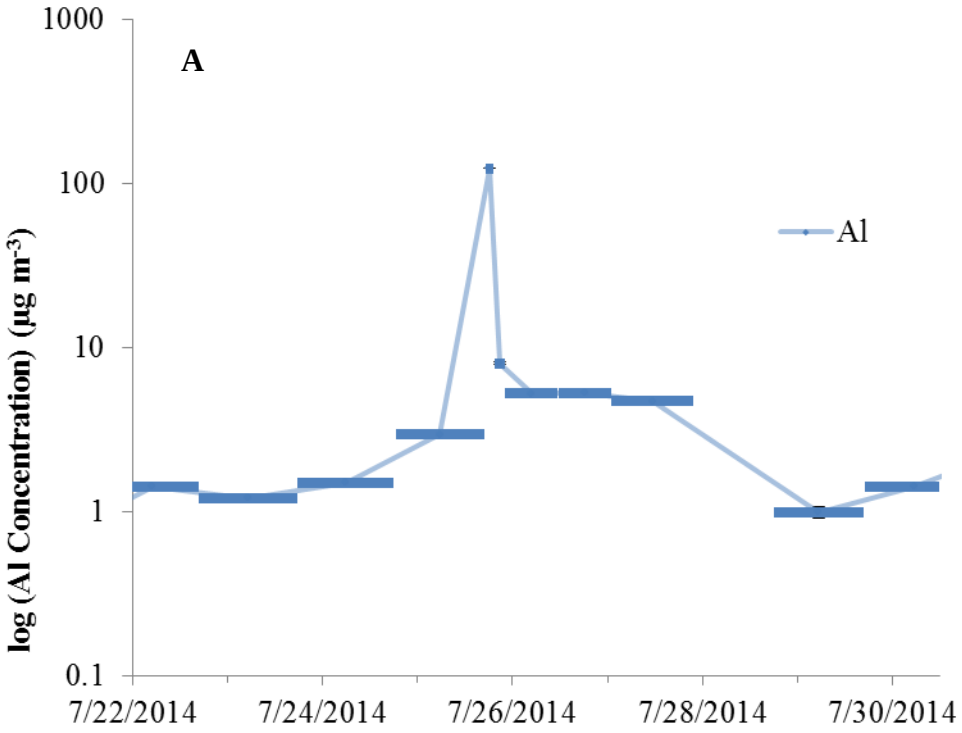


Figure 2.5. Particulate matter (PM) concentrations of Al (Blue; A) in µg m^{-3} and Cd (Red; B) in ng m^{-3} in aerosol samples collected during the summer of 2013 at ASU Tempe Campus. Arrows represent periods during which haboobs occurred. $PM_{2.5}$ (gray) concentrations are plotted on the primary y-axis (µg m^{-3}).

To study the temporal effect of haboobs, aerosol samples were collected before, during, and after haboob events. During haboob events, PM concentrations increase significantly for a very short period of time with PM_{10} increasing an order of magnitude more than $PM_{2.5}$. This is corroborated by the increased concentration of Al during haboob events, which is used as a tracer for mineral dust (Figure 2.5A). Cd can be used as an indicator of anthropogenic sources as Cd is not a naturally abundant trance metal. Aerosol samples collected during haboob events had elevated Cd concentrations (Figure 2.5B) suggesting a resuspension of anthropogenic PM from the greater Phoenix area.



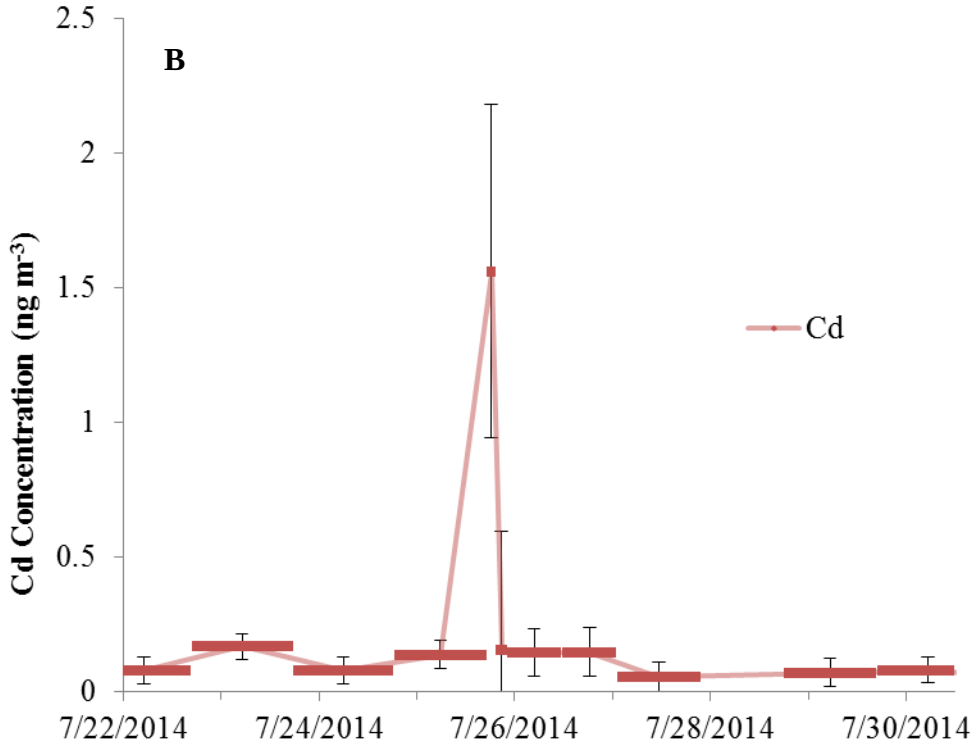
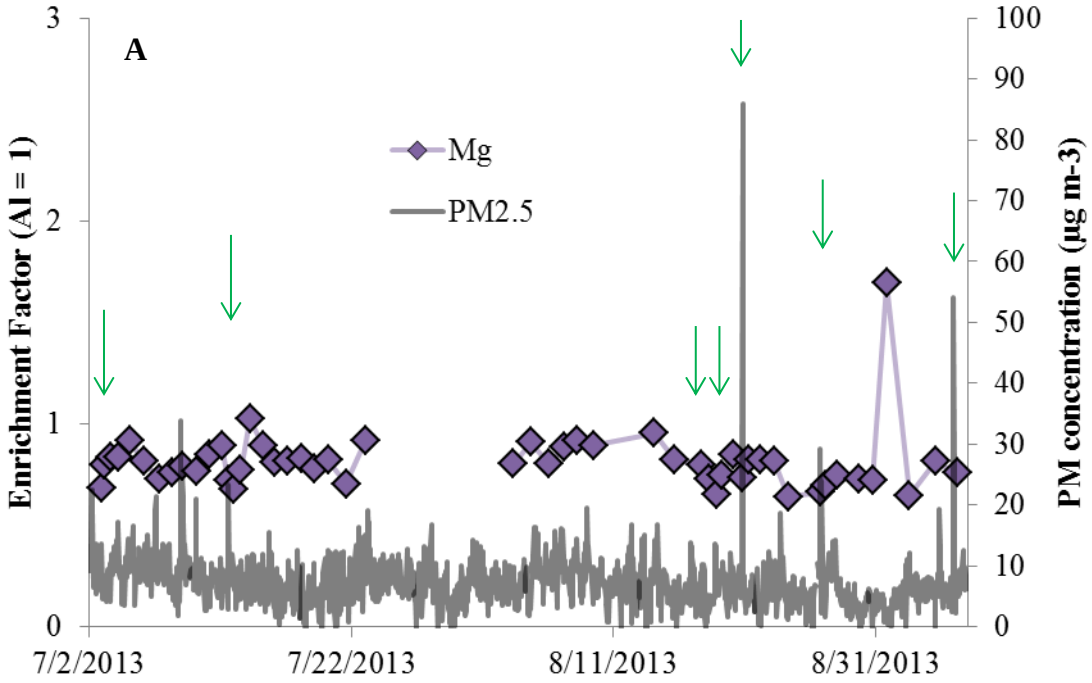


Figure 2.6. Al (Blue; A) and Cd (Red, B) concentrations in $PM_{2.5}$ samples collected during 2014 at the ASU Tempe Campus in µg and ng m^{-3}, respectively.

In 2014, PM samples were collected with better time resolution (i.e. shorter and more sampling periods after a haboob) to study if PM and elemental concentrations remain elevated after a haboob. PM, Al, Cd, and other metal concentrations decrease rapidly immediately after the haboob event. Haboob events bring a large influx of dust into the Phoenix area; however, all the dust does not remain in the region. Instead, the haboob moves through the region, which is why there is a significant decrease in PM concentration after the event is over. On July 25th, 2014 (Figure 2.6) it shows that after the haboob event PM decreases significantly, but does stay elevated for several days. This phenomenon can be observed with changes in Al concentrations before, during and after the haboob event. Ambient concentrations of Al are around 1 µg m^{-3}, during the haboob event the Al concentration increases to 123µg m^{-3}, and after the event

concentrations decrease rapidly to 7µg m^{-3} and remain around 5µg m^{-3} for the next 24 to 48 hours. This haboob event did not have any rain associated with it, which would alter the PM concentrations after the event, as rain/humidity has been known to scavenge atmospheric particles. Approximately 2 out of 3 haboob events are followed by rain (Idso, 1972).



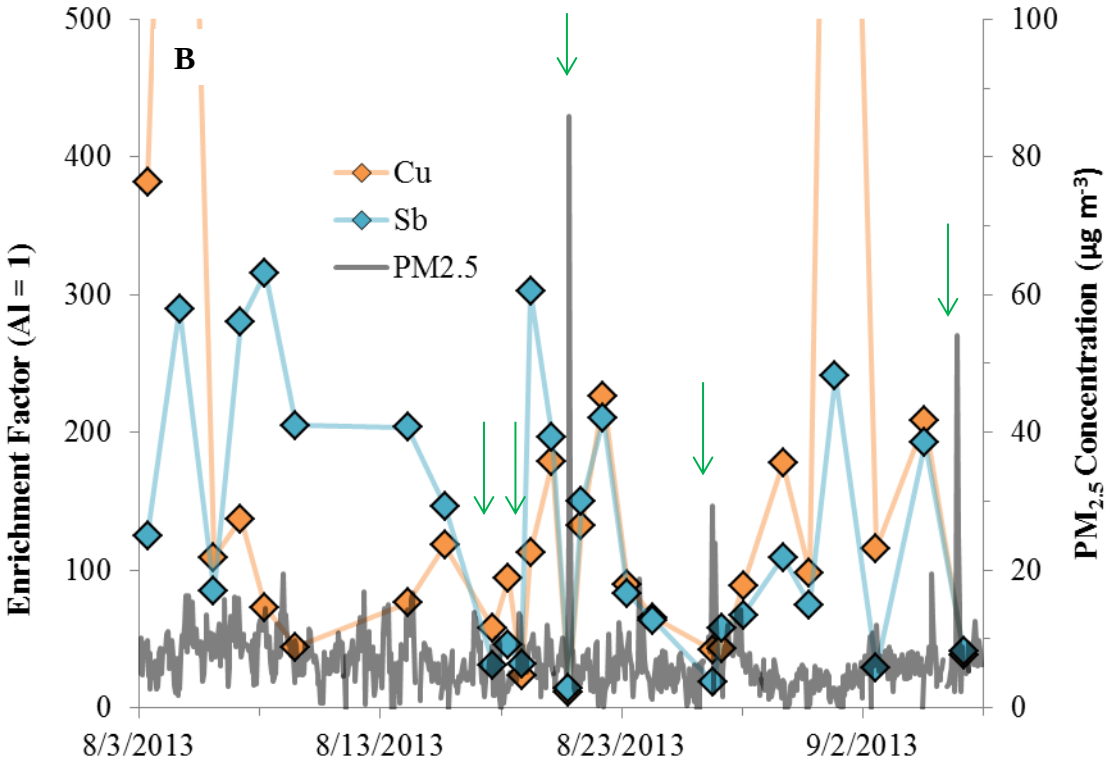


Figure 2.7. Enrichment factors (EF) of Mg (purple; A) and Cu and Sb (orange and teal; B) in $PM_{2.5}$ samples collected during the summer of 2013 at ASU Tempe Campus. Arrows represent periods during which haboobs occurred. $PM_{2.5}$ concentrations (grey) is plotted on the secondary y-axis.

Figure 2.7A shows the enrichment factor of Mg in haboob PM samples collected during 2013. The enrichment factors throughout the sampling period at approximately 1, which shows the Mg from the samples is similar in abundance as compared to the upper continental crust (i.e. natural sources). There is not a significant difference between haboob events and non-haboob events suggesting the influx of dust is mainly crustal in composition and/or the Mg is all associated with crustal material.

Enriched elements (EF > 10) in haboob particulate matter included Cd, Cu, Mo, Sb, Sn, W, Zn, and in some samples Pb. Enrichment factors of these anthropogenic elements decrease during haboob events as more PM and mineral dust is brought into the area. However, their enrichment factors return to previous values within approximately

24 hours after the haboob event as PM and mineral dust particles fall out of suspension (Ex. Cu and Sb; Figure 2.7B).

Conclusions

This work examined time resolved haboob particulate matter samples collected on the ASU Tempe Campus during the summers of 2013 and 2014. In particular, this work and other work done by the Herckes group at ASU sought to chemically characterize these haboob samples. In this work, trace metal composition of samples collected before, during, and after the haboob event was determined. In general, during haboob events PM increased significantly then rapidly decreased after the event. This trend was also seen with all trace metals, which increases 1-2 orders of magnitude during the haboob events. Enrichment factors of anthropogenic elements decreased significantly during haboob events as mineral dust floods the area effectively diluting the anthropogenic signal even though anthropogenic elements are also increasing during the events. Compounds examined in other work by members of the Herckes' group shows that organic carbon and polycyclic aromatic hydrocarbons (PAHs) increase during haboob events as well. Future work should include more time resolved samples, single particle characterization, and possible biological characterization to determine if the fungus that causes Valley Fever is more prevalent during haboob events.

CHAPTER 3

FOG PROCESSING OF TRACE METALS IN CALIFORNIA'S CENTRAL VALLEY

Introduction

Aerosols can enter the atmosphere as sea spray, mineral dust, and from anthropogenic sources. Once in the atmosphere, processing during short and long range transport can alter the chemical speciation of the aerosols, which can have various effects on human health, climate, and the biosphere. An important atmospheric transformation process is atmospheric aqueous phase processing by fogs and clouds. First, incorporation of particulate metals into fogs and clouds will enhance their removal probability through precipitation (clouds) or droplet sedimentation and impaction (fogs) processes. Therefore incorporation into fog and clouds or scavenging by fogs and clouds has a substantial impact on the lifetimes of atmospheric compounds, including metals. Second, scavenging into the aqueous phase will allow PM to undergo aqueous phase chemistry, which provides ample opportunities for particles to undergo solubilization, photochemical, and redox and other reaction processes. Finally, only a small number of cloud/fog droplets end up precipitating (Warneck, 1994) and hence most aerosol particles can undergo several aerosol/cloud/aerosol processes during their transport and atmospheric lifetime.

Numerous studies exist on fog and cloud composition in terms of acidity and major ions (Hoag et al., 1999; Collett et al., 2008; Wang et al., 2011), while fewer studies focus on organic matter in the atmospheric aqueous phase (Herckes et al., 2013 and references therein), and even less on trace metals (Fuzzi et al., 1984; Hallberg et al., 1992; Gordon et al., 1994; Straub et al., 2012). The latter is likely the result of the experimental challenges in such measurements which, in some parts, only recently were

overcome with the use of aerosol mass spectrometers (Girardoni et al., 2014). Most observational studies on metals are limited to metals of interest to sulfur oxidation such as Mn and Fe (Hegg and Hobbs, 1978; Brandt and van Eldik, 1995; Seifert et al., 1998). In addition, there are several studies that investigated, in detail, iron and iron speciation because of the indirect effect on global climate (ocean primary productivity; Chapter 5) (Kumar et al., 2010; Chuang et al., 2005; Journet et al., 2008). Very few studies included trace metals in clouds and are often from a deposition perspective and enhancement of deposition fluxes by direct fog deposition (e.g. Klemm and Wrzesinsky, 2007). Finally, several studies aiming at fog and cloud water collection for agricultural or domestic use also included metals as to assess the water quality of fog and cloud water (Schemenauer and Cereceda, 1992).

Studying the cloud and fog processing of aerosols is of importance when examining the fate of these aerosols species. Radiation fogs, prevalent during the wintertime in the Central Valley of California, form when high pressure systems force marine air to remain in a region, especially regions surrounded by mountain ranges. These fog episodes can last on a timescale of hours to days (longest fog episode between 1954 and 1980 was 13 days; Holets and Swanson, 1981). Since fogs are comprised of water droplets (size ranges between 0.4μm to tens of microns) (Pruppacher and Klett, 1980), and can last for extended periods of time, this can lead to aqueous phase reactions as well as deposition of aerosol particles.

The Central Valley of California has been one of the most studied areas in regards to fog chemistry. Studies have included fog processing of organic matter (Herckes et al., 2007a, Collett et al., 2008, Mazzoleni et al., 2010, Ervens et al., 2013, Wang et al., 2013),

polycyclic aromatic hydrocarbons (Ehrenhauser et al., 2012), and major inorganic ions (Herckes et al., 2007b, Collett et al., 1999a) as well as sulfur oxidation (Collett et al., 1999a and b, Hoag et al., 1999) and hydroxyl radical chemistry (Anastasio and McGregor, 2001) among many other studies (McGregor and Anastasio, 2001, Zhang and Anastasio, 2001, Ge et al., 2012, Moore et al., 2012). There is however limited data from this region on trace elements in the aerosols and fogs (Munger et al., 1983, Siefert et al., 1998).

Trace elements and their processing by fogs in this region are of importance because of the aqueous phase reactions that can occur solubilizing harmful metals making them more easily uptaken in biological systems. In this study, select trace metals in fog water and aerosol ($PM_{2.5}$) samples collected during two sampling campaigns in the Central Valley of California, Fresno and Davis, between 2010 and 2011 are examined. Cloud water samples were also collected in Whistler, BC in 2010 to compare to fog trace metal composition in the Central Valley. Aerosol samples in Davis and Fresno were collected before, during, and after fog events to determine the effect of fog processing/scavenging efficiency on atmospheric aerosols.

Materials and Methods

Fog and aerosol samples were collected during January 2010 in Fresno, CA and January 2011 in Davis, CA and cloud water samples were collected in Whistler, BC in 2010. The experimental set-ups, local conditions and additional chemical results are described in detail elsewhere (Ehrenhauser et al., 2012; Wang et al., 2013).

Sample Collection

Fog water samples were collected using Caltech Active Strand Cloud Collectors (CASCC) (Demoz et al., 1996). In Davis and Fresno, fog collection was triggered automatically based on liquid water content (typically LWC > 60mg/m^3) as measured by a CSU optical fog detector (Carillo et al., 2008). In Whistler, cloud collection was triggered by LWC measurements using a particulate volume monitor PVM 100. Samples for metal analysis were collected in pre-cleaned HDPE bottles, filtered with 0.45µm glass fiber filters (GFF, Whatman, GE Healthcare Life Sciences) and acidified with nitric acid (OmniTrace, EMD, Darmstadt, Germany; 70%) in the field and then refrigerated until analysis.

High-volume air samplers (Tisch Environmental, Village of Cleves, OH; flow rate 1.13 m^3 min^{-1}) equipped with a $PM_{2.5}$ impactor stage (Tisch-Environmental Inc., TE 231) were used to collect fine ($PM_{2.5}$ or particles with an aerodynamic diameter smaller than 2.5 µm) and large ($PM_{>2.5}$ or particles with an aerodynamic diameter larger than 2.5 µm) particles. Particulate matter samples were collected on quartz fiber (QFF, Whatman QM-A, GE Healthcare Life Sciences) and cellulose (CL, Whatman 41, GE Healthcare Life Sciences) filters. Cellulose filters were pre-cleaned in a 0.5% hydrochloric acid bath and quartz fiber filters were pre-fired overnight at 650°C.

Trace metal analysis

In the laboratory, fog and cloud water samples were diluted with 1% nitric acid and spiked with an indium internal standard for analysis using a double focusing magnetic sector inductively coupled plasma mass spectrometer (ICP-MS, ThermoFinnigan ELEMENT 2). Aerosol samples were digested and prepared similarly

to previous methods outlined in Upadhyay et al. (2008). Briefly, samples were digested with 10mL nitric acid (OmniTrace, EMD; 70%), 4mL deionized water (18.2MΩ), and 1mL hydrofluoric acid (EMD; 36%) in 22mL Teflon bombs using a Mars 5 Microwave Digestion System (CEM Corporation, Matthews, NC). Included in each digestion batch were standard reference materials (SRM 2709 and 1649a), a reagent blank, and a filter blank. Standard reference materials, which are samples of known composition, were used to check the digestion procedure. Reagent and filter blanks were analyzed to subtract their trace metal contribution from the ambient aerosol samples. Samples were then dried down to 1mL and brought up in 1% nitric acid and spiked with an indium internal standard for ICP-MS analysis for Fresno and Davis aerosols.

Scavenging Efficiency

Scavenging efficiencies for Fresno and Davis were calculated similarly to previous studies (Collett et al., 2008) using the equation:

$$\text{Scavenging Efficiency} = 1 - (X_{interstitial}/X_{pre}) \quad (1)$$

Where X is the concentration of the element in the aerosol sample (in ng m^{-3}), "interstitial" refers to the aerosol sample collected during the fog and "pre" is the aerosol sample collected before the fog event.

Results and discussion

Metal concentrations in fog and cloud water samples

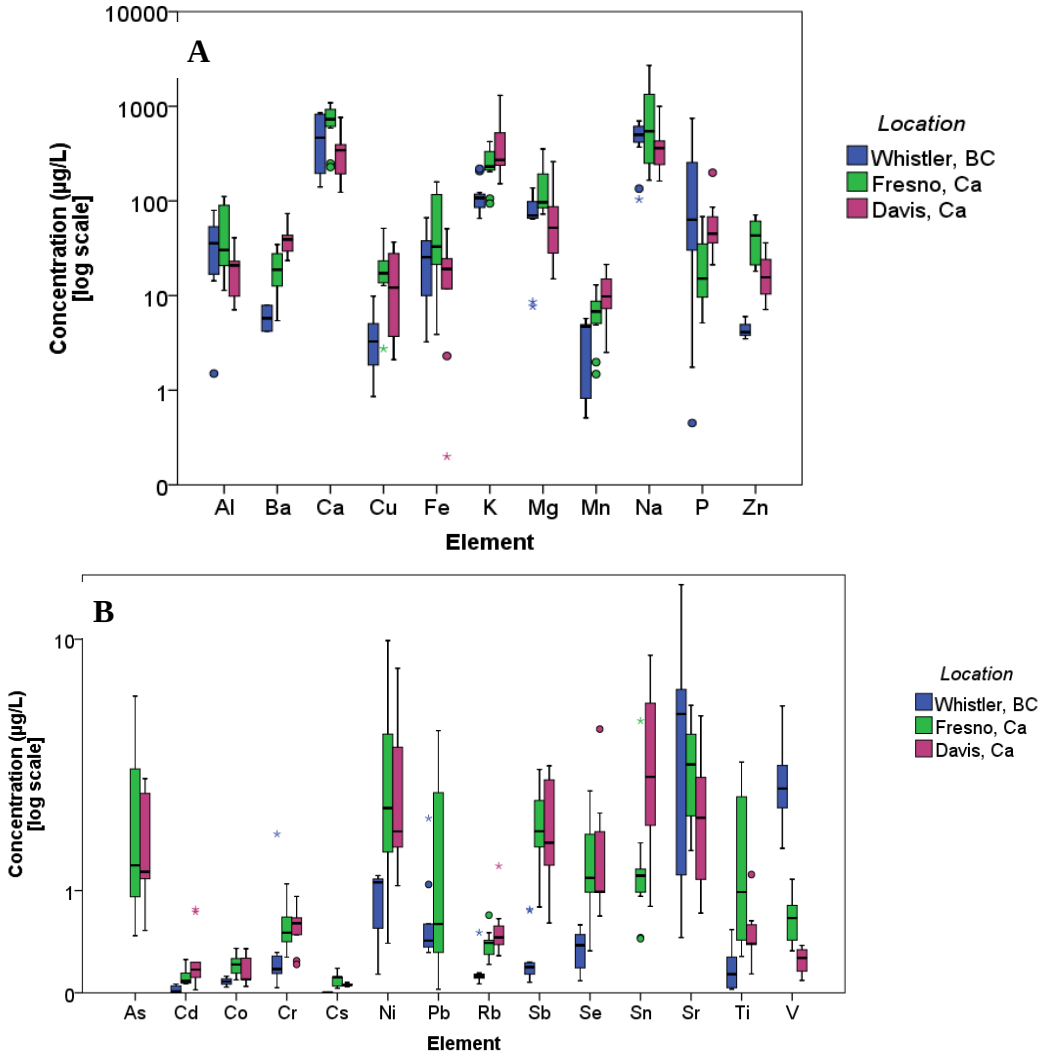


Figure 3.1. Box and whisker plots for major (A) and minor (B) element concentrations in fog and cloud water collected in Whistler, BC (Blue), Fresno, CA (Green) and Davis, CA (Purple). The black line represents the median, whiskers represent range, the top and bottom of the boxes indicate the 75th and 25th percentile, respectively, circles represent outliers and asterisks represent extreme outliners.

Figure 3.1 shows metal concentrations in fog samples collected in Fresno, CA and Davis, CA as well as cloud samples from Whistler, BC for comparison purposes. Metal concentrations overall were consistent with the local environment. In general, Whistler presented the lowest trace metal concentrations, consistent with the more pristine

location, while Fresno presented highest concentrations, consistent with the polluted nature of the location. There was a substantial inter- and intra-event variability at each site, which might be driven by changes in liquid water content (LWC) and changes in local atmospheric composition. In fact, increased LWC may lead to more dilute metal concentrations in fog/cloud water samples. This has been shown for ions in previous studies (e.g. Elbert et al., 2000; Aleksic and Dukett, 2010, Straub et al., 2012). The range of concentrations for most metals even at a given site is substantial, up to one order of magnitude and more (Figure 3.1). Higher, and largely variable, concentrations in P in Whistler may be due to the location of the sampling sites, which were midway up the mountain and at the peak. The midpoint was located in a forest which is likely the source of higher P concentrations from biological material in the summer. Wang et al. (2013) also showed the presence of biological macromolecular material at this site in Whistler. Sr was another element that showed higher, and largely variable, concentrations in Whistler. Elevated Sr concentrations may be linked to a mineral dust or marine contribution; although, more investigation is needed.

Table 3.1. Select metal concentrations in fog and cloud studies around the world, past and present

Site (μg L^{-1})	Fe	Mn	Pb	Cu	Ni	Reference
Fresno, CA 2010	62 (3.9-159)	6.7 (1.5-13)	1.4 (<0.3-4.9)	16 (<0.1-51)	3.6 (0.4-9.9)	this work
Davis, CA 2011	20 (0.2-51)	11 (2.5-21)	<0.003 (<0.003-0.6)	14 (<0.01-37)	3.4 (1.1-8.0)	this work
Whistler, BC 2010	29 (3.2-66)	3.6 (<0.1-5.7)	0.7 (<0.1-2.3)	3.9 (<0.1-9.9)	0.8 (<0.1-1.2)	unpublished
Norway 2011	53 (1.0-211)	10 (1.1-37)	0.3 (0.2-0.3)	9.1 (5.5-14)	49 (5.3-130)	Wang et al., 2015
Pennsylvania	34 (26.3-99)	4.4 (3.2-14)		0.6 (0.4-2.3)	2.4 (1.9-8.5)	Straub et al., 2012
IMS95 (Bakersfield/Kern and Fresno)	339 (16-886)	12.7 (1.6-118)				Hoag et al., 1999
Oildale/Bakersfield 1982	240-6400	97-800	241-366	45-401	124-586	Munger et al., 1983

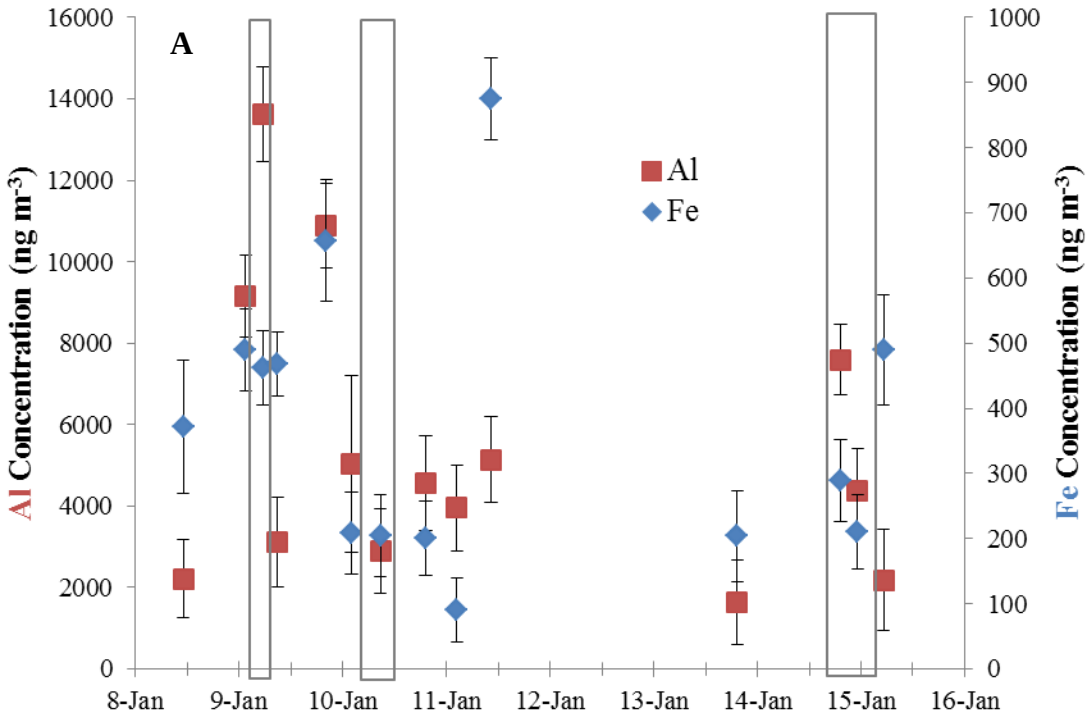
Table 3.1 shows the concentrations of select metals in our study with other fog and cloud studies as well as earlier studies in the Central Valley. The concentrations of trace metals in the Central Valley have overall decreased since fog samples were collected in Oildale in 1982. In addition, trace metal concentrations continued to decrease from fog samples collected in the 1990's in Bakersfield and Fresno. These decreases will be discussed further in regards to trace metals concentration in $PM_{2.5}$ found in this study compared to other studies in the Central Valley.

While more studies exist on metal concentrations in fogs and clouds, it is important to note that here we compare against temporally similar studies at other sites. A reason is that fog composition tends to reflect local air quality and substantial changes over time might occur as a result of policy changes and be directly reflected in fog composition. This has been shown for fog and cloud acidity, ions and organic matter in various locations as well as in the Central Valley (e.g. Herckes et al., 2002; Aikawa et al., 2007; Blas et al, 2008; Aleksic et al., 2009; Gioda et al., 2013; Herckes et al., 2015). For metals, time series samples are less frequently included in observational studies.

The fog water data can also be compared to earlier studies in the Central Valley. In Frenso, there are studies as far back as 1995 that included metal concentrations (Hoag et al., 1995), while other locations, like Oildale (Bakersfield area), there are data that goes back all the way to the early 1980s (Munger et al., 1982). Overall, metal concentrations in fog water collected from Fresno and Davis, CA between 2010 and 2011 were much lower than reported concentrations from Munger and coworkers suggesting that air quality has significantly improved over the past 30 years. Improvements in air quality are largely due to the Clean Air Act implemented in 1963, with major reforms in

the late 1970's which required the federal and state governments to make regulations on industrial and mobile pollution sources. Notably, Pb has decreased in fog water concentrations by 3-5 orders of magnitude over the past 30 years. This is consistent with the phasing out of leaded gasoline. Similar observations on a shorter time scale (10 years) were seen by Herckes et al. (2002) in Strasbourg (France), where Pb concentrations in fog had decreased by more than an order of magnitude between 1990 and 1999 following the phasing out of leaded gasoline. These changes over time are even more impressive as in our recent work, looking at 30 years of fog chemistry data in the Central Valley (but not metal concentrations), it was shown that there was a significant decrease in liquid water content (Herckes et al.,2015).

Metal processing by fogs events



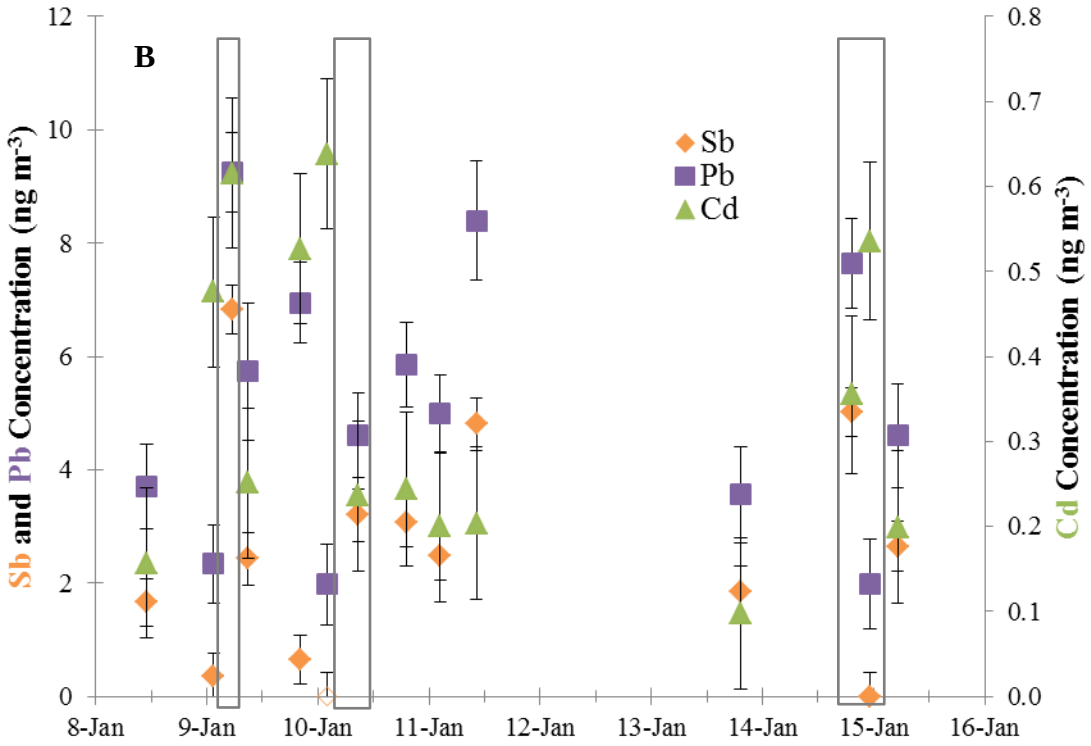
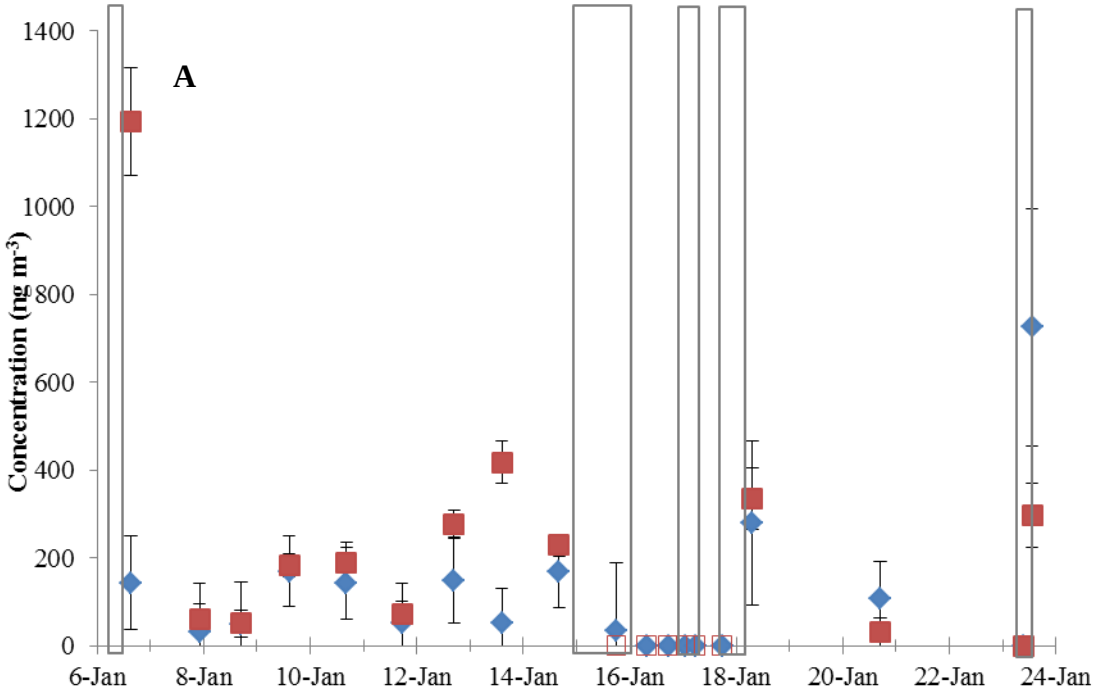


Figure 3.2. $PM_{2.5}$ concentrations of Al and Fe (**A**) and Sb, Pb, and Cd (**B**) (ng m^{-3}) from Fresno, CA. Grey bars represent periods of fog.



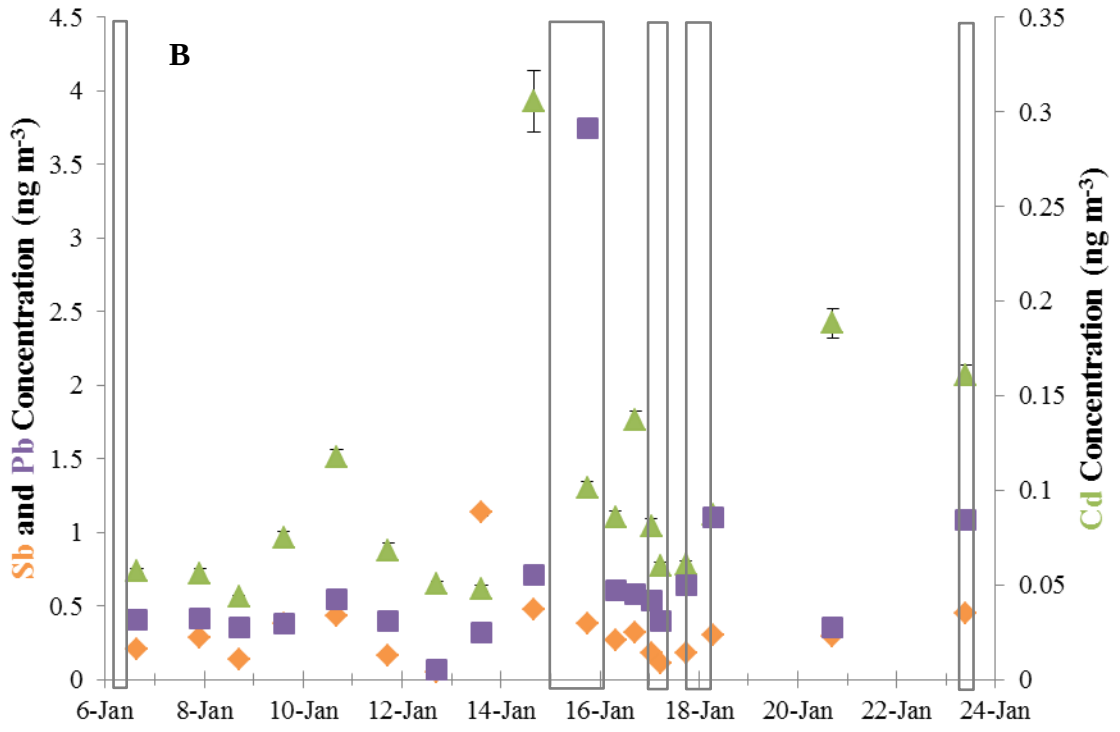


Figure 3.3. $PM_{2.5}$ concentrations of Al and Fe (**A**) and Sb, Pb, and Cd (**B**) (ng m^{-3}) from Davis, CA. Grey bars represent periods of fog.

Figure 3.2 shows $PM_{2.5}$ concentrations of select metals in Fresno, CA. No statistically significant differences were observed between pre-, post- or interstitial ($PM_{2.5}$ collected during a fog event in grey bars). Figure 3.2A shows Fe and Al concentration timelines in $PM_{2.5}$ samples from Fresno. These elements are generally representative of natural contributions (i.e. from mineral dust); although, it is possible that anthropogenic sources may also contribute to these metal concentrations (Majestic et al., 2009). Figure 3.2B shows Sb, Pb, and Cd concentrations in $PM_{2.5}$ samples from Fresno, which is meant to act as a proxy for anthropogenic sources as Sb, Pb, and Cd have very low concentrations in natural samples.

In Fresno, Fe and Al concentrations in $PM_{2.5}$ samples are approximately 2 and 10 times greater, respectively, than in Davis (Figures 3.2A and 3.3A, respectively). During

fog events in Davis, Al and Fe concentrations decrease significantly while during fog events in Fresno, Al and Fe concentrations decrease very little. There are different explanations for a difference in scavenging.

The scavenging of aerosol particles depends on their size, their hygroscopicity and the humidity (degree of supersaturation). The supersaturation was not observed in our case, but one indicative parameter could be liquid water content which was higher in Fresno as compared to Davis. This is opposite of what we would expect based on the scavenging of trace metals in Davis (i.e. expected Davis to have higher LWC than Fresno). A lower LWC results in higher solubility and larger particles being scavenged first, while smaller and less soluble particles would be scavenged later. Additionally, lower LWC suggests a larger abundance of secondary inorganic particles that are highly hygroscopic and hence grow faster into fog droplets, preventing the activation of larger amounts of mineral dust particles that tend to be less soluble, while at the same time limiting the range towards small particles on what will be activated. The latter could mean that the interstitial aerosol tends to be enriched in the smallest particles (less than 200nm, might not get activated into fog droplets; Gilardoni et al., 2014). Measurements of particle size distributions containing Fe in Bakersfield in the wintertime 2000 - 2001, showed a pseudo-Gaussian distribution with a peak at 0.4μm (Ham et al., 2010). Also, Cahill et al. (2011) shows that (non-soil) iron is found in very fine (0.09 to 0.26 μm) and ultrafine (<0.09 μm) aerosols in Fresno and Bakersfield. The concentration of very fine particles in Fresno and Bakersfield were 2 and 15 times greater, respectively, than in Sacramento, which is 14 miles from Davis. Since ideal activation sizes for particles to become CCN usually falls about > 0.5μm, this leaves particles less than this suspended

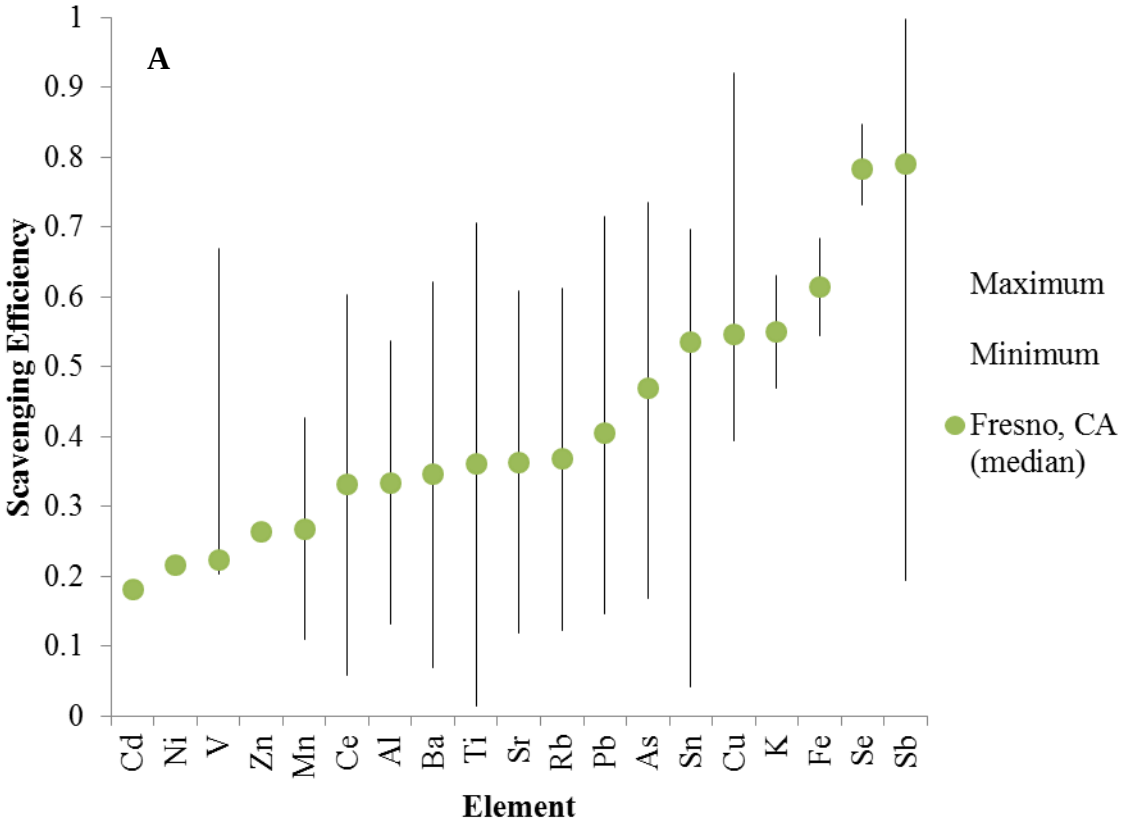
even during fog events, which may be the case in Fresno. Mineral dust particles, as may be more prevalent in Davis, can span across a large size range (< 0.1 to > 10µm), but the majority of particles fall within the 0.5 - 2µm (Tegan and Lacis, 1996), which is in the ideal activation range. Unfortunately, in this work, no simultaneous measurements of particles sizes were available.

An additional consideration, and possible interpretation of this data, is that aged particles tend to become more hygroscopic after processing. In an area like Davis, where there are less fresh emissions, aerosols might be overall more hygroscopic. On the other hand, if there are consecutive fog events (as in Davis on January 15 - 18th), a first fog event can scavenge and deposit the most hygroscopic particles resulting in a less scavenging of those particles in the follow-up event.

In some instances, a higher concentration in interstitial aerosol compared to pre-fog aerosol illustrates the impact of physical processes including horizontal air mass movements, entrainment of air masses from above the fog into the fog layer and local emissions. As a result, rather than just seeing a decrease in concentrations as expected in a closed system, where particles can only go into the fog phase (as shown in models and some observations; Fahey et al., 2005), the concentrations occasionally increase, which is clear evidence of entrainment/advection/emissions. The latter is a challenge in our measurement approach, where long integration times are needed to collect sufficient aerosol for offline analysis, increasing the likelihood of these phenomena, besides the challenge to "time" perfectly the onset and dissipation of the fog. A novel approach is the use of aerosol mass spectrometry (AMS) in such studies. In recent years, AMS was successfully used to study organics and ionic species (Ge et al., 2012; Gilardoni et al.,

2014), but not yet on Fe and other trace metal. Therefore, the offline methods, while prone to artifacts, are our best available tools. To capture all fog events in our studies, we proceeded to calculate scavenging efficiencies.

Observed trace metals scavenging efficiencies for Davis and Fresno fog events



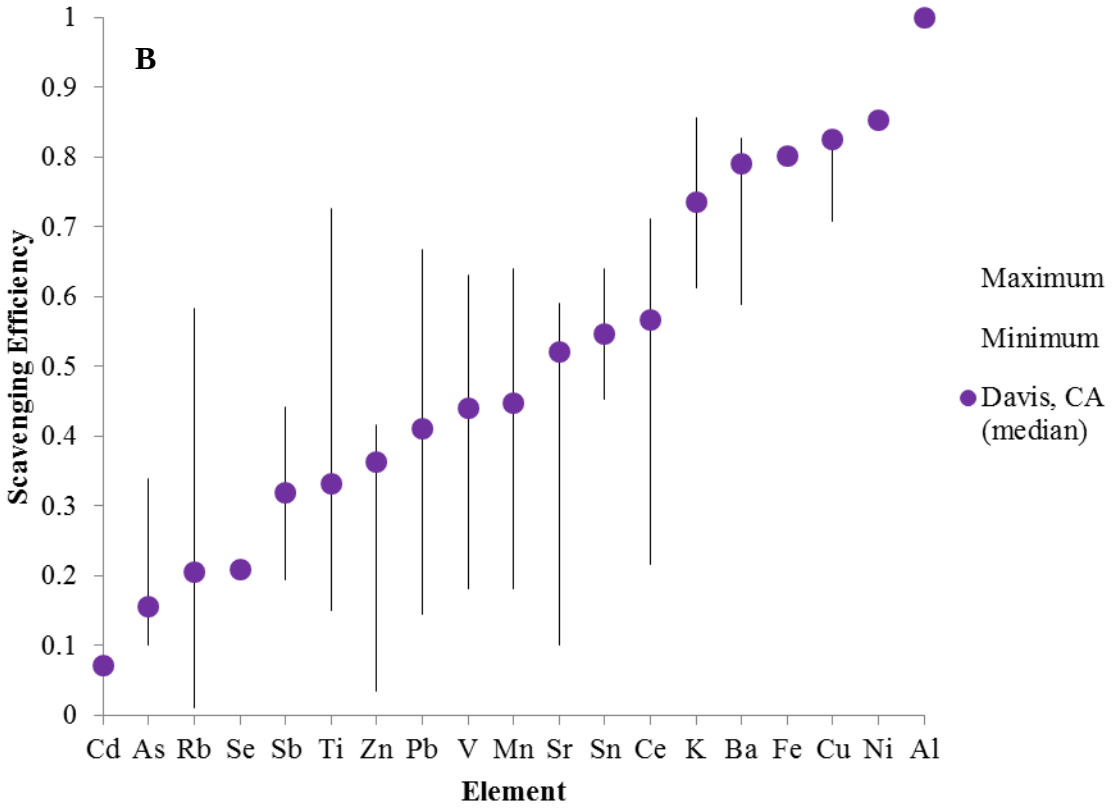


Figure 3.4. Calculated scavenging efficiencies in Fresno (**A**) and Davis (**B**), CA. Circles represent medians and lines represent maximum and minimum values.

Scavenging efficiency can be defined as the fraction of aerosol that is incorporated and/or removed by a fog event by measuring the pre- and interstitial aerosol. While scavenging efficiency calculations can be a useful tool, they are difficult to estimate using our methods. Typically, plates are used to physically collect droplets. These droplets are then evaporated and the remaining aerosol if used to determine scavenging efficiency (Collett et al., 2008). Some scavenging efficiency calculations resulted in negative values, indicating that the interstitial aerosol concentration was greater than the pre-aerosol concentration. These values were eliminated as they were clearly entrainment events (cf. previous section).

Figure 3.4 shows large variability in $PM_{2.5}$ scavenging efficiencies within samples collected from each site as well as between sites. In the case of consecutive fog events occurring, the scavenging efficiency calculated for the second fog event was typically lower than the first, which shows easily scavenged materials get removed by fog deposition processes. For several elements, only very few measurements were available because of the low concentrations in the aerosol phase. A large variability between events even for a given site is not unusual and was observed for organic and elemental carbon too (Herckes et al., 2013). Given the analytical challenges detailed before, very few measurements exist, especially for metals. One comparative study by Hallberg et al. (1992) used scavenging efficiency to determine the scavenged fraction of sulfate, elemental carbon, and a few metals by fogs collected in the Po Valley, Italy. They defined scavenging efficiency as:

$$\text{Scavenging efficiency} = X_{fog} / (X_{interstitial} + X_{fog})$$

This study found low scavenging efficiencies for the reported metals (less than 0.4) suggesting other aerosol components (e.g. salts) are being more preferentially scavenged.

Calculated scavenging efficiencies show greater scavenging of Fe and Al in Davis (~0.8 and 1, respectively) than in Fresno (~0.6 and 0.4, respectively) (Figure 3.4). Scavenging of Fe in Davis may be linked to lower concentrations PM in the appropriate CCN range. Fresno may have higher PM concentrations and particles containing salts, sulfate and nitrate which are more likely to become activated first as they are more hygroscopic.

Sb, Pb and Cd are elements generally associated with anthropogenic emissions (especially traffic related). Concentrations of all three elements were approximately

twice as high in Fresno as they were in Davis, which is consistent with Fresno being a more urban area. During fog events in Fresno and Davis, Sb, Pb and Cd concentrations did not significantly decrease suggesting tiny particles that were not activated or scavenged by the fog events. This hypothesis is supported by low scavenging efficiencies (0.1-0.4; with the exception of highly variable Sb scavenging efficiencies in Fresno) in both Fresno and Davis and was consistent with the majority of anthropogenic elements.

Conclusions

In this work, metal concentrations in fog/cloud water and $PM_{2.5}$ are reported. Metal concentrations in fog/cloud water samples were mostly consistent with the local environment. $PM_{2.5}$ samples showed increased metal concentrations in Fresno as compared to Davis, in general. In Davis, fog seemed to incorporate/deposit metals in $PM_{2.5}$, while Fresno did not, suggesting other components of Fresno $PM_{2.5,}$ such as carbonaceous compounds and salts are being preferentially incorporated into the fog over metal components.

This work found large inter- and intra-site variability in fog/cloud water samples as well as aerosol samples collected in Whistler, Fresno, and Davis. Sources of variability may be linked to air mass movement or aerosol entrainment above the fog. Additionally, size distributions of aerosols can shift which could change which particles are scavenged. Finally, aerosol ageing and processing has the possibility to play a large role in which particles become CCN or are scavenged by fog. Highly processed aerosols can be associated with more soluble material making aerosols more hygroscopic.

Although this data shows interesting differences between sampling sites and trace metals in fog/cloud water and aerosols, improved observation studies are needed. Size resolved aerosol and fog droplet samples and more time resolved samples would be beneficial to better understand fog and cloud microphysics. Deposition measurements would significantly improve scavenging efficiency calculations.

CHAPTER 4

PROCESSING OF ATMOPSHERIC AEROSOLS IN RURAL AND URBAN ENVIRONMENTS: SOLUBLE IRON CONTENT

Introduction

The chemical composition and speciation of metals in atmospheric aerosols is dependent on their emission source and the atmospheric processing they undergo during transport. The solubility of metals in aerosols is dependent on both of these processes. When an aerosol is emitted, the process by which it is produced can affect its solubility. Vehicle emissions can have increased solubility due to their small particle size (Shi et al., 1999) and the hot combustion process by which they are formed. Mineral dust aerosols on the other hand tend to have lower solubility as they do not undergo significant processing during emission, besides erosion, and they tend to be larger particles. During atmospheric transport, aerosols can undergo aqueous phase processing as well as processing by anthropogenic gases and photochemistry. This atmospheric processing can solubilize metals changing their reactivity and fate in the environment.

The solubility and speciation of metals in atmospheric aerosols is important because of their impact on ecosystems and organisms. In the environment, soluble metal species from atmospheric aerosols provide nutrients to the open ocean and other biologically active surfaces. In remote areas of the ocean, aerosol deposition can act as a large or dominant source of nutrients including select metals; therefore, trace metal solubility plays an important role in marine productivity. On the ocean surface, trace metal nutrients, such as Fe, Cu, Co, Cd, and Zn have been found to be depleted (Butler, 1998).

The solubility of metals in aerosols is also important for health purposes. Small particles (< 2.5μm) can penetrate the lungs and interact with lung fluid, which acts as an aqueous medium for solubilization to occur (Morrow, 1972). Smaller particles can cross into the blood and potentially travel to the brain. This was especially important in the case of lead, which was emitted from cars as tetraethyllead, before leaded gasoline was banned in the mid-1970's. It was banned because lead is a neurotoxin, mainly affecting the decision making part of the brain (Needleman, 1990). Copper is another metal that can be particularly harmful because soluble Cu in aerosols has been shown to enhance the formation of ROS species in lung fluid, which causes irritation and inflammation (Charrier et al., 2014).

In regards to iron, solubility in atmospheric aerosols has been widely studied primarily in response to its limitation in the open ocean affecting primary productivity, which in turn affects the amount of CO_2 uptaken by the ocean from the atmosphere. Martin (1990) was one of the first to examine what he calls the "iron hypothesis". Since then researchers have been trying to determine why soluble iron content in the open ocean is low. Baker et al. (2006) found that Saharan dust, which is a major aerosol source contributing to the Atlantic Ocean, had a soluble iron content around 1.7%, while other sources had on average a solubility of 5.2%. In iron solubility studies, speciation of iron (Fe(II) vs Fe(III)) is also considered as Fe(II) has been found to be more soluble, and hence bioavailable, than Fe(III) (Zhuang et al., 1992). Cloud/fog processing has also been found to increase iron solubility as they provide an aqueous medium for reactions to occur (Desboeufs et al., 2001). Interactions with gas phase species such as SO_x and NO_x

have been suggested to increase iron solubility in atmospheric aerosols (Meskhidze et al., 2005).

In this chapter, iron solubility in aerosols collected in Tempe, AZ and in California's Central Valley is examined. Iron solubility measurements are discussed in terms of source (natural vs anthropogenic) and atmospheric processing of the aerosols and are compared to literature observations. It is hypothesized that aerosol samples from more polluted regions will have higher soluble iron content due to processing by anthropogenic gases (NO_x and SO_x) and emission from sources that already start most soluble. Additionally, we want to test the hypothesis that aqueous phase processing (i.e. fog) will result in higher iron solubility in ambient particulate matter.

Materials and Methods

Sample collection

$PM_{2.5}$ and $PM_{>2.5}$ samples were collected using a Tisch High Volume Sampler (Tisch Environmental,Village of Cleves, OH) operating at a flow rate of $1.13 m^3 min^{-1}$ and fitted with a $PM_{2.5}$ impactor plate (Tisch Environmental, TE 231). Aerosol samples were collected on cellulose (CL, Whatman 41, GE Healthcare Life Sciences) and quartz fiber filters (QFF, Whatman QM-A, GE Healthcare Life Sciences). Prior to use, cellulose filters were cleaned in a 0.5% hydrochloric acid bath and quartz fiber filters were baked overnight at 650°C. Field blanks were taken before and after the sampling period. Particulate matter samples were collected at 24 hour intervals. During fog events, particulate matter samples were collected for at least one hour to ensure enough particle (mass) loading for analysis. After PM collection, samples were stored in a freezer until analysis.

Aerosol samples were collected during January 2010 in Fresno, CA. Sampling was performed at the experimental farm at the California State University at Fresno, located on a large agricultural plot, but close to major highways and residential areas.

A second field study was conducted in January 2011 in Davis, CA during January 2011. The sampling site was on an agricultural field close to the California State University at Davis campus as well as less than a mile from a major highway.

A third and final field study in the Central Valley of California was conducted in in Bakersfield/Oildale, CA during January and February 2013. The sampling site was in a lot situated between a church and a residential community. Across the street (approximately 100 yards away) was an oil field.

Finally, local samples were collected in Tempe, AZ during the summer of 2013. The Tempe sampling site was located on the roof of the Life Sciences A-wing building on the Tempe campus of Arizona State University. Tempe is an urban area located on the border of Phoenix. During the summer monsoon season it occasionally experiences massive dust storms, also known as haboobs (Chapter 2).

Sample extraction

Samples were extracted following a well-established procedure (Upadhyay et al. 2011). In brief, 3 x 3 cm squares of $PM_{2.5}$ filters and 2 strips of $PM_{>2.5}$ filters were cut up using a ceramic blade on a Teflon cutting board. Samples were placed in 50mL plastic centrifuge tubes (VWR, Radnor, PA) to which 8mL of 5mM acetate buffer (pH 4.3) was added. Samples were extracted for soluble iron by shaking in a rotisserie shaker for 150 minutes. Samples were covered with aluminum foil to reduce the amount of light present

as photochemical reactions on the surface of particles have been shown to increase iron solubility (Borer et al., 2009).

Soluble iron analysis

Sample extracts were filtered using a plastic syringe and a PES membrane filter (0.22µm pore size, Millex, Millipore Corporation, Cork, Ireland). Aliquots were taken for Fe(II) and FeT (total soluble iron = Fe(II) + Fe(III)) measurements. To measure Fe(II) by UV-Vis a 5.2mM ferrozine reagent solution (3-(2-Pyridyl)-5,6-diphenyl-1,2,4-triazine-4',4"-disulfonic acid sodium salt, Sigma-Aldrich) was added, which forms a colored complex with Fe(II) (pink). To reduce all the Fe(III) to Fe(II) in the Fe_T sample to be measured by UV-Vis spectroscopy, 5.5mM hydroxylamine hydrochloride (99.999% metals basis, Sigma Aldrich, St. Louis, MO) was first added followed by the ferrozine reagent. A Shimadzu UV-1700 Spectrophotometer was used with the wavelength set at 562nm and a 1cm pathlength plastic cuvette. Samples were measured within 30 minutes of the ferrozine reagent being added (Upadhyay et al., 2011).

Results and Discussion

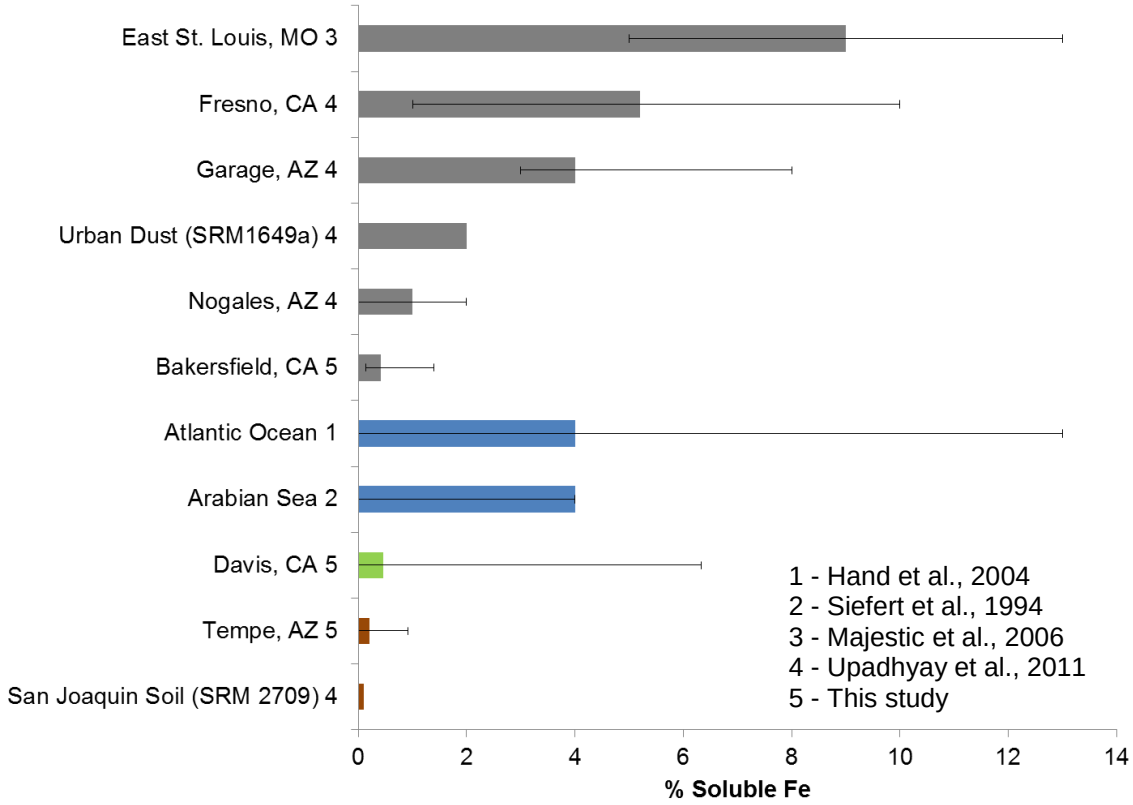


Figure 4.1. Percent soluble iron in $PM_{2.5}$ samples collected from various sites. Bars represent averages and black line represents maximum and minimum values. Grey represents urban areas, blue represents ocean regions, green represents agricultural areas, and brown represents areas with mineral dust aerosol sources. All samples were analyzed similarly to make a more accurate comparison.

Figure 4.1 shows the soluble iron content (%) in $PM_{2.5}$ samples collected in this study compared to $PM_{2.5}$ samples from other locations. Variability between sites was observed as was variability within a site, which is denoted by the maximum/minimum bars in Figure 4.1. Variability across sites is due to the local environment (i.e. sources of particles). Urban areas typically have higher soluble iron content as the areas are heavily influenced by anthropogenic emissions (i.e. vehicles, industry, etc.). The San Joaquin Soil (SRM2709), however, which is used as a reference material for crustal samples, has

low soluble iron content since mineral dust in not very soluble. Samples collected over the ocean generally can be influenced by a variety of sources, which explains the mid-range but variable soluble iron contents shown in Figure 4.1. In addition, they are likely to have undergone long range transport to the sampling locations with the corresponding opportunities for atmospheric processing and hence enhanced solubilization. Variability within a site is partly due to changes in meteorological conditions throughout the sampling period. For example, periods of high humidity or fog could allow for aqueous phase reactions to occur as particles can act as CCN. Another possible explanation for intra-site variability is changes in wind direction, which could result in differences in particle sources and hence, solubility being sampled. The samples analyzed in this work are examined further for their intra-site variability focusing on how local meteorological events impact iron solubility. More specifically, in Fresno and Davis, the impact of fog on iron solubility in aerosols will be examined, then "haze" (i.e. high humidity) events in Bakersfield, and finally haboob dust storms impact on iron solubility in aerosols from Tempe, AZ.

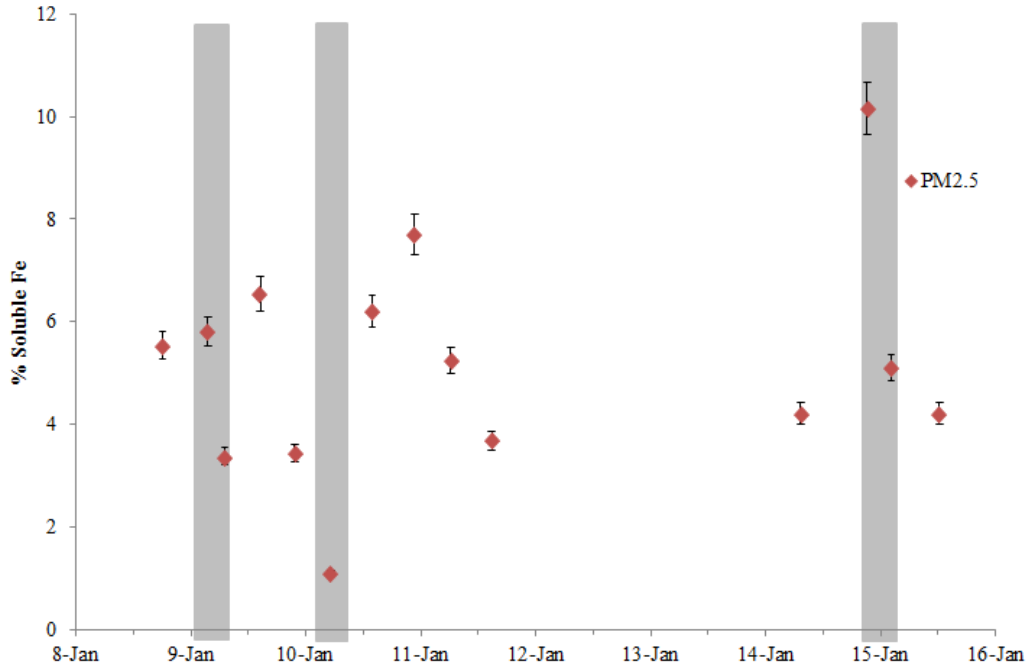


Figure 4.2. Soluble iron content in $PM_{2.5}$ samples collected in Fresno, CA during the winter of 2010. Grey bars represent periods of fog. (data from Upadhyay et al., 2011)

Figure 4.2 shows the soluble iron content of $PM_{2.5}$ collected in Fresno, CA, an urban area in the San Joaquin Valley. Fresno has historically bad air quality and generally, the soluble iron content of Fresno aerosols was high (average of 5.2%) (Upadhyay et al., 2011). Comparatively, Saharan dust has an average soluble iron content of 1.7% (Baker et al., 2006; Trapp et al., 2010), suggesting that in Fresno there is an input from anthropogenic sources or extensive processing. Smaller particles have higher surface area and more highly processed aerosols have been found to have higher iron solubility. The grey bars in Figure 4.2 represent periods of fog and were included to examine the effect of aqueous phase processing on aerosol iron solubility. In Fresno, there does appear to be an effect on solubility during periods of fog. As the fog forms iron solubility increases indicating the aerosol population is being processed by the high humidity conditions before the fog forms. During the fog event, there is a decrease in

solubility during the fog, suggesting the more soluble aerosols are being incorporated into the fog. After the fog dissipates, the soluble iron fraction returns to average, which shows an input from "fresh" anthropogenic emissions. This suggests that in this region, iron solubility is dependent on emission sources, with scavenging of more soluble particles during fog events.

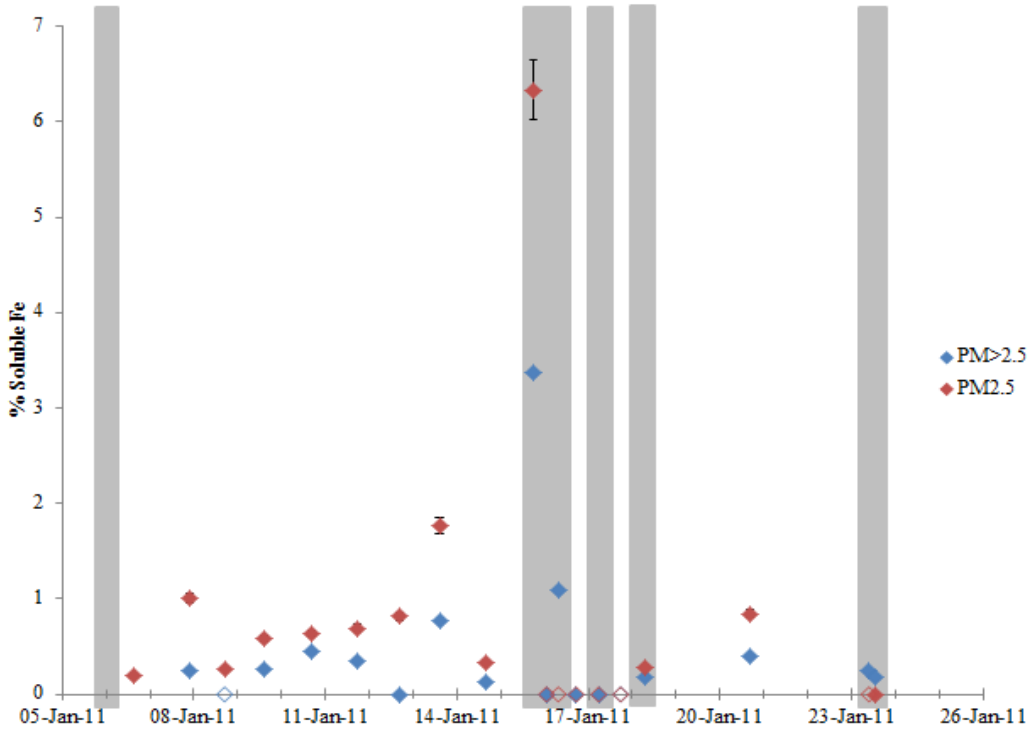


Figure 4.3. Soluble iron content in $PM_{2.5}$ and $PM_{>2.5}$ samples collected in Davis, CA during the winter of 2011. Grey bars represent periods of fog.

Figure 4.3 shows the soluble iron content of $PM_{2.5}$ and $PM_{>2.5}$ samples collected in Davis, CA. Davis is a mostly agricultural, sub-urban city in northern California at the inlet of the San Joaquin Valley. In Davis, soluble iron content was low (average of 0.72% for $PM_{2.5}$), which is consistent with mineral dust sources and few anthropogenic inputs. The soluble iron content of $PM_{2.5}$ was slightly higher than that of $PM_{>2.5}$ (average of 0.41%), which shows the impact of particle size on iron solubility. The effect of aqueous

processing on the iron solubility in this region is similar to that of Fresno, but more extreme. When examining the January 15th to 18th fog periods, it is observed that as the fog forms, iron solubility increases. During the fog, the more soluble particles are scavenged, leaving less soluble particles in the interstitial aerosol. Considering the low solubility of these aerosols, other factors affecting solubility are unlikely.

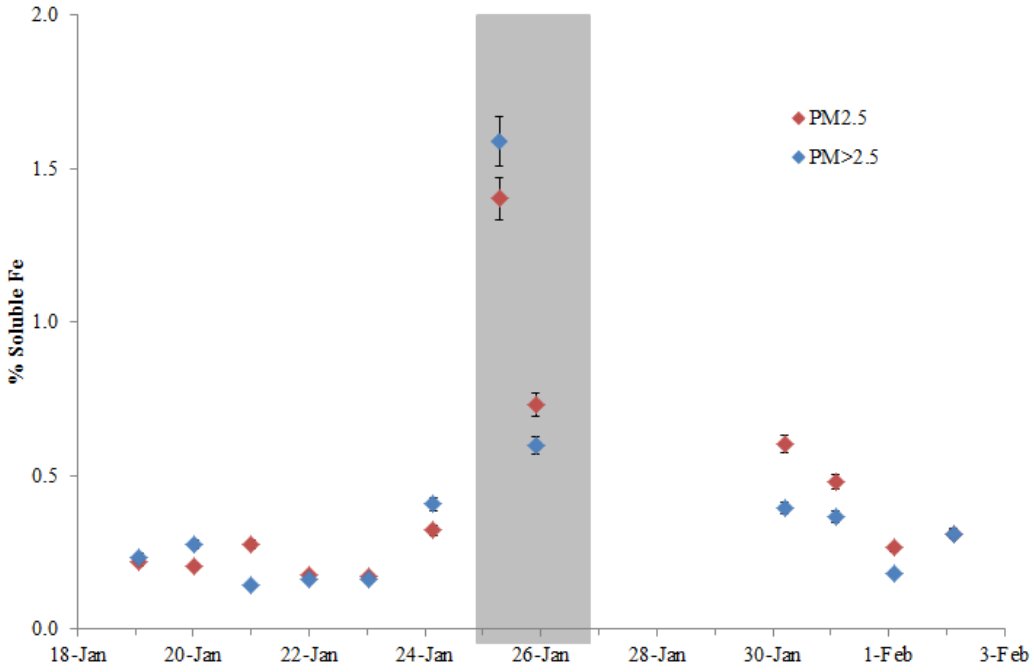


Figure 4.4. Soluble iron content in $PM_{2.5}$ and $PM_{>2.5}$ samples collected in Bakersfield, CA during the winter of 2013. The grey bar represents a period of haze (RH > 90%).

Figure 4.4 shows the soluble iron content of $PM_{2.5}$ and $PM_{>2.5}$ samples collected in Bakersfield, CA. Similarly to Davis, the samples collected in Bakersfield had low soluble iron content (average of 0.38% in $PM_{2.5}$). This result was unexpected in Bakersfield as it appears to be heavily influenced by anthropogenic sources, especially from oil refineries. Although, in a study by Majestic et al. (2006), urban areas were found to have iron solubility in $PM_{2.5}$ samples ranging from 0.2 to 13%. During the sampling period in Bakersfield there was no fog events; therefore, the grey bar in this plot

represents a period of high relative humidity (RH > 90%) to examine the effect of aqueous phase processing on iron solubility. In Bakersfield, it appears that iron solubility in atmospheric aerosols might be greatly influenced by haze/fog events. During the January haze event, iron solubility increased from 0.5 to 1%. Since there was no fog formation, these more soluble aerosols were not scavenged and remained in the interstitial aerosol. This increased solubility during fog/haze events is important to consider as other metals may also become soluble during this time.

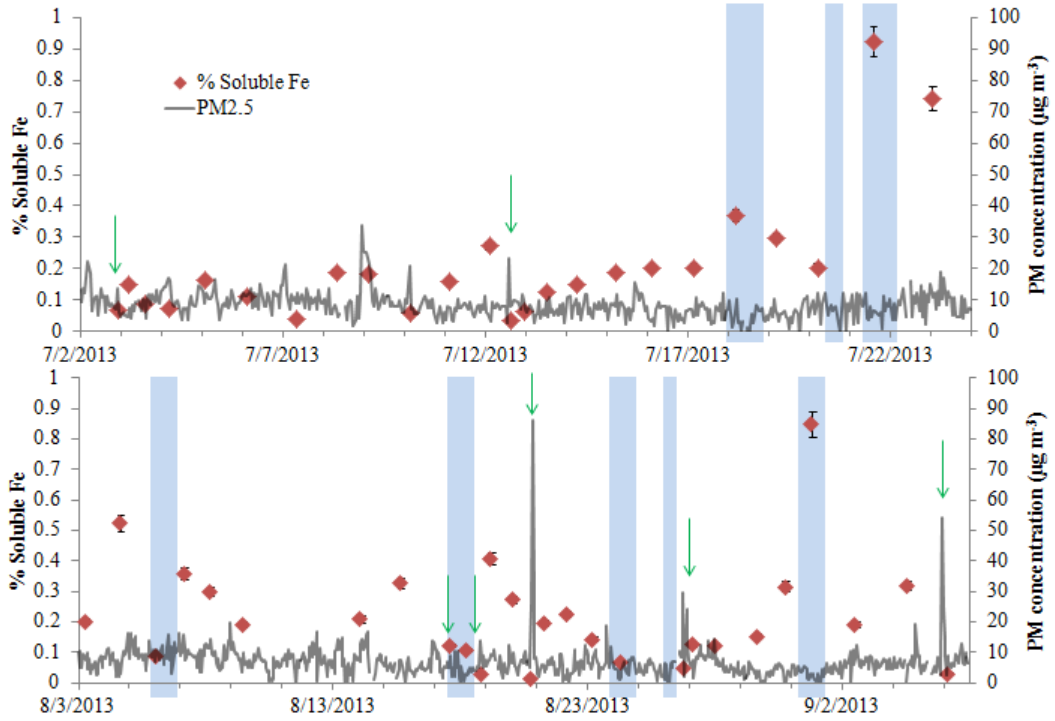


Figure 4.5. Soluble iron content in $PM_{2.5}$ samples collected in Tempe, AZ during the summer 2013 monsoon season. Blue bars represent periods of rain. Green arrows represent haboob events.

Figure 4.5 shows the soluble iron content of $PM_{2.5}$ samples collected in Tempe, AZ. Soluble iron content was low in aerosols from Tempe (average of 0.21%). Although Tempe is an urban area it is strongly influenced by mineral dust, especially in the summer when these samples were collected. Upadhyay et al., (2011) found iron solubility of

$PM_{2.5}$ samples collected in Nogales, AZ was around 1%. To study the effect of scavenging on iron solubility in atmospheric aerosols in Tempe, Figure 4.5 shows periods during which rain occurred (blue bars). During periods of rain, it iron solubility tends to increase. While increases in relative humidity may play a role in this, a more likely explanation is that when it rains, larger particles are scavenged first leaving smaller, more soluble particles in the atmosphere. The green arrows in Figure 4.5 represent periods during which a haboob occurred. During a haboob there is a rapid increase in mineral dust in the area for a relatively short period of time (minutes to hours). Iron solubility was at its lowest during these events, which reflects this excess contribution of mineral dust.

Table 4.1. Percent of total soluble Fe that is Fe(II) in $PM_{2.5}$ samples.

Site	Fe(II) % (min-max)
Fresno, CA	97 (50-100)
Davis, CA	68 (20-100)
Bakersfield, CA	87 (71-100)
Tempe, AZ	72 (43-100)

Table 4.1 shows the percent of soluble iron that is Fe(II) (the remaining fraction is assumed to be Fe(III)). Across all sites, the fraction of Fe(II) is greater than 50% suggesting some form of processing at all sites since iron bearing minerals are more typically comprised of Fe(III). Fresno, CA had the highest fraction of Fe(II), which is consistent with an urban area with anthropogenic inputs. It was hypothesized that Bakersfield would have high soluble iron content in $PM_{2.5}$ samples due to the industrial sources in the region, but this was not observed. However, Fe(II) seems to be the dominating species in these samples suggesting that of the soluble iron present it is likely from an anthropogenic source. Intra-site variability is likely due to changes in meteorology throughout the sampling period.

Conclusions

This chapter examined the solubility of iron in aerosol samples collected in the Central Valley of California and in Tempe, AZ. Soluble iron content was found to be the highest in Fresno, followed by Bakersfield and Davis, and then Tempe (results summarized in Table 4.1). These findings are consistent with the local environment as Fresno is an area with significant anthropogenic input. It is also possible that increased soluble iron content might be due to interactions with anthropogenic gases from the local environment. Although Tempe, AZ is an urban area, PM in the summer months can be largely attributed to dust resuspension, including special events like haboobs, and mineral dust aerosols has been previously shown to have low soluble iron content.

The effect of meteorological events like fog and rain on iron solubility in aerosols from these cities was studied. In Fresno, Davis and Bakersfield, soluble iron content increased with increases in humidity (i.e. pre-fog/haze events) suggesting aqueous phase processing of aerosols. These increases in solubility were followed by scavenging of the more soluble aerosols during the fog, leaving less soluble material in the interstitial aerosol, which was sampled. In Tempe, higher iron solubility may be due to rain out of larger, less soluble particles, so smaller particles are left, increasing the soluble iron fraction.

CHAPTER 5

EFFECT OF PARTICLE SIZE ON IRON SOLUBULITY IN ATMOPSHERIC AEROSOLS

Introduction

Plankton blooms affect the biogeochemical cycles of carbon, nitrogen, silicon, and sulfur, thereby affecting the earth's climate (Boyd et al., 2007). For example, oceans are responsible for removing approximately one-third of anthropogenic CO_2 from the earth's atmosphere (Zeebe, 2012) with marine phytoplankton playing a large role in that removal. A process called upwelling, which transfers nutrients, such as nitrogen, phosphorus, and potassium, to the photic zone from deep waters, controls photosynthesis; however, in parts of the ocean where concentrations of these nutrients exceed the demand, other limiting nutrients emerge. Iron has been determined to be the limiting factor in the high nutrient, low chlorophyll (HNLC) areas (Figure 5.1), which dominate the southern ocean (Martin, 1990; Falkowski et al., 1998).

There are a variety of iron sources to the open ocean, which are largely dependent on sampling location. In remote ocean regions, such as the sub-arctic and Southern Ocean, atmospheric mineral dust is a major source of iron in addition to upwelling of iron rich waters, resuspension of coastal sediments, glacial melt, hydrothermal vents, sediment interactions, volcanic activity, etc. (Boyd and Ellwood and references herein, 2010; Jinkells et al., 2005). In coastal waters, sedimentary and riverine sources usually supply materials to the oceans. In other ocean regions, atmospheric inputs from extraterrestrial dust and urban pollution can be a major source of iron. The concentration of iron in the ocean is limited by the scavenging of the less soluble form of iron, Fe (III), from

seawater. Also, the iron concentration in surface seawater is depleted compared to deeper ocean, which is consistent with biologic uptake close to the surface and release from organic matter in the deep ocean (Archer and Johnson, 2000).

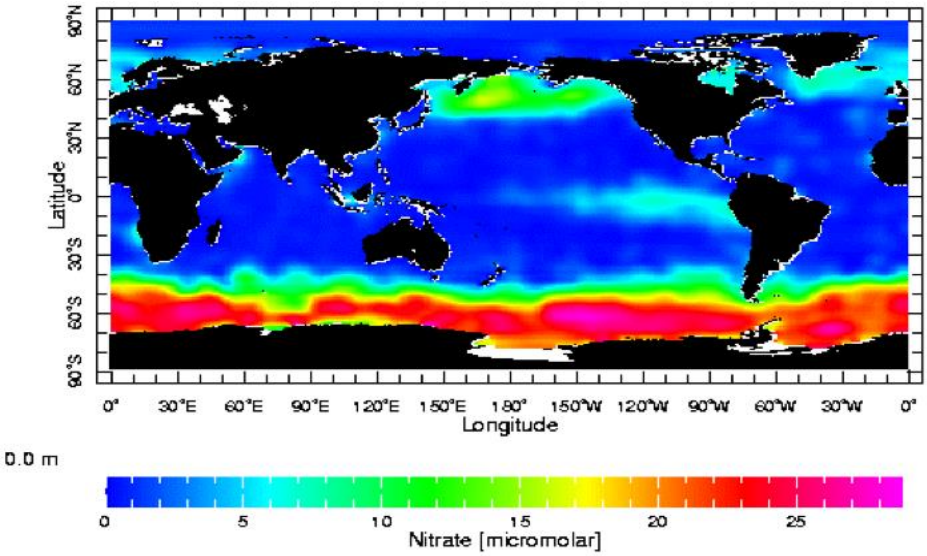


Figure 5.1. Distribution of HNLC regions in the oceans (data from the Levitus World Ocean Atlas, 1994).

Mineral dust aerosols contain approximately 3% iron by mass (Jinkells et al., 2005) and can undergo long range transport resulting in an estimated 14-16 Tg of iron deposited into the oceans annually (Gao et al., 2003). Although this is a significant amount of iron, only a very small fraction of it is soluble (~2-4% from clays and ~0.003% from iron (oxyhydr)oxides) and thus bioavailable (Journet et al., 2008). It is possible that the soluble iron fraction in aerosols is the result of reactions during atmospheric transport or from anthropogenic iron sources, which have been found to be highly soluble (10-50%; Kumar et al., 2010; Chuang et al., 2005), mixing with mineral dust aerosols. Iron containing minerals can dissolve via three different mechanisms: 1) proton-promoted dissolution, where high proton concentrations disrupt Fe-O bonds in the crystal lattice, 2) ligand-controlled dissolution, where ligand molecules form surface

complexes with iron and detach to form soluble Fe(III), and 3) reductive dissolution, where Fe(III) forms soluble Fe(II) generally by photochemical reactions (Fu et al., 2010).

Fe(II) is considered to be the more bioavailable form of iron because less organic ligands in the ocean complex with Fe(II) than Fe(III) (Cwiertny et al., 2008). In most mineral dust found in the atmosphere iron is presumed to be in the Fe(III) form, which is substituted into aluminosilicate minerals and present in (oxyhydr)oxides such as goethite and hematite (Cwiertny et al., 2008). Fe(II) can be produced by the dissolution of Fe(II) compounds or by the reduction of Fe(III) at the solid/liquid boundary layer when O_2, O_3, H_2O_2, and other oxidants are present. The photochemical reduction of Fe(III) to Fe(II), which then is rapidly reoxidized to Fe(III), is also a major source of Fe(II) (Dedik et al., 1993, Arakaki and Faust, 1998).

The factors affecting iron solubilization during atmospheric transport need to be considered as aerosol particles are a large source of soluble iron the open ocean. Figure 5.2 represents three main processes a mineral dust aerosol may undergo during atmospheric transport: environmental processing (i.e. cloud and marine processing, changes in relative humidity), interactions with anthropogenic gases, and photochemical processes. Two other factors affecting iron solubilization during transport are related to mineral dust aerosol directly: mineralogy and particle size.

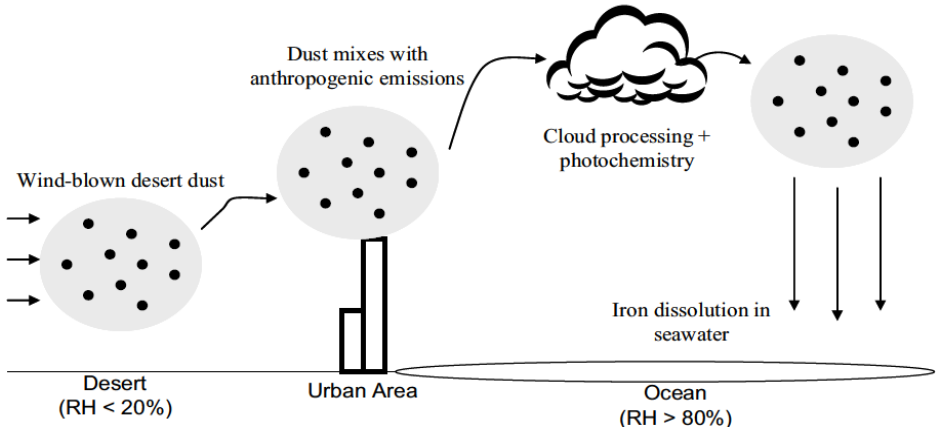


Figure 5.2 Schematic diagram of atmospheric processing and transport of mineral dust aerosols to the open ocean.

In this section, the hypothesis that iron solubilization varies as a function of particle size and mineralogy is examined. According to Buseck and Adachi (2008), dust particles can range from 200nm to 100µm and particles less than 10µm can be transported long distances. The average dust particle size, hundreds of kilometers from its source, is approximately 3µm (Buseck and Adachi, 2008). This work examines particle sizes ranging from 10µm to less than 250nm with a specific focus on particle sizes between 2.5µm and 250nm, since smaller particles are most likely to travel further distances and decreased particle size leads to increased surface reaction sites for iron to be solubilized. Atmospheric dust typically contains quartz, feldspar, calcite, gypsum, illite, kaolinite, smectite, and hematite (Claquin et al., 1999). In this work, illite, kaolinite, magnetite, hematite, and goethite are examined as they are relevant iron bearing minerals. Particles are size fractionated then extracted into a simulated cloudwater buffers as well as a marine aerosol solution. The extracts were analyzed for soluble iron content by inductively coupled plasma mass spectrometry (ICP-MS) as well as their oxidation states by UV-VIS spectroscopy. Photochemical experiments were performed to determine the role of photochemistry during atmospheric transport.

Materials and Methods

Reagents

Acetate and simulated cloudwater buffer solutions (Table 1)were made from chemicals obtained from Sigma-Aldrich including glacial acetic acid (99.8%), sodium acetate (99.0%), formic acid (≥96%), sodium formate (99+%), ammonium nitrate (99.999%). The marine aerosol solution was prepared with sulfuric acid (10N, Fisher Scientific) and sodium chloride (≥99.5%, Fluka).

Table 5.1. Composition of extraction solutions in solubility experiments

Solution	Composition
Acetate Buffer (pH 4.3)	5mM acetate buffer*
Simulated Cloudwater Buffer (pH 4.25)	5mM acetate buffer, 5mM formate buffer**, 5mM ammonium nitrate
Marine Aerosol Solution pH (1.7)	0.1M sulfuric acid, 0.1M sodium chloride

*Acetate buffer has a ratio of 0.36 (acetate/acetic acid).
** Formate buffer has a ratio of 3.63 (formate/formic acid).

All plasticware was soaked overnight in a 10% nitric acid (OmniTrace, EMD) bath. Mineral extracts were filtered with PES membrane filters (0.22μm pore size, Millex, Millipore Corporation, Cork, Ireland). For ICP-MS analysis, iron standards were made from a J. T. Baker iron standard (1000ppm). For UV-Vis analysis, Fe(III) was reduced to Fe(II) with 5.5mM hydroxylamine hydrochloride (99.999% metals basis, Sigma Aldrich) then complexed with 5.2mM ferrozine solution (3-(2-Pyridyl)-5,6-diphenyl-1,2,4-triazine-4',4"-disulfonic acid sodium salt, Sigma-Aldrich). UV-VIS standards for Fe(II) and Fe(III) were made from ammonium iron(II) sulfate hexahydrate (minimum 99%, Sigma-Aldrich) and ammonium iron(III) sulfate dodecahydrate (minimum 99%, Sigma-Aldrich), respectively.

Sample preparation

Five pure mineral phases (kaolinite, illite, magnetite, goethite, and hematite) were obtained from Ward Life Sciences (kaolinite, illite, goethite) and Fisher Scientific (hematite, magnetite). The samples were ground using a ceramic ball mill. The ground mineral phases were then resuspended using a laboratory set-up described in detail in Upadhyay et al., 2015. The resuspended particles were collected onto solvent cleaned/sonicated aluminum (Alfa Aesar Puratronic, 99.997% metals basis) substrates (25mm) using a Sioutas Personal Cascade Impact Sampler (PCIS) (SKC Inc.), which size segregates the resuspended particles into 5 different size fractions: >2.5, 2.5-1.0, 1.0-0.5, 0.5-0.25, and <0.25μm. The last, "catch", stage (<0.25μm) was a 37mm Teflon filter (Teflo, Pall Life Sciences, Port Washington, NY). The flow rate of the resuspension system was 9 L min^{-1}. The aluminum substrates and Teflon "catch" stage were extracted into three buffer solutions: an acetate buffer, a simulated cloud water buffer, and a marine aerosol solution (compositions shown in Table 5.1). The extracts were then filtered through a PES membrane filter (0.22μm pore size, Millipore, Millex) and subsequently aliquoted for analysis by ICP-MS for total soluble iron content and by UV-Vis for iron speciation. Light exposure was limited by keeping the extracts covered with aluminum foil at all times.

Scanning electron microscopy (SEM)

SEM coupled with energy-dispersive X-ray spectroscopy (EDX) was used to confirm the particle size distribution obtained by sampling with the PCIS. Three mineral phases representing the three classes of minerals investigated (quartz, clay, iron (oxyhydr)oxide) were examined using SEM. The bottom "catch" stage (< 0.25μm)

could not be examined by SEM because gold and carbon coating disintegrated the Teflon filters.

Surface area measurements

Brunauer-Emmett-Teller Theory (BET) was used to determine the surface area of kaolinite and magnetite at the following particle sizes: 10-2.5, 2.5-1.0, 1.0-0.5, and 0.5-0.25 μm. In BET, surface area is determined by the physical adsorption of N_2 gas to the surface of the mineral and the difference in mass before and after gas adsorption is proportional to the surface area.

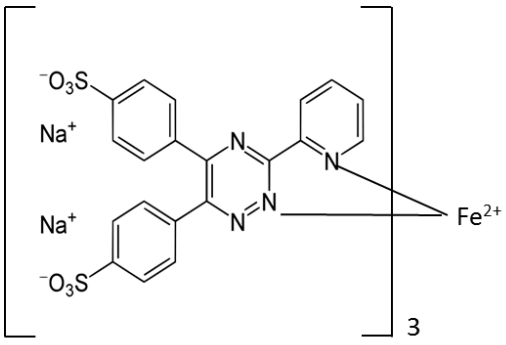
Inductively coupled plasma mass spectrometry (ICP-MS) analysis

Filtrates were diluted with 0.32M nitric acid and analyzed using a quadrupole ICP-MS (X Series 2, Thermo Fischer Scientific) for soluble iron content.

Illite and kaolinite have varying iron content, so the minerals were digested following a method detailed in Uphadhyay et al. (2009) then analyzed by ICP-MS for their total iron content.

UV-Vis spectroscopy analysis

To determine the Fe(II) content, 5.2mM ferrozine solution was added to the extracts. Ferrozine complexes with the free Fe(II) producing a light pink color (Reaction 1), so the absorbance can be measured by UV-VIS spectroscopy at a wavelength of 562nm. To determine the total iron content and subsequently the Fe(III) composition, 5.55mM hydroxylamine hydrochloride was added to the extract (Reaction 2) before adding ferrozine to reduce the Fe(III) to Fe(II).

$$3(C_{20}H_{13}N_4NaO_6S_2 \cdot xH_2O) + Fe^{2+} \rightarrow$$  (1)

$$2HONH_3^+Cl^- + 2Fe^{3+} \leftarrow\rightarrow 4H^+ + 2H_2O + N_2 + 2Fe^{2+} + 2Cl^- \quad (2)$$

Photochemical Experiments

To determine the effect of photochemistry on iron solubility as it relates to particle size, size segregated minerals were extracted into marine aerosol and simulated cloud water buffer solutions and split into irradiated and non-irradiated ("dark" control) samples. The irradiated samples were placed in solar simulator, the set-up of which is described in detail elsewhere (e.g. Chen at al., 2010; Hutchings et al., 2010). In brief, samples were irradiated with simulated sunlight in a double jacketed wall reactor for temperature control. The simulated light was provided by a 300 W xenon arc lamp (Spectraphysics Oriel, 91160A), and the output of the arc lamp is filtered through a standardized air mass 1.5 filter (AM 1.5 Global), which yields a spectrum representative of the solar spectrum at ground level when the sun is at a zenith angle of 48.2°. The power supply can be changed, but the lamp output power was set at a typical ambient value of 1325 W m^{-2}. Figure 5.3 shows the photochemistry reaction set-up. Non-irradiated samples were run at the same time in a dark environment to directly observe differences between having and not having photochemical reactions. Aliquots were taken at 1, 30, 60, and 150 minutes to observe the reaction rate of iron dissolution. Samples were then filtered (0.22μm) and analyzed by ICP-MS for soluble iron content.

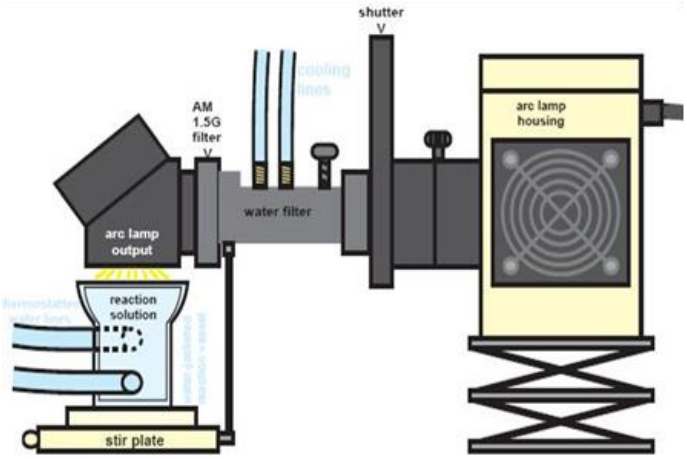


Figure 5.3. Schematic diagram of photochemical experimental set-up.

Results and discussion

Confirmation of particle size distribution by SEM and surface area measurements by BET: iron oxides vs clays

Scanning electron microscopy (SEM) was used to verify sample preparation and the re-suspension processes as well as the collection of particulates on the different stages of the aerosol sampler. Figure 5.4 shows the SEM images for illite (A) and magnetite (B). One of each type of mineral phase (clay and iron oxide) was chosen to be representative of the other minerals for validation of the re-suspension protocol. The <0.25µm size fraction is not shown here because it was collected on a Teflon filter to act as a "catch" stage for the smallest particle. The Teflon filter cannot be analyzed by SEM because the sputter coating, which is necessary to prevent charging during imaging, disintegrates the Teflon filter. The images show that the particles appear to have the right sizes and distributions as expected; although, there does appear to be some small particles "sitting" on top of the larger particles in the largest size fraction. This small particle adhesion was not considered to be an issue because even though this may slightly increase the surface

area of the particle, the mass contribution of those small particles can be considered negligible and will not contribute significantly to the iron mass fraction. It was more important to ensure that no large particles were in the smallest size fraction, which is common in impaction methods from particle bounce between impaction stages. There was no large particles observed in the smallest size fractions, and hence the sample preparation protocols hence were considered validated.

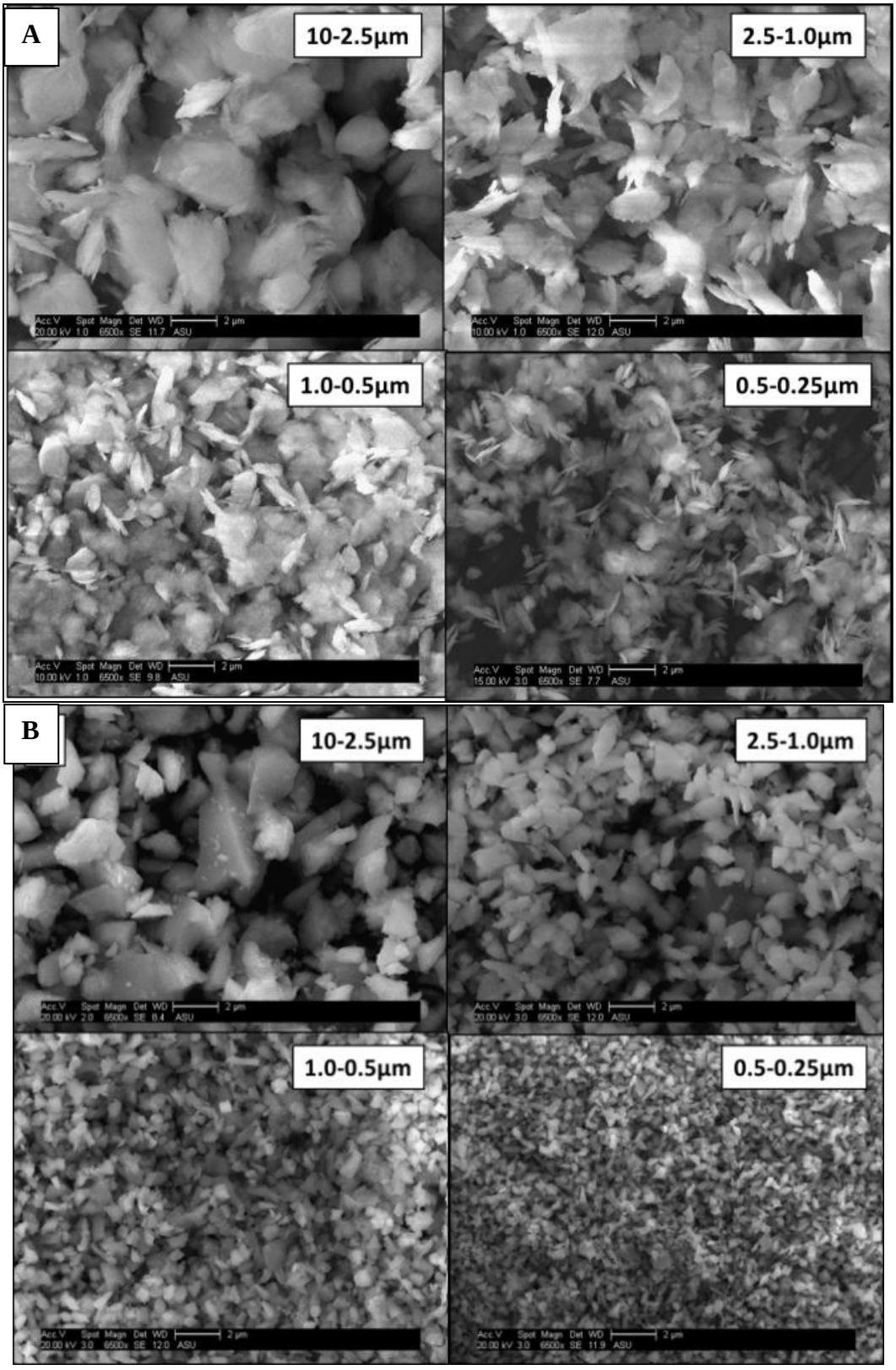


Figure 5.4. Scanning Electron Microscopy (SEM) images for illite (A) and magnetite (B). The SEM images are shown at the same magnification, 6500x, with a scale of 2µm.

Surface area measurements of kaolinite and magnetite using BET (Brunauer-Emmett-Teller) theory show potential differences between clays and iron oxides as particle size decreases. One of each category of mineral (clay and iron oxide) was chosen because their mineral structures are quite different. Clay minerals have a structure resembling stacked "plates" and are typically more "spongy" with a lot of pores (Figure 5.4A). Iron oxide minerals are much more compact and geometric, with very small pores (Figure 5.4B). Surface area measurements were made on each set of particle sizes (10-2.5, 2.5-1.0, 1.0-0.5, and 0.5-0.25μm) for kaolinite and magnetite. Table 5.2 shows that the surface area of kaolinite does not change with decreasing particle size while magnetite has an approximately 3-fold increase in surface area with decreasing particle size. The BET results for kaolinite reveal that since clays are already porous, changing their particle size does not significantly alter their surface area. Conversely, BET analysis of magnetite shows that since iron oxides are more geometric and not porous, decreasing their particle size increases their surface area.

Table 5.2. Surface area measurements of kaolinite and magnetite made by the BET method.

Mineral (m^2/g)	**10-2.5μm**	**2.5-1.0μm**	**1.0-0.5μm**	**0.5-0.25μm**
Kaolinite	31.3	21.7	30.2	29.9
Magnetite	7.1	9.4	11.3	20.9

Iron dissolution of minerals extracted into simulated cloud water and marine aerosol solutions

Figure 5.5 shows that, on average, the percent soluble iron is an order of magnitude greater in the clays, illite and kaolinite, as compared to magnetite, hematite, and goethite. First, the results of the solubility studies indicate that **mineralogy greatly**

affects iron solubilization. These findings are in agreement with a study by Journet et al. (2008), who observed increased iron solubility in clays (~4%) as compared to iron (oxyhydr)oxides (<1%). In mineral dust, clays are much more prevalent than iron (oxyhydr)oxides and in the long range transport of mineral dust, clays have been found to be the most prevalent phase followed by quartz, feldspars and calcite (Jeong and Achterberg, 2014). Even though the weight percent of iron in clays is much lower than in iron (oxyhydr)oxides, the iron is much more soluble. In iron oxide minerals, iron is inferred to be in strong Fe-O lattice bonds. Clays have nano-thin platelet layers, resulting in high surface area (confirmed by BET; Table 5.2) and therefore more reaction sites for iron to solubilize. There are also differences in how the iron is bound in the crystal structure of clays. In clays, iron can "sit" in the interstitial layers as an impurity or can substitute in the crystal lattice for Mg or K, which is bound by ionic bonds. Although clays have higher surface area overall, their surface area does not greatly change as a function of particle size, unlike iron oxides. These relative changes in surface area may not explain the effect of particle size on iron solubility in the simulated cloud water solution because no change was observed for the clays and iron oxides (Figure 5.5A and 5.5B). There is a greater increase in iron solubility with decreasing particle size in the iron oxides as compared to the clays in the marine aerosol solution, which may be a result of the relative change in surface area with particle size (Figure 5.5C and 5.5D).

As the pH of the extraction solution decreases, there is an increase in the fraction of soluble iron in the mineral. When clays were extracted into a simulated cloud water buffer (pH 4.3; Figure 5.5A) approximately 0.5-4% of the iron in the clay was soluble, but when extracted into a marine aerosol solution (pH 1-2; Figure 5.5C) the solubility

increased to 5-14%. A similar trend is observed in iron oxides where the solubility increased from <0.3% to 0.5-2% when extracted into a simulated cloud water buffer (Figure 5.5B) and marine aerosol solution (Figure 5.5D), respectively. This is consistent with previous studies reported in the literature (Bonnet and Guieu, 2004, Cwiertny et al., 2008) that showed an increase in iron solubility with a decrease in solution pH.

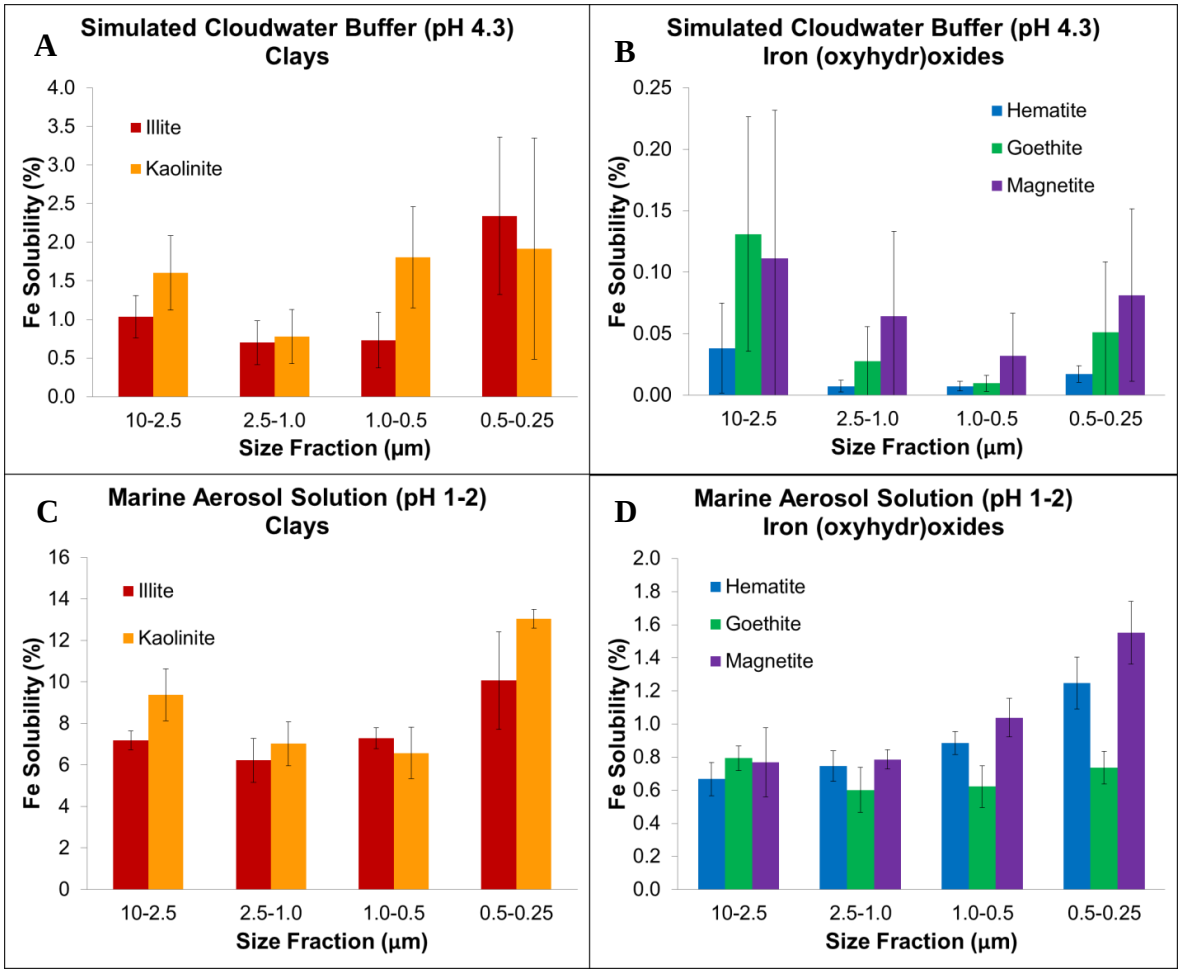


Figure 5.5. Total soluble iron content (as a percentage) of the extracted mineral samples into simulated cloudwater and a marine aerosol solution at the various size fractions. The graphs on the left show the two clay minerals, while the graphs on the right show the three iron (oxyhydr)oxide minerals, which are substantially less soluble. Error bars are representative of the standard deviation of three replicate experiments.

Figure 5.5 shows the effect of particle size and atmospheric processing on iron solubility in atmospheric aerosols. In the simulated cloudwater buffer, at sizes greater than 0.25µm, particle size does not appear to have a statistically significant effect on iron solubility. This is likely due to the low solubility of the iron in these minerals at this pH, which could make changes in solubility difficult to observe. At particle sizes smaller than 0.25µm, there could be a size effect on solubility, but this was not determined in this study. Samples collected at <0.25µm were on Teflon substrates and were difficult to

remove from the filter for analysis in addition to having very low mass loadings (iron content below detection limit in many instances).

In the marine aerosol solution (pH 1-2), it appears that as particle size decreases, soluble iron increases, indicating that surface area of the particle is one factor driving iron solubility (Figure 5.5C and 5.5D). Baker and Jickells (2006) performed field studies examining the solubility of iron as compared with particle size. They showed that iron solubility is an inverse function of mineral aerosol concentration, proposing that the surface area to volume ratio, or specific surface area, is a contributing factor to solubility. Since smaller particles have more volume exposed, the iron solubility of fine aerosols as compared to coarse is greater. To show this relationship, the soluble iron fraction was normalized to surface area for hematite and magnetite (Figure 5.6). Goethite was not shown due to its different structure, and hence surface area, which will be discussed further. The clay minerals are not shown because their surface area does not change with changes in particle size. When soluble iron is normalized to particle surface area in figure 5.6, there appears to be competing processes affecting solubility although the uncertainty of these measurements makes it difficult to conclude a definitive trend. In figure 5.5D, there is increasing iron solubility with decreasing particle size for magnetite and hematite; however, figure 5.6 shows decreasing chemical solubility possibly due to changing composition with size.

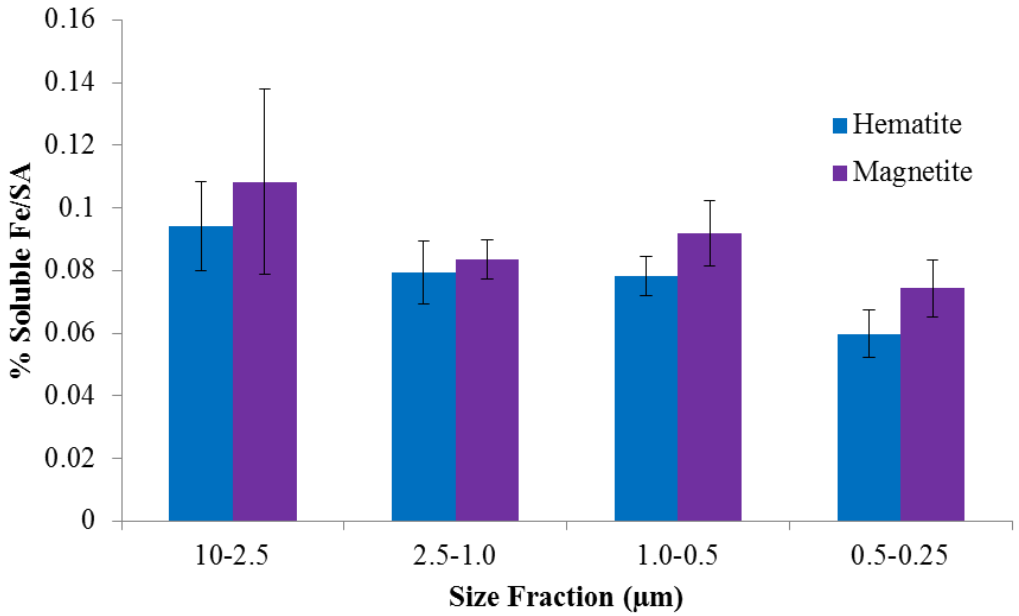


Figure 5.6. Percent soluble iron normalized to surface area (SA) for hematite (blue) and magnetite (purple). Error bars represent 3 replicate experiments.

Iron speciation measurements of minerals in simulated cloud water

In addition to total soluble iron measurements, we also measured the speciation of iron (Fe(II) or Fe(III)) using the UV-Vis/ferrozine method. Figure 5.7 shows the results of speciation measurements for clays and iron oxides extracted into a simulated cloud water buffer, which contained acetate, formate, and ammonium nitrate (Table 5.1). In this experiment, it was observed that the clays, illite and kaolinite contain more Fe(II), which might explain their higher solubility as compared to iron oxides as Fe(II) has been found to be the more soluble form of iron (Cwiertny et al., 2008). Iron (oxyhydr)oxides typically have a high Fe(III) content, although magnetite should have a higher Fe(II) content as its chemical composition is Fe_3O_4 (mix of Fe(II) and Fe(III)).

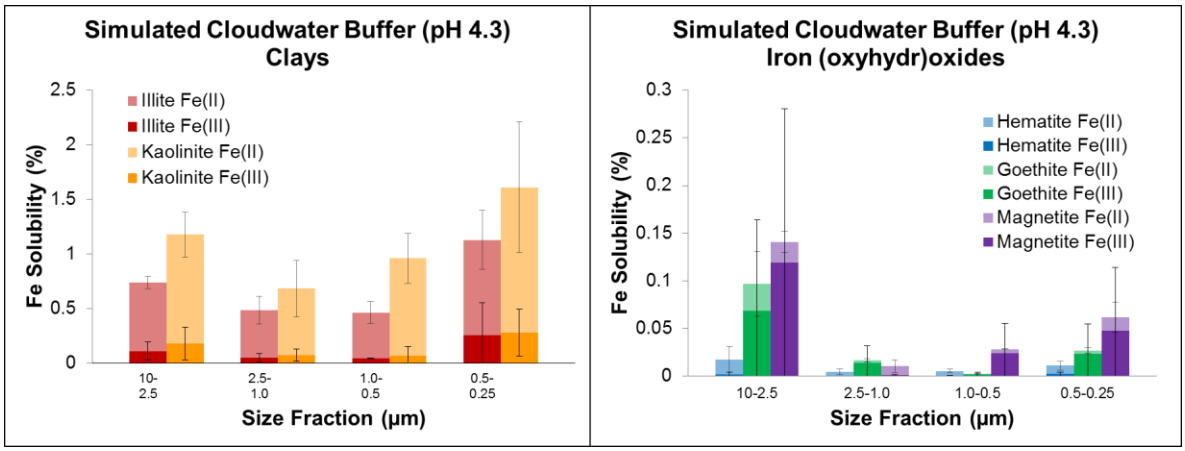


Figure 5.7. Soluble iron fraction (as a percentage) and speciation of the size fractionated minerals. The graphs on the left show the two clay minerals, while the graphs on the right show the three iron (oxyhydr)oxide minerals, which are substantially less soluble. Fe(II) (shaded) is stacked on top of Fe(III) (solid) and total soluble iron is shown as the height of the column. Error bars are representative of the standard deviation of three replicate experiments.

Impact of photochemistry on iron solubility in mineral dust aerosols.

Next, photochemical experiments were performed on size segregated mineral phases to determine the role of photochemistry in the solubilization of iron during atmospheric transport. In Figures 5.8 and 5.9, increased solubility over time is observed for all mineral phases when extracted into the marine aerosol solution. Dissolution of iron oxides is slower than that of clays, which is consistent with mineral/particle structural observations. The highly porous nature of clay materials allows for faster dissolution, while iron oxides typically have very few and small pores resulting in slower dissolution. A trend of increased iron solubility with decreasing particle size was observed, which is consistent with earlier experiments (Figure 5.5C and 5.5D). Irradiation of iron oxides (hematite and magnetite; Figure 5.8A and 5.8B) in a marine aerosol solution showed increased iron solubility with decreasing in particle size which was enhanced by photochemistry. Figure 5.5 also shows iron solubility in goethite was enhanced by

photochemistry, but the effect of particle size on iron solubility in goethite was variable, which was also observed in the initial particle size experiments (Figure 5.5D). The addition of photochemistry does not appear to affect the dissolution of clay minerals (illite and kaolinite; Figure 5.9) in a marine aerosol solution although a trend of increasing iron solubility with decreasing particle size is observed.

Iron solubilization from iron oxides in the presence of solar irradiation might be caused by the photoreduction of the Fe(III) at the surface, which releases the surface bound Fe(II) into solution (Faust and Hoigne, 1990; Rubasinghege et al., 2010a). Organic ligands play a large role in the photoreduction of Fe(III) to Fe(II) as they can act as electron donors for the reaction (Zhu et al., 1993; Pehkonen et al., 1993 and 1995). While organic ligands can promote this photoreduction, they are not required. Specifically, photoreduction of Fe(III) on the surface of iron oxides is cause by light induced ligand to metal charge transfer excitations (LMCE). As Fe(III) is reduced to Fe(II), a hydroxyl group gets oxidized to form a radical. The Fe(II) and OH radical in solution can then further react to for reactive oxygen species in the presences of O_2 (Borer et al., 2009 and references herein). As shown in Sherman (2005), thermodynamics suggest this reaction can only happen at a low pH, in the absence of ligands.

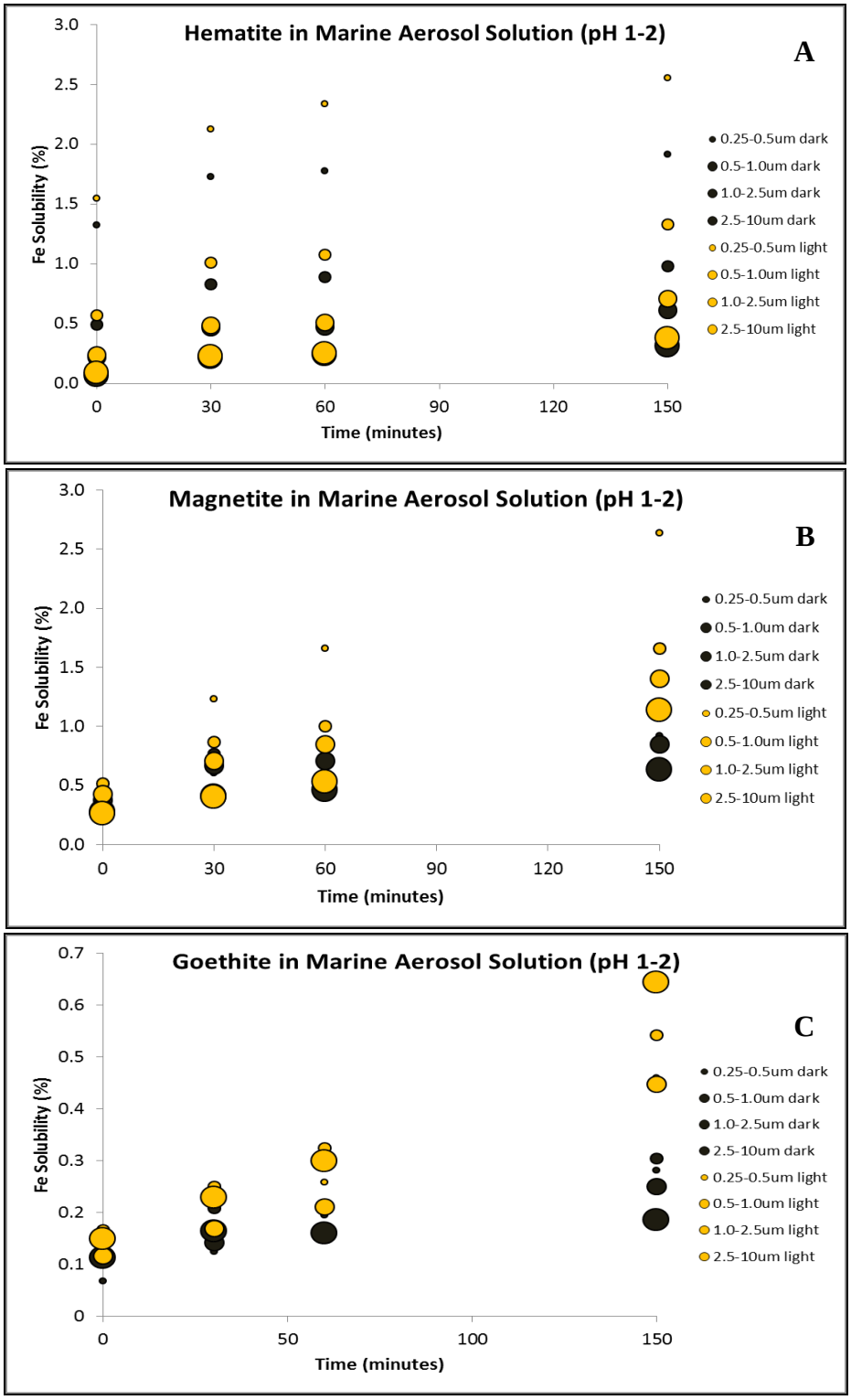


Figure 5.8. The fraction of soluble iron (as a percentage) of the iron (oxyhydr)oxide minerals studied as a function of the time (in minutes) of the photochemical reaction in the marine aerosol solution (pH 1-2). Circles are representative of relative particle size with non-irradiated samples in black and irradiated samples in yellow.

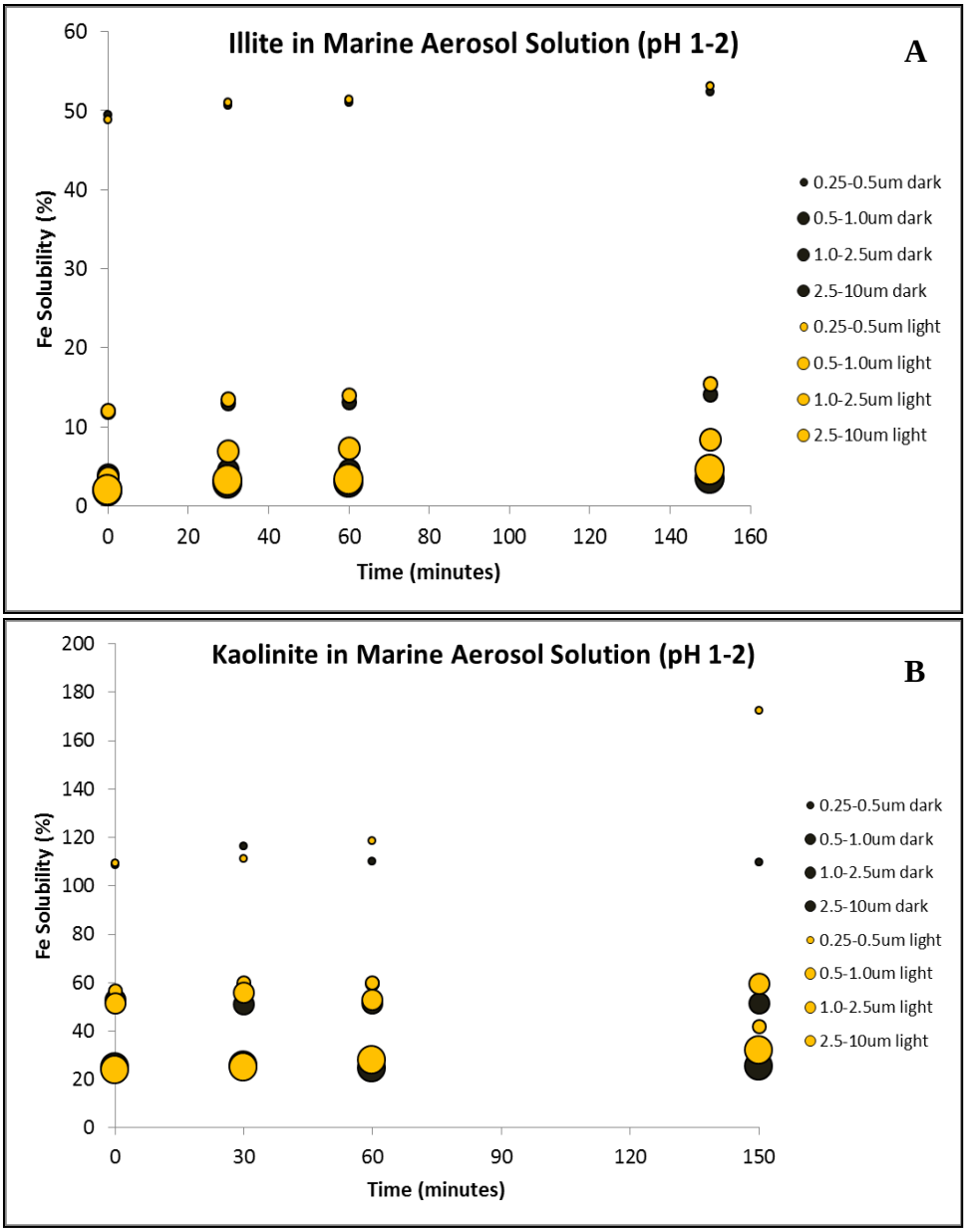


Figure 5.9. The fraction of soluble iron (as a percentage) of the clay minerals studied as a function of the time (in minutes) of the photochemical reaction in the marine aerosol solution (pH 1-2). Circles are representative of relative particle size with non-irradiated samples in black and irradiated samples in yellow.

Results from the photochemical experiments in the simulated cloudwater buffer (pH 4.3) were highly variable (not shown here). A possible reason is that photochemical reduction of Fe(III) to Fe(II) is not thermodynamically favorable in the iron (oxyhydr)oxides (Sherman, 2005) and likely clay minerals under these conditions (pH >

4). We observed also that the solubility decreased occasionally over the duration of the experiment suggesting iron sorption to the centrifuge tube. Common practice in trace metal analysis of aqueous samples requires acidification to approximately pH 2 to ensure all the metal stays in solution.

Variable and unexpected results for goethite

Goethite exhibits a trend of no change in soluble Fe with changes in particle size unlike the iron oxides, magnetite and hematite. Additionally, photochemical experiments show that photochemistry enhances iron dissolution, but an inverse trend of large particles having higher solubility than smaller particles. Originally goethite was grouped with the iron oxides, magnetite and hematite; however, goethite has a different structure and exhibits different characteristics unlike originally thought. Instead of being more spherical in shape, goethite is more rod-like. In Rubasinghege et al. (2010b), it was shown that decreasing pH from 2 to 1 caused micro-goethite to have higher solubility than nano-goethite. This is unusual as nano-goethite has higher surface area than micro-goethite, but aggregation of nano-goethite at pH 1 (confirmed by TEM), reduces the reactive surface area, and appears to quench the dissolution of iron. Rubasinghege and coworkers attribute this phenomenon to the increased ionic strength of the solution at pH 1 compared to pH 2 and confirms this with measurements of the zeta potentials. In the pH 2 solution the zeta potential of nano-goethite is 75mV, but when the pH is reduced to 1 the zeta potential drops to 35mV. Micro-goethite, on the other hand, had greater zeta potentials and is stable under all conditions.

Conclusions

In this section, the effect of particle size on iron solubility was examined. It was found that the largest factor affecting iron solubility during atmospheric transport was mineralogy with clays having higher solubility overall than iron oxide minerals. Solution pH also plays a large role in iron solubility; as pH decreases, iron solubility increases. Both of these results are consistent with previous work in the literature. At lower pH environments a trend of increasing iron solubility with decreasing particle size can be observed for iron oxide minerals. Iron solubility in clay minerals seems mostly unaffected by particle size. This trend is explained by surface area measurements taken in this work, which shows greater changes in surface area as a function of particle size in iron oxides as compared to clays. Photochemical experiments showed that iron solubility increases with exposure to solar irradiation in iron oxides, but not in clays.

CHAPTER 6

SUMMARY AND FUTURE WORK

This dissertation focuses on the trace metal composition and processing of atmospheric aerosols. Trace metals in aerosols are important on local, regional and global scales and their impact on health and the biosphere drives research on this topic. This work combines field and laboratory studies to understand trace metal processing in the atmosphere. Iron was a specific focus of this work, although other trace metals were also examined. Field sampling spanned from 2010 to 2014 and included the following sites: Fresno, Davis, and Bakersfield, CA as well as Tempe, AZ and Whistler, Canada. ICP-MS was employed for the majority of the analyses although a variety of other characterization techniques were used.

In Chapter 2, the trace metal composition of particulate matter (PM) samples collected during the summers of 2013 and 2014 in Tempe, AZ was determined. The haboob dust storms in the summer can bring a large influx of dust into the area in a very short amount of time. It was hypothesized that haboobs derived from the south bring an influx of mineral dust into the greater Phoenix area, but also resuspend anthropogenic matter along the way. PM samples were collected before, during, and after haboob events and analyzed by ICP-MS for metal concentrations. Using data from ADEQ, PM spikes were observed during haboob events. During haboob events increases in trace metals common of mineral dust were observed, but also were elements common of anthropogenic emissions. The influx of high concentrations of mineral dust during a haboob causes decreases in enrichment factors for anthropogenic elements. Finally, PM associated with anthropogenic emissions remains suspended after a haboob, which can be

potentially harmful to residents. Members of the Herckes group at ASU have focused on other components of these aerosol samples (i.e. organic and elemental carbon, polycyclic aromatic hydrocarbons, alkanes, etc.). Future work should focus on potential nutrient deposition (nitrate, phosphate, ammonium, etc.) from haboob events and changes in soil composition in the greater Phoenix area. Future sampling campaigns should focus on collection of haboob PM samples for biologic analysis because there may be a correlation between increased haboob occurrences and cases of Valley Fever in this region.

To study the effect of fog processing on trace metals in aerosols, aerosol samples were collected in California's Central Valley before, during, and after fog events. Aerosol samples were collected in Fresno and Davis, CA in the winters of 2010 and 2011, respectively, to examine differences between urban and rural areas. Trace metal concentrations in fog and cloud water samples from Fresno, Davis, and Whistler, CA were also reported. It was hypothesized that trace metals are being incorporated into fog water droplets by particles acting as cloud condensation nuclei or being scavenged effectively removing them from the atmosphere. Trace metal concentrations in fog from Whistler were the lowest followed by Davis then Fresno, which is consistent with the local environment as Whistler is a remote location, Davis is an agricultural suburban city, and Fresno is an urban location. Fog was effective at activating or scavenging particles containing Fe and Al more effectively in Davis than in Fresno. This may be a result of the activation size of the particles, with larger particles being activated first over smaller particles. Additionally, the overall composition of particles in Davis and Fresno may be different such that other particles are scavenged first in Fresno, while trace metal containing aerosols in Davis are scavenged first in lieu of the other particles. Fog in

Davis and Fresno were not effective at activating or scavenging particles containing Sb, Cd, and Pb. Anthropogenic, highly processed particles may be too small to be incorporated into fogs/clouds. Future work needs to focus on scavenging measurements using deposition plates to quantify trace metal deposition/scavenging from fog events.

Chapter 4 focused on atmospheric processing of iron, which has anthropogenic and natural sources. In this chapter, aerosol samples collected from California's Central Valley and Tempe, AZ were extracted and their soluble iron content was determined using UV-Vis spectroscopy. It was hypothesized that samples from more polluted regions will have higher soluble iron content due to aerosol sources. Also, samples that have undergone aqueous phase processing (i.e. fog) will have higher iron solubility. The highest soluble iron content in atmospheric aerosols was found in Fresno, CA (> 5%), an urban area with historically bad air quality. Higher iron solubility in Fresno was likely due to the sources of the PM, but also may be due to interactions with anthropogenic gases and fog processing. Davis, Bakersfield, and Tempe all had low soluble iron content (< 1%). In California's Central Valley, there were some instances where iron solubility increased as the humidity increased (i.e. pre-fog/haze). During periods of fog those more soluble particles were scavenged removing them from the interstitial aerosol, which was sampled. Periods of increased iron solubility in Tempe may be due to rain out of larger less soluble particles, so smaller more soluble particles left. Future work should focus on solubility of other trace metals in $PM_{2.5}$ as metal solubility in aerosols is an important area of study due to the potential health effects.

The final portion of this work (Chapter 5) focused on laboratory studies to determine the effect of particle size on iron solubility in atmospheric aerosols. Iron-

bearing mineral phases were ground and resuspended to simulate mineral dust aerosols characteristic of the Saharan Desert, as this is the largest contributor of iron to remote regions of the Atlantic Ocean. Resuspended samples were size segregated into 5 particle sizes to examine the effect of particle size and then extracted into solutions simulating aqueous atmospheric processing. It was observed that mineralogy and solution pH greatly affect iron solubility, with clays having higher solubility than iron oxides and increased solubility in more acidic environments, which is consistent with previous work. Clays have higher surface area than iron oxides, which explains their higher solubility. Iron oxides, however, have greater changes in surface area with particle size, so a trend of increasing solubility with decreasing particle size was observed in the marine aerosol solution (low pH). After samples were irradiated, it was observed that photochemical reactions likely play a role in the solubilization of iron from iron oxides, but not clays. This is likely due to the slow release of iron from iron oxides, while clays solubilize rapidly because of their high surface area. Future work in this field should focus on smaller particle sizes and what happens to the iron after deposition into seawater.

REFERENCES

Aleksic, N., and J.E. Dukett, (2010). Probabilistic relationship between liquid water content and ion concentrations in cloud water. *Atmos. Res*., 98, 400–405.

Alfarra, M. R., Paulsen, D., Gysel, M., Garford, A. A., Dommen, J., Prevot, A. S. H., Worsnop, D. R., Baltensperger, U., and H. Coe (2006). A mass spectrometric study of secondary organic aerosols formed from the photooxidation of anthropogenic and biogenic precursors in a reaction chamber. *Atmos. Chem. Phys.*, 6, 5279–5293.

Anastasio C. and K. G. McGregor (2001). Chemistry of fog waters in California's Central Valley: 1. In situ photoformation of hydroxyl radical and singlet molecular oxygen. *Atmos. Env.*, 35, 6, 1079-1089.

Andreae, M. O. and D. Rosenfeld (2008). Aerosol–cloud–precipitation interactions. Part 1. The nature and sources of cloud-active aerosols. *Earth-Science Reviews*, 89, 13-41.

Arakaki, T., and B. C. Faust (1998). Sources, sinks, and mechanisms of hydroxyl radical photoproduction and consumption in authentic acid continental cloud waters from Whiteface Mountain, New York: The role of the Fe(r) (r=II,III) photochemical cycle. *Journal of Geophys. Res.,* 103, 3487-3504.

Archer, D. E., and K. Johnson (2000). A model of the iron cycle in the ocean. Global *Biogeochem. Cycles*, 14, 269-279.

Baker, A. R., and T. D. Jinkells (2006). Mineral particle size as a control on aerosol iron solubility. *Geophys. Res. Letters*, 33.

Baker, A. R., Jickells, T. D., Witt, M., and Linge, K. L. (2006). Trends in the solubility of iron, aluminium, manganese and phosphorus in aerosol collected over the Atlantic Ocean. *Marine Chemistry*, 98, 43-58.

Baker, A. R., M. French, and K. L. Linge (2006). Trends in aerosol nutrient solubility along a west–east transect of the Saharan dust plume. *Geophys. Res. Lett.*, 33, L07805, doi:10.1029/2005GL024764.

Bauer, S. E., Y. Balkanski, M. Schulz, D. A. Hauglustaine, and F. Dentener (2004). Global modeling of heterogeneous chemistry on mineral aerosol surfaces: Influence on tropospheric ozone chemistry and comparison to observations. *J. Geophys. Res.*, 109.

Bonnet S. and C. Guieu (2004). Dissolution of atmospheric iron in seawater. *Geophys. Res. Letters*, 31.

Borer, P., Sulzberger, B., Hug, S. J., Kraemer, S. M., and R. Kretschmar (2009). Photoreductive Dissolution of Iron(III) (Hydr)oxides in the Absence and Presence of

Organic Ligands: Experimental Studies and Kinetic Modeling. *Environ. Sci. Technol.,* 43 (6), 1864–1870.

Boyd, P. W. and M. J. Ellwood (2010). The biogeochemical cycle of iron in the ocean. *Nature Geoscience*, 3, 675-682.

Boyd, P. W., Jinkells, T., Law, C. S., Blain, S., Boyle, E. A., Buesseler, K. O., Coale, K. H., Cullen, J. J., de Baar, H. J. W., Follows, M., Harvey, M., Lancelot, C., Levasseur, M., Owens, N. P. J., Pollard, R., Rivkin, R. B., Sarmiento, J., Schoemann, V., Smetacek, V., Takeda, S., Tsuda, A., Turner, S., and A. J. Watson (2007). Mesoscale iron enrichment experiments 1993-2005: synthesis and future directions. *Science*, 315, 612-617.

Buseck P. R. and K. Adachi (2008). Nanoparticles in the atmosphere. *Elements*, 4, 389-394.

Brandt, C., and R. van Eldik (1995). Transition Metal-Catalyzed Oxidation of Sulfur(IV) Oxides. Atmospheric-Relevant Processes and Mechanisms. *Chem. Rev.*, 95, 119-190.

Butler, A. (1998). Acquisition and utilization of transition metal ions by marine organisms. *Science*, 280, 207–210.

Cahill, T. A., Barnes, D. E., Spada, N. J., Lawton, J. A., and T. M. Cahill (2011). Very Fine and Ultrafine Metals and Ischemic Heart Disease in the California Central Valley 1: 2003–2007, *Aerosol Science and Technology*, 45(9), 1123-1134.

Cakmur, R. V., R. L. Miller, J. Perlwitz, I. V. Geogdzhayev, P. Ginoux, D. Koch, K. E. Kohfeld, I. Tegen, and C. S. Zender (2006). Constraining the magnitude of the global dust cycle by minimizing the difference between a model and observations, *J. Geophys. Res.*, 111.

Carrillo, J.H., Emert, S.E., Sherman, D.E., Herckes, P., and J. L. Collett Jr. (2008). An economical optical cloud/fog detector. *Atmos. Res.*, 87, 259–267.

Carvalho, T. C., Peters, J. I., and R. O. Williams III (2011). Influence of particle size on regional lunch deposition—What evidence is there? *International Journal of Pharmaceuticals*, 406, 1-10.

Centers for Disease Control and Prevention (CDC).”Fungal Diseases: Valley Fever (Coccidioidomycosis) Statistics.” http://www.cdc.gov/fungal/diseases/coccidioidomycosis/statistics.html.

Chapman, R.S., Watkinson, W.P., Dreher, K.L., and D. L. Costa (1997). Ambient Particulate Matter and Respiratory and Cardiovascular Illness in Adults: Particle-Borne Transition Metals and the Heart-Lung Axis. *Environ. Toxicol. Pharmacol.*, 4, 331-338.

Charlson, R. J., Lovelock, J. E., Andreae, M. O., and S. G. Warren (1987). Oceanic phytoplankton, atmospheric sulphur, cloud albedo and climate. *Nature*, 326, 655-661.

Charrier, J. G., McFall, A. S., Richards-Hernderson, N. K., and C. Anastasio (2014). Hydrogen Peroxide Formation in a Surrogate Lung Fluid by Transition Metals and Quinones Present in Particulate Matter. *Environmental Science and Technology*, 48, 7010-7017.

Chen, B., W. Lee, P.K. Westerhoff, S.W. Krasner and P. Herckes (2010). Solar photolysis kinetics of disinfection byproducts. *Water Research*, 44 , 3401 -3409.
Chen, W., and D. W. Fryrear (2002). Sedimentary characteristics of a haboob dust storm. *Atmos. Res.*, 61, 75-85.

Chuang, P. Y., Duvall, R. M., Shafer, M. M., and J. J. Schauer (2005). The origin of water soluble particulate iron in the Asian atmospheric outflow. *Geophys. Res. Letters* 32.

Claquin, T., Schulz, M., and Y. J. Balkanski (1999). Modeling the mineralogy of atmospheric dust sources. *Journal of Geophys. Res.* 104, 22243-22256.

Collett, J. L. Jr., Daube, B. C. Jr., Munger, J. W., and M. R. Hoffmann (1990). A comparison of two cloudwater/fogwater collectors: The Rotating Arm Collector and the CalTech Active Strand Cloudwater Collector. *Atmospheric Environment*, 24A (7), 1685-1692.

Collett, Jr., J. L., Hoag, K. J., Rao, X., and S. N. Pandis (1999b). Internal acid buffering in San Joaquin Valley fog drops and its influence on aerosol processing. *Atmos. Env.*, 33, 4833-4847.

Collett, Jr., J. L., Hoag, K. J., Sherman, D. E., Bator, A., and L. W. Richards (1999a). Spatial and temporal variation in San Joaquin Valley fog chemistry. *Atmos. Env.*, 33, 129-140.

Collett, Jr., J.L., Herckes, P., Youngster, S., T. Lee (2008). Processing of atmospheric organic matter by California radiation fogs. *Atmos. Res*., 87, 232–241.

Cwiertny, D. M., Baltrusaitis, J., Hunter, G. J., Laskin, A., Scherer, M. M., and V. H. Grassian (2008). Characterization and acid-mobilization study of iron-containing mineral dust source minerals. *Journal of Geophys. Res*., 113.

Cwiertny, D. M., Young, M. A., and V. H. Grassian (2008). Chemistry and photochemistry of mineral dust aerosol. *Annu. Rev. Phys. Chem*., 59, 27-51.

Daube, B.C., Jr, Flagan, R.C. and M. R. Hoffmann (1987). Active cloudwater collector. United States Patent No. 4,697,462.

Dedik, A. N., Hoffman, P., and J. Ensling (1992). Chemical characterization of iron in atmospheric aerosols. *Atm. Environ.*, 26A, 2545-2548.

Demoz, B. B., Collett, J. L. Jr., and B. C. Daube Jr. (1996). On the Caltech Active Strand Cloudwater Collectors. *Atmospheric Research*, 41, 47-62.

Demoz, B.B., Collett, Jr., J.L., and B.C. Daube (1996). On the Caltech Active Strand Cloudwater Collectors. *Atmos. Res.*, 41, 47–62.

Desboeufs, K. V., Losno, R., and J. L. Colin (2001). Factors influencing aerosol solubility during cloud processes, *Atmospheric Environment*, 35 (20), 3529-3537.

Desboeufs, K. V., Sofikitis, A., Losno, R., Colin, J. L., and P. Ausset (2005). Dissolution and solubility of trace metals from natural and anthropogenic aerosol particulate matter. *Chemosphere*, 58, 195-203.

Doherty, S.J., T.L. Anderson, and R. J. Charlson (1999). Measurement of the lidar ratio for atmospheric aerosols with a 180degree backscatter nephelometer, *Applied Optics*, 38(9), 1823-1832.

Doubovik, O., Holben, B., Eck, T. F., Smirnov, A., Kaufman, Y. J., King, M. D., Tanre, D., and I. Slutsker (2001). Variability and Absorption of Optical Properties of Key Aerosol Types Observed in Worldwide Locations. *Journal of Atmospheric Sciences*, 59, 590-608.

Dumont, M., Brun, E., Picard, G., Michou, M., Libois, Q., Petit, J-R., Geyer, M., Morin, S., and B. Josse (2014). Contribution of light-absorbing impurities in snow to Greenland's darkening since 2009. *Nature Geoscience*, 7, 509–512.

Ehrenhauser, F.S., Khadapkar, K., Wang, Y., Hutchings, J.W., Delhomme, O., Kommalapati, R. R., Herckes, P., Wornat, M.J., K. T. Valsaraj (2012). Processing of atmospheric polycyclic aromatic hydrocarbons by fog in an urban environment. *J. Environ. Mon.*, 14, 2566–79.

Ehrenhauser, F.S., Khadapkar, K., Wang, Y., Hutchings, J.W., Delhomme, O., Kommalapati, R. R., Herckes, P., Wornat, M.J., and K. T. Valsaraj (2012). Processing of atmospheric polycyclic aromatic hydrocarbons by fog in an urban environment. *J. Environ. Mon.*, 14, 2566–79.

Elbert, W., Hoffmann, M.R., Kraemer, M., Schmitt, G., and M.O. Andreae (2000). Control of solute concentrations in cloud and fog water by liquid water content. *Atmos. Environ.*, 34, 1109-1122.

Environmental Protection Agency (EPA). Air Quality Index Daily Values Report: $PM_{2.5}$ and PM_{10} for 2013 and 2014.

http://www.epa.gov/airquality/airdata/ad_rep_aqi_daily.html.

Environmental Protection Agency (EPA). Particulate Matter (PM) Standards - Table of Historical PM NAAQS (2012).
http://www.epa.gov/ttn/naaqs/standards/pm/s_pm_history.html.

Ervens, B., Wang, Y., Eagar, J., Leaitch, W. R., Macdonald, A. M., Valsaraj, K. T., and P. Herckes (2013). Dissolved organic carbon (DOC) and select aldehydes in cloud and fog water: the role of the aqueous phase in impacting trace gas budgets. *Atmos. Chem. Phys.*, 12, 33083-33125.

Fahey, K. M., Pandis, S. M., Collett, J. L. Jr., and P. Herckes (2005). The influence of size-dependent droplet composition on pollutant processing by fogs. *Atmospheric Environment*, 39 (25), 4561-4574.

Falkowski, P. G., Barber, R. T., and V. Smetacek (1998). Biogeochemical controls and feedbacks on ocean primary productivity. *Science*, 281, 200-206.

Faust, B. C. and J. Hoigne (1990). Photolysis of Fe(III)-hydroxy complexes as sources of OH radicals in clouds, fog and rain. *Atmospheric Environment*, 24A, 79-89.

Finlayson-Pitts, B. J., and Pitts Jr, J. N., Chemistry of the Upper and Lower Atmosphere, edited by: Pitts, B. J. F.-P. N., Academic Press, San Diego, 2000.

Fu, H., Cwiertny, D. M., Carmichael, G. R. , Scherer, M. M., and V. H. Grassian (2010). Photoreductive dissolution of Fe-containing mineral dust particles in acidic media. *Journal of Geophys. Res.*, 115.

Fuzzi, S., Castillo, R. A., Jiusto, J. E., and G. G. Lala (1984). Chemical composition of radiation fog water at Albany, New York, and its relationship to fog microphysics. *Journ. Geophys. Res.*, 89, D5, 7159-7164.

Gantt, B. and N. Meskhidze (2013). The physical and chemical characteristics of marine primary organic aerosol: a review. *Atmos. Chem. Phys.*, 13, 3979-3996.

Gao, Y., Fan, S. M., and J. L. Sarmiento (2003). Aeolian iron input to the ocean through precipitation scavenging: A modeling perspective and its implication for natural iron fertilization in the ocean. *Journal of Geophys. Res.*, 108, 1-13.

Gaudichet, A., Echalar, F., Chatenet, B., Quisefit, J. P., Malingre, G., Cachier, H., Buat-Menard, P., Artaxo, P., and W. Maenhaut (1995). Trace elements in tropical African savanna biomass burning aerosols. *Journal of Atmospheric Chemistry*, 22, 19-39.

Ge, X., Setyan, A., Sun, Y., and Q. Zhang (2012). Primary and secondary organic aerosols in Fresno, California during wintertime: Results from high resolution aerosol mass spectrometry. *Journal of Geophysical Research Atmospheres*, 117, D19.

Ge, X., Zhang, Q., Sun, Y., Ruehl, C. R., and A. Setyan (2012). Effect of aqueous-phase processing on aerosol chemistry and size distributions in Fresno, California during wintertime. *Env. Chem.*, 9 (3), 221-235.

Gilardoni, S., Massoli, P., Guilianelli, L., Rinaldi, M., Paglione, M., Pollini, F., Lanconelli, C., Poluzzi, V., Carbone, S., Hillamo, R., Russell, L. M., Facchini, M. C., and S. Fuzzi (2014). Fog scavenging of organic and inorganic aerosol in the Po Valley. *Atmos. Chem. Phys.*, 14, 6967-6981.

Gillies, J. A., Nickling, W. G., and G. H. McTainsh (1996). Dust concentrations and particle size characteristics of an intense dust haze event: Inland Delta Region, Mali, West Africa. *Atmos. Env.*, 30, 1081-1090.

Gonzalez-Maddux, C., Marcotte, A., Upadhyay, N., Herckes, P., Williams, Y., Haxel, G., and M. Robinson (2014). Elemental composition of $PM_{2.5}$ in Shiprock, New Mexico, a rural community located near coal-burning power plants and abandoned uranium mine tailings sites. *Atmospheric Pollution Research*, 5, 511-519, doi: 10.5094/APR.2014.060.

Gordon, C. A., Herrera, R., and T. C. Hutchinson (1994). Studies of fog events at two cloud forests near Caracas, Venezuela—II. Chemistry of fog. *Atmos. Env.*, 28, 2, 323-337.

Grob, S., Esselborn, M., Weinsierl, B., Wirth, M., Fix, A., and A. Petzold (2013). Aerosol classification by airborne high spectral resolution lidar observations. *Atmos. Chem. Phys.*, 13, 2487-2505.

Gurgueira, S. A., Lawrence, J., Coull, B., Murthy, G. G. K., and B. Gonzalez-Flecha (2002). Rapid increases in the steady-state concentration of reactive oxygen species in the lungs and heart after particulate air pollution inhalation. *Environ. Health Perspect.*, 110(8), 749–755.

Hallberg, A., Ogren, J. A., Noone, K. J., Heintzenberg, J., Berner, A., Solly, I., Kruisz, C., Reischl, G., Fuzzi, S., Facchini, M. C., Hansson, H. C., Wiedensohler, A., and I. B. Svenningsson (1992). Phase partitioning for different aerosol species in fog. *Tellus B*, 44(5), 545-555.

Ham, W. A., Herner, J. D., Green, P. G., and M. J. Kleeman (2010). Size Distribution of Health-Relevant Trace Elements in Airborne Particulate Matter During a Severe Winter Stagnation Event: Implications for Epidemiology and Inhalation Exposure Studies. *Aerosol Science and Technology*, 44(9), 753-765.

Han, Y.M., Du, P.X., Cao, J.J., and E. S. Posmentier (2006). Multivariate analysis of heavy metal contamination in urban dusts of Xi'an, Central China. *Science of the Total Environment*, 355, 176–186.

Harrison, R. M. and C. A. Pio (1983). Size-differentiated composition of inorganic atmospheric aerosols of both marine and polluted continental origin. *Atmos. Environ.*, 17 (9), 1733-1738.

Hegg, D. A., and P. V. Hobbs (1978). Oxidation of sulfur dioxide in aqueous systems with particular reference to the atmosphere. *Atmospheric Environment*, 12, 241-253.

Herckes, P., and J. L. Collett Jr. (2015). Cloud Chemistry. In: Gerald R. North (editor-in-chief), John Pyle and Fuqing Zhang (editors). Encyclopedia of Atmospheric Sciences, 2nd edition, Vol 6, pp. 218–225.

Herckes, P., Leenheer, J. A., J. L. Collett, Jr. (2007a). Comprehensive characterization of atmospheric organic matter in Fresno, California fog water. Environ. Sci. Technol., 41, 393‑399.

Herckes, P., Chang, H., Lee, T., J.L. Collett, Jr. (2007b). Air Pollution Processing by Radiation Fogs. *Water, Air, Soil Poll.*, 181, 65–75.

Herckes, P., Wortham, H., Mirabel, P., and M. Millet (2002). Evolution of the fogwater composition in Strasbourg (France) from 1990 to 1999. *Atmospheric Research*, 64, 53-62.

Heyder, J., Genhart, J., Rudolf, G., Schiller, C. F., and W. Stahlhofen (1986). Deposition of particles in the human respiratory tract in the size range 0.005-15µm. *Journal of Aerosol Science*, 17(5), 811-825.

Hinds, W. C. (2012). Aerosol Technology: Properties, Behavior, and Measurement of Airborne Particles 2nd Edition (3.3 Settling Velocity and Mechanical Mobility), John Wiley and Sons.

Hoag, K. J., Collett, Jr., J. L., and S. N. Pandis (1999). The influence of drop size-dependent fog chemistry on aerosol processing by San Joaquin Valley fogs. *Atmos. Env.*, 33 (29), 4817-4832.

Hobbs, P. V. (1993). Chapter 2 Aerosol-Cloud Interactions. *International Geophysics*, 54, 33-73.

Holets, S. and R. N. Swanson (1981). High-Inversion Fog Episodes in Central California. *Journal of Applied Meteorolgy*, 20, 890-899.

Hopke, P.K. (1991). An Introduction to Receptor Modeling. *Chemomet. Intell. Lab. Syst.*, 10, 21-43.

Hutchings, J. W., Ervens, B., Straub, D., and P. Herckes (2010). N-nitrosodimethylamine occurrence, formation and cycling in clouds and fogs. *Environmental Science and Technology*, 44, 8128–8133.

Idso, S. B., Ingram, R.S., and J. M. Pritchard (1972). An American Haboob. *Bull. Amer. Meteor. Soc.*, 53, 930–935.

Jacob D. J., Wang R. F. T. and R. C. Flagan (1984) Fogwater collector design and characterization. *Envir. Sci. Technol*., 18, 827-833.
Jeong, G. Y., and E. P., Achterberg (2014). Chemistry and mineralogy of clay minerals in Asian and Saharan dusts and the implications for iron availability. *Atmos. Chem. Phys. Discuss.*, 14, 15735–15770.

Jacob, D. J. (1999). Chapter 4: Atmospheric Transport, Introduction to Atmospheric Chemistry. *Princton University Press*.

Jinkells, T. D., An, Z. S., Andersen, K. K., Baker, A. R., Bergametti, G., Brooks, N., Cao, J. J., Boyd, P. W., Duce, R. A., Hunter, K. A., Kawahata, H., Kubilay, N., laRoche, J., Liss, P. S., Mahowald, N., Propero, J. M., Ridgwell, A. J., Tegen, I., and R. Torres (2005). Global iron connections between desert dust, ocean biogeochemistry, and climate. *Science*, 308, 67-71.

Journet, E., Desboeufs, K. V., Caquineau, S., and J-L. Colin (2008). Mineralogy as a critical factor of dust iron solubility. *Geophys. Res. Letters*, 35.
Karlsson, H.L., Nilsson, L., and L. Moller (2005). Subway Particles are More Genotoxic than Street Particles and Induce Oxidative Stress in Cultured Human Lung Cells. *Chem. Res. Toxicol.*, 18, 19-23.

Kiehl, J. T., and H. Rodhe (1995). Modeling geographic and seasonal forcing due to aerosols, in Aerosol Forcing of Climate, edited by R. J. Charlson and J. Heintzenberg. Wiley, NY, 281-296.

Klemm, O., and T. Wrzesinsky (2007). Fog deposition fluxes of water and ions to a mountainous site in Central Europe. *Tellus B*, 59, 705-714.

Kong, L. D., Zhao, X., Sun, Z. Y., Yang, Y. W., Fu, H. B., Zhang, S. C., Cheng, T. T., Yang, X., Wang, L., and J. M. Chen (2014). The effects of nitrate on the heterogeneous uptake of sulfur dioxide on hematite. *Atmos. Chem. Phys.*, 14, (17), 9451-9467.

Krämer M. and L. Schütz (1994). On the collection efficiency of a rotating ARM collector and its applicability to cloud- and fogwater sampling. *Journal of Aerosol Science*, 25, 137-148.

Kumar, A., Sarin, M.M., and B. Srinivas (2010). Aerosol iron solubility over Bay of Bengal: Role of anthropogenic sources and chemical processing. *Marine Chemistry*, 212, 167-175.

Lawson, T. J. (1971). Haboob structure at Khartoum. *Weather*, 26.

Lee, M. Y. H. (2014). Valley dust levels receive federal approval. *The Arizona Republic*, azcentral.com.

Lim et al. (2012). A comparative risk assessment of burden of disease and injury attributable to 67 risk factors and risk factor clusters in 21 regions, 1990–2010: a systematic analysis for the Global Burden of Disease Study 2010. *The Lancet*, 380, 2224-2260.

Liu, B. Y. H. (1976). Fine Particles: Aerosol Generation, Measurement, Sampling and Analysis. Academic Press Inc.

Lohse, K. A., Hope, D., Sponseller, R., Allen, J. O., and N. B. Grimm (2008). Atmospheric deposition of carbon and nutrients across an arid metropolitan area. Science of The Total Environment, 402, 95-105.

Majestic, B. J., Schauer, J. J., Shafer, M. M., Turner, J. R., Fine, P. M., Singh, M., and C. Sioutas (2006). Development of a wet-chemical method for the speciation of iron in atmospheric aerosols. *Environmental Science & Technology*, 40, 2346-2351.

Majestic, B.J., Anbar, A.D., and P. Herckes (2009). Stable isotopes as a tool to apportion atmospheric iron. *Environmental Science & Technology*, 43, 4327–4333.

Martin, J. H. (1990). Glacial-interglacial CO2 change: the iron hypothesis. *Paleoceanography*, 5, 1-13.

Mazzoleni, L.R., Ehrmann, B.M., Shen, X., Marshall, A.G., and J. L. Collett Jr. (2010). Water-soluble atmospheric organic matter in fog: exact masses and chemical formula identification by ultrahigh-resolution fourier transform ion cyclotron resonance mass spectrometry. *Env. Sci. Technol.*, 44, 3690– 3697.

McGregor K. G. and C. Anastasio (2001). Chemistry of fog waters in California's Central valley: 2. Photochemical transformations of amino acids and alkyl amines. *Atmos. Env.*, 35 (6), 1091-1104.

Meskhidze, N., Chameides, W. L., and A. Nenes (2005). Dust and pollution: a recipe for enhanced ocean fertilization? *Journal of Geophysical Research-Atmospheres*, 110, D03301.

Miller, S. D., Kuciauskas, A. P., Liu, M., Ji, Q., Reid, J. S., Breed, D. W., Walker, A. L., and A. Al Mandoos (2008). Haboob dust storms of the southern Arabian Peninsula. *Jour. Geophys. Res. Atmos.*, 113.

Monger, J. W., Collett, J. L. Jr., Daube, B. Jr., and M. R. Hoffmann (1989). Chemical composition of coastal stratus clouds: Dependence on droplet size and distance from the coast. *Atmospheric Environment*, 23 (10), 2305-2320.

Moore, K. F., Sherman, D. E., Reilly, J. E., and J. L. Collett Jr. (2002). Development of a multi-stage cloud water collector. Part 1: Design and field performance evaluation. *Atmospheric Environment,* 36, 31-44.

Moore, R. H., Cerully, K., Bahreini, R., Brock, C. A., Middlebrook, A. M., and A. Nenes (2012). Hygroscopicity and composition of California CCN during summer 2010. *Jour. Geophys. Res.,* 117, D21.

Morrow, P. E. (1972). Pulmonary absorption'of toxic metals, Rep. UR-3490- 136, Univ. of Rochester, Rochester, N.Y.

Munger, J. W., Jacob, D. J., Waldman, J. M., and M. R. Hoffman (1983). Fogwater Chemistry in an Urban Atmosphere. *Jour. Geophys. Res*., 88, 5109-5121.

Needleman, H. L., Schell, A., Bellinger, D., Leviton, A., and E. L. Allred (1990). The long-term effects of exposure to low doses of lead in childhood: An 11-year follow-up report. The New England Journal of Medicine 332, 83-88.

Nemmar, A., Hoet, P.H.M., Vanquickenborne, B., Dinsdale, D., Thomeer, M., Hoylaerts, M.F., Vanbilloen, H., Mortelmans, L., and B. Nemery (2002). Passage of Inhaled Particles Into the Blood Circulation in Humans. *Circulation*, 105, 411-414, doi:10.1161/hc0402.104118.

O'Dowd, C. D., Smith, M. H., Consterdine, I. E., and J. A. Lowe (1997). Marine aerosol, sea salt, and the marine sulphur cycle: a short review. *Atmos. Environ*., 31, 73–80.
Pewe, T. L. (1981). Desert Dust: Origin, Characteristics, and Effect on Man. *Assoc. for the Advancement of Sci.,* 177.

Pehkonen, S. O., Siefert, R. L., Erel, Y., Webb, S., and M. R. Hoffmann (1993). Photoreduction of iron oxyhydroxides in the presence of important organic compounds. *Environ. Sci. Technol.*, 27, 2058-2062.

Pehkonen, S. O., Siefert, R. L., and M. R. Hoffmann (1995). Photoreduction of iron oxyhydroxides and the photooxidation of halogenated acetic acids. *Environ. Sci. Technol.*, 29, 1215-1222.

Prahalad, A.K., Soukup, J.M., Inmon, J., Willis, R., Ghio, A.J., Becker,S., and J.E. Gallagher (1999). Ambient Air Particles: Effects on Cellular Oxidant Radical Generation in Relation to Particulate Elemental Chemistry. *Toxicol. Appl. Pharmacol.,* 158, 81-91.

Pruppacher, H. R. and J. D. Klett (1980). Microphysics of Clouds and Precipitation.
Ramadan, Z., Song, X.H., and P.K. Hopke (2000). Identification of sources of Phoenix aerosol by positive matrix factorization. *Journal of the Air & Waste Management Association*, 50, 1308–1320.

Raman, A., Arellano Jr., A. F., and J. J. Brost (2014). Revisiting haboobs in the southwestern United States: An observational case study of the 5 July 2011 Phoenix dust storm. *Atmospheric Environment*, 89, 179-188.

Rattigan, O. V., Mirza, M. I., Ghauri, B. M., Khan, A. R., Swami, K., Yang, K., and L. Husain (2002). Aerosol sulfate and trace elements in urban fog. *Energy Fuels*, 16, 3, 640-646.

Reid, J. S., et al. (2003). Comparison of size and morphological measurements of coarse mode dust particles from Africa, *J. Geophys. Res.*, 108, 8593, doi:10.1029/2002JD002485, D19.

Rubasinghege, G., Elzey, S., Baltrusaitis, J., Jayaweera, P. M., and V. H. Grassian (2010a). Reactions on Atmospheric Dust Particles: Surface Photochemistry and Size-Dependent Nanoscale Redox Chemistry. *J. Phys. Chem. Lett.*, 1, 1729‑1737

Rubasinghege, G., Lentz, R. W., Park, H., Scherer, M. M., and V. H. Grassian (2010b). Nanorod Dissolution Quenched in the Aggregated State. *Langmuir*, 26(3), 1524‑1527

Rudnick, R.L., and S. Gao (2005). Composition of the Continental Crust, in The Crust—Treatise on Geochemistry. Edited by Rudnick R.L., Elsevier Ltd., Oxford, 3, 1–64.

Schemenauer, R. S. and P. Cereceda (1992). The Quality of Fog Water Collected for Domestic and Agricultural Use in Chile. *Journal of Applied Meteorology*, 31, 275-290.

Schwartz, J., Laden, F., and A. Zanobetti (2002). The concentration-response relation between PM (2.5) and daily deaths. *Environ. Health Perspect*., 110, 1025–1029.

Seifert, R. L., Johansen, A. M., Hoffmann, M. R., and S. O. Pehkonen (1998). Measurements of Trace Metal (Fe, Cu, Mn, Cr) Oxidation States in Fog and Stratus Clouds. *Journal of Air and Waste Management Association*, 48, 128-143

Seinfeld, J. H., and S. N. Pandis (2006). Atmospheric Chemistry and Physics: From Air Pollution to Climate Change, 2nd ed., John Wiley & Sons.

Sherman, D. M. (2005). Electronic structures of iron(III) and manganese(IV) (hydr)oxide minerals: Thermodynamics of photochemical reductive dissolution in aquatic environments. *Geochimica et Cosmochimica Acta,* 69 (13), 3249-3255.

Shi, J.P., Khan, A.A., and R. M. Harrison (1999). Measurements of ultrafine particle concentration and size distribution in the urban atmosphere, *Sci. Total Environ.*, 235, 51-64.

Siefert, R. L., Johansen A. M., Hoffman, M. R., and S. O. Pehkonen (1998). Measurements of Trace Metal (Fe, Cu, Mn, Cr) Oxidation States in Fog and Stratus Clouds. *Journal of Air and Waste Management Association,* 48, 128-143.

Smith, K. R., Frumkin, H., Balakrishnan, K., Butler, C. D., Chafe, Z. A., Fairlie, I., Kinney, P., Kjellstrom, T., Mauzerall, D. L., McKone, T. E., et al. (2013). Energy and human health. *Annu. Rev. Public Health*, 34, 159–188.

Solomon, P.A. and P.K. Hopke (2008). A Special Issue of JA&WMA Supporting Key Scientific and Policy- and Health-relevant Findings from EPA's Particulate Matter Supersites Program and Related Studies: An Integration and Synthesis of Results. *J. Air Waste Manage. Assoc.*, 58, 137–139.

Sorooshian, A., Wonaschütz, A., Jarjour, E. G., Hashimoto, B. I., Schichtel, B. A., and E. A. Betterton (2011). An aerosol climatology for a rapidly growing arid region (southern Arizona): Major aerosol species and remotely sensed aerosol properties. Journal of Geophysical Research: Atmospheres, 116, DOI: 10.1029/2011JD016197.

Spokes, L. J., Jickells, T. D., and B. Lim (1994). Solubilisation of aerosol trace metals by cloud processing: A laboratory study. *Geochimica et Cosmochimica Acta,* 58 (15), 3281-3287.

Straub, D. J., Hutchings, J. W., and P. Herckes (2012). Measurements of fog composition at a rural site. *Atmospheric Environment*, 47, 195-205.

Tao, F., Gonzalez-Flecha, B., and L. Kobzik (2003). Reactive oxygen species in pulmonary inflammation by ambient particulates. *Free Radical Biology and Medicine,* 35 (4), 327-340.

Tegen, I. and A. A. Lacis (1996). Modeling of particle size distribution and its influence on the radiative properties of mineral dust aerosol. *Journal of Geophysical Research*, 101, D14, 19237–19244.

Trapp, J. M., Millero, F. J., and J. M. Prospero (2010). Trends in the solubility of iron in dust-dominated aerosols in the equatorial Atlantic trade winds: Importance of iron speciation and sources. *Geochemistry, Geophysics, Geosystems*, 11, Q03014.

Upadhyay, N., Clements, A. L., Fraser, M. P., Sundblom, M., Solomon, P., and P. Herckes (*in press*). Size-Differentiated Chemical Composition of Re-Suspended Soil Dust from the Desert Southwest United States. *Aerosol and Air Quality Research*.
Upadhyay, N., Clements, A., Fraser, M., and P. Herckes (2011). Chemical speciation of $PM_{2.5}$ and PM_{10} in South Phoenix, Arizona. *Journal of the Air & Waste Management Association*, 61, 302–310.

Upadhyay, N., Majestic, B. J., and P. Herckes (2011). Solubility and speciation of atmospheric iron in buffer systems simulating cloud conditions. *Atmospheric Environment*, 45 (10), 1858-1866.

Upadhyay, N., Majestic, B. J., Prapaipong, P., and P. Herckes (2009). Evaluation of polyurethane foam, polypropylene, quartz fiber, and cellulose substrates for multi-element analysis of atmospheric particulate matter by ICP-MS. *Anal. Bioanal. Chem.*, 394, 255-266.

Upadhyay, N., Majestic, B.J., Prapaipong, P. and P. Herckes (2009). Evaluation of Polyurethane Foam, Polypropylene, Quartz Fiber, and Cellulose Substrates for Multi-Element Analysis of Atmospheric Particulate Matter by ICP-MS. *Anal. Bioanal. Chem.*, 394: 255–266.

Usher, C. R, Michel, A. E., and V. H. Grassian (2003). Reactions on Mineral Dust, *Chem Rev*., 103, 4883-4939.

Wang, Y. Chiu, C., Westerhoff, P., Valsaraj, K. T., and P. Herckes (2013). Characterization of atmospheric organic matter using size exclusion chromatography with inline organic carbon detection. *Atmos. Env*., 68, 326-332.

Wang, Y., Guo, J., Wang, T., Ding, A., Gao, J., Zhou, Y., Collett, Jr., J. L., and W. Wang (2011). Influence of regional pollution and sandstorms on the chemical composition of cloud/fog at the summit of Mt. Taishan in northern China. *Atmospheric Research*, 99, 434-442.

Wang, Y., Zhang, J., Marcotte, A. R., Karl, M., Dye, C., and P. Herckes (2015). Fog Chemistry at Three Sites in Norway. *Atmospheric Research*, 151, 72-81.

Warneck, P. (1994). Clouds, Rain, and Aerosols. *Low-Temperature Chemistry of the Atmosphere NATO ASI Series*, 21, 49-68.

Woolf, D. K., Bowyer, P. A., E. C. Monahan (1987). Discriminating Between the Film Drops and Jet Drops Produced by a Simulated Whitecap. *Journal of Geophysical Research*, 92, 5142-5150.

Xu, M.H., Yan, R., Zheng, C.G., Qiao, Y., Han, J., and C.D. Sheng (2004). Status of trace element emission in a coal combustion process: A review. *Fuel Processing Technology*, 85, 215–237.

Zeebe, R. E. (2012). History of Seawater Carbonate Chemistry, Atmospheric CO_2, and Ocean Acidification. *Annu. Rev. Earth Planet. Sci*., 40.

Zhang Q. and C. Anastasio (2001). Chemistry of fogwaters in California's Central Valley—Part 3: concentrations and speciation of organic and inorganic nitrogen. *Atmos. Env.*, 35, 32, 5629-5643.

Zhu, X., Propero, J. M., Savoie, D. L., Millero, F. J., Zika, R. G., and E. S. Saltzman (1993). Photoreduction of iron (III) in marine mineral aerosol solutions. *Journal of Geophys. Res.*, 98, 9039-9046.

Zhuang, G. S., Yi, Z., Duce, R. A., and P. R. Brown (1992). Link between iron and sulfur cycles suggested by detection of Fe(II) in remote marine aerosols. *Nature*, 355, 537-53.

APPENDIX A

SAMPLE INFORMATION FOR FOG WATER AND AEROSOL SAMPLES COLLECTED IN FRESNO AND DAVIS, CALIFORNIA

Table A1. Sample information for fog water collected in Fresno and Davis, CA.

Sample ID	Collection Location	Collection Date	Start Time (Local)	Duration (min)	Weight (mg)	LWC (mg/m^3)	pH
F010910 P1	Fresno, CA	9-Jan-10	1:30	120	100.78	39.86	6.97
F010910 P2	Fresno, CA	9-Jan-10	3:30	120	171.7	67.91	6.63
F010910 P3	Fresno, CA	9-Jan-10	5:30	180	241.44	63.66	7.3
F011010 P1	Fresno, CA	10-Jan-10	1:45	420	186.22	21.60	6.66
F011410 P1	Fresno, CA	14-Jan-10	20:00	60	90.98	71.97	6.41
F011410 P2	Fresno, CA	14-Jan-10	21:00	60	89.32	70.65	6.48
F011410 P3	Fresno, CA	14-Jan-10	22:00	60	88.78	70.23	6.62
F011410 P4	Fresno, CA	14-Jan-10	23:00	60	77.38	61.21	6.66
F011410 P5	Fresno, CA	15-Jan-10	0:00	60	99.22	78.48	6.88
F011410 P6	Fresno, CA	15-Jan-10	1:00	60	128.3	101.49	7.01
F011410 P7	Fresno, CA	15-Jan-10	2:00	60	100	79.10	7.15
DAA010611	Davis, CA	6-Jan-11	5:31	260	291.08		6.915
DAMIX011511	Davis, CA	15-Jan-11	9:50	460	322.88	4.74	6.91
DAA011511P1	Davis, CA	15-Jan-11	17:30	170	335.8	16.60	6.67
DAA011511P2	Davis, CA	15-Jan-11	20:20	216	344.54	58.83	6.835
DAA011511P3	Davis, CA	15-Jan-11	23:56	449	381.86	51.57	6.855
DAMIX011611	Davis, CA	17-Jan-11	0:57	258	423	6.47	6.42
DAA011711P1	Davis, CA	17-Jan-11	20:57	191	248.54	9.68	6.555
DAA011711P2	Davis, CA	18-Jan-11	0:08	382	138.54		6.685
DAMIX012311	Davis, CA	23-Jan-11	9:30	175	198	92.57	6.805
DAA012511	Davis, CA	25-Jan-11	6:35	205	566.18		6.36

Table A2. Sample information for aerosol samples ($PM_{2.5}$ and $PM_{>2.5}$) collected in Fresno and Davis, CA.

Sample ID	Collection Date	Start Time (Local)	Time total (min)	Air volume (m^3)	Comments
010810HVI_QFF	1/8/2010	11:04	847	958.014	PRE
010910HVIP1_QFF	1/9/2010	1:30	240	271.2	INTERSTITIAL
010910HVIP2_QFF	1/9/2010	5:30	187	191.196	INTERSTITIAL
010910HVI After_QFF	1/9/2010	8:56	673	760.038	POST
010910HVI_QFF	1/9/2010	20:13	180	202.044	PRE
011010HVIP1_QFF	1/10/2010	2:00	394	444.768	INTERSTITIAL
011010HVI After_QFF	1/10/2010	8:46	612	691.56	POST
011010HIV_QFF	1/10/2010	19:10	428	482.736	PRE
011110HIVP1_QFF	1/11/2010	2:24	465	525.45	INTERSTITIAL
011110HIVA_QFF	1/11/2010	10:17	541	577.656	POST
011310HIV_QFF	1/13/2010	19:19	1435	1623.132	PRE
011410HIVP1_QFF	1/14/2010	19:17	233	263.064	INTERSTITIAL
011410HIVP2_QFF	1/14/2010	23:15	355	401.376	INTERSTITIAL
011510HIVA_QFF	1/15/2010	5:12	846	957.336	POST
01062011DavisA_CL PM2.5	1/6/2011	15:17	1167	1318.71	INTERSTITIAL
01072011Davis_CL	1/7/2011	22:05	1113	1257.69	POST
01082011Davis_CL	1/8/2011	16:46	1296	1464.48	POST
01092011Davis_CL	1/9/2011	14:31	1540	1740.2	no fog
01102011Davis_CL	1/10/2011	16:18	1501	1696.13	no fog
01112011Davis_CL	1/11/2011	17:25	1401	1583.13	no fog
01122011Davis_CL	1/12/2011	16:54	1272	1437.36	stopped sometime between 4am and 2pm
01132011Davis_CL	1/13/2011	14:25	1531	1730.03	PRE
01142011Davis_CL	1/14/2011	16:04	1546	1746.98	INTERSTITIAL
01152011Davis_CL	1/15/2011	17:58	804	908.52	INTERSTITIAL
01162011Davis_CL	1/16/2011	7:29	583	658.79	POST
B01162011Davis_CL	1/16/2011	17:19	456	515.28	PRE
C01162011Davis_CL	1/16/2011	1:02	267	301.71	INTERSTITIAL
01172011Davis_CL	1/17/2011	5:36	716	809.08	POST
B01172011Davis_CL	1/17/2011	17:38	796	899.48	INTERSTITIAL
01182011Davis_CL	1/18/2011	7:01	664	750.32	POST
01202011DavisBK_CL	1/20/2011	16:47	1	1.13	Field Blank
01202011Davis_CL	1/20/2011	16:54	1486	1679.18	PRE
01232011Davis_CL	1/23/2011	9:38	217	245.21	INTERSTITIAL

QFF = Quartz Fiber Filter, CL = Cellulose Filter, FBK = Field Blank